Assessing diurnal variability of rainfall: A remote sensing based approach

Ayele Almaw Fenta

March, 2010

Assessing diurnal variability of rainfall: A remote sensing based approach

by

Ayele Almaw Fenta

Thesis submitted to the International Institute for Geo-information Science and Earth Observation in partial fulfilment of the requirements for the degree of Master of Science in Geo-information Science and Earth Observation, Specialisation: (Integrated Watershed Modelling and Management-Surface Water Hydrology)

Thesis Assessment Board

Chairperson	Dr. Ir. M. W. Lubczynski	(WREM department, ITC Enschede)
External Examiner	Dr. Ir. P. Reggiani	(WL Delft-Hydraulics)
First supervisor	Dr. Ing. T. H. M. Rientjes	(WREM department, ITC Enschede)
Second supervisor	Dr. A.S.M. Gieske	(WREM department, ITC Enschede)
Advisor	MSc. Alemseged Tamiru	(WREM department, ITC Enschede)

ITC

INTERNATIONAL INSTITUTE FOR GEO-INFORMATION SCIENCE AND EARTH OBSERVATION
ENSCHEDE THE NETHERLANDS

Abstract

Rainfall variability studies have wide range of applications in meteorology, climatology and hydrological processes. The assessment of the diurnal cycle of rainfall requires rainfall data at relatively high temporal resolution with large spatial coverage using evenly distributed rain gauges. In most tropical regions, however, observations are commonly available only at daily time steps from rain gauges that are sparsely and unevenly located. The objectives of this study are: to assess the diurnal cycle of rainfall using Tropical Rainfall Measuring Mission (TRMM) satellite observations, validate TRMM rainfall diurnal cycle estimates using ground observations and assess the spatial pattern of the rainfall diurnal cycle. One year (2005) of TRMM Microwave Imager (TMI) data for French Guiana and seven years (2002-2008) of Precipitation Radar (PR) and TMI data for the Upper Blue Nile basin were used for the rainy season. These two areas are selected since the areas are characterized by different latitudinal locations, different climatic and topographic settings. The analysis was based on GIS operations, statistical techniques such as correlation matrix and harmonic analysis. Moreover, since the Upper Blue Nile basin is characterized by high topographic variation, the spatial variability and the relation between rainfall and elevation was assessed taking transects across the basin. Over the two study areas the diurnal cycles of rainfall occurrence from TRMM estimates show significant correlation with the ground observations at 95 % confidence level. In the Upper Blue Nile basin, the PR conditional mean rain rate estimates are closer to the ground observations than the TMI. Over most parts of French Guiana, the maximum rainfall occurrence and conditional mean rain rate are observed from mid to late afternoon between 1500-1800 local standard time (LST). Observations from PR and TMI reveal that over most areas of the Upper Blue Nile basin, the rainfall occurrence and conditional mean rain rate are maximum between mid to late afternoon (1500-1800LST). However, exceptions to this are Lake Tana and the southwest and southeast parts of the basin where midnight and early morning maximum are observed. Along the Blue Nile River gorge the rainfall occurrence and conditional mean rain rate are maximum during the night (2000-2300LST). In general, the mean of the diurnal cycle, the amplitude and the time of amplitude show spatially varying diurnal cycle owing to the high topographic variability of the basin. Along transects that are taken across the basin from north to south and east to west, it is observed that areas on the windward side of the high mountain ranges receive higher amount of rainfall than areas on the leeward side. As such, mountain orientation in relation to general pattern of air circulation influences the rainfall distribution resulting in rain shadow effect in the northeast parts of Choke mountain and the ridges in the northeast of the basin. Moreover, a direct relation between rainfall occurrence and elevation is observed especially for 1700-1800LST. The seasonal mean rainfall depth is highest in the southwest areas and central highlands of the basin while the areas in the north, northeast and along the Blue Nile gorge receive the least amount of rainfall. This study provides relevant information to understand the effect of terrain on diurnal variability of rainfall and variation of rainfall with elevation and mountain orientation using satellite based rainfall observations. As such, it is of high use for meteorological, climate and hydrological studies, water resources planning and management and hydropower development.

Key words: French Guiana, Upper Blue Nile basin, TRMM, PR, TMI, rainfall variability, diurnal cycle

Acknowledgements

Table of contents

List of figures

List of tables

List of Acronyms

AMJJ	Aril, May, June and July
CERES	Cloud and the Earth's Radiant Energy System
DEM	Digital Elevation Model
METEOSAT	Meteorological Satellites
EUMETSAT	European Organization for the Exploitation of Meteorological Satellites
ESA	European Space Agency
GCM	Global Circulation Model
GPROF	Goddard profiling Algorithm
GSC	Guiana Space Centre
HDF	Hierarchical Data Files
ILWIS	Integrated Land and Water Information System
IR	Infrared
ITCZ	Intertropical Convergence Zone
JAXA	Japan Aerospace Exploration Agency
JJAS	June, July, August and September
LIS	Lightning Imaging Sensor
LST	Local Standard Time
MSG-2	Meteosat Second Generation
MW	Microwave
MPE	Multi-sensor Precipitation Estimator
NASA	National Aeronautics and Space Administration
NIR	Near-Infrared
NWP	Numerical Weather Prediction
PR	Precipitation Radar
PUMA	Preparation for the Use of MSG in Africa
SRTM	Shuttle Radar Topography Mission
SSM/I	Special Sensor Microwave Imager
SEVIRI	Spinning Enhanced Visible and Infrared Imager
TMI	TRMM Microwave Imager
TSDIS	TRMM Science Data and Information System
TRMM	Tropical Rainfall Measuring Mission
UTM	Universal Traverse Mercator
DMSP	Defence Meteorological Satellite Program
VIS	Visible
VIRS	Visible and Infrared Radiometer System
WV	Water Vapour

1. Introduction

1.1. Background

The tropics play an important role in the global hydrological cycle with high rainfall rates and depth. The atmosphere receives three-fourth of the heat energy from the latent heat released by tropical rainfall (Kummerow et al., 1998; Kummerow et al., 2000). Two-third of the global rainfall falls in the tropical regions of the earth between 300N and 300S (Kummerow et al., 1998; Simpson et al., 1988). Rainfall and its variability are important constituents of the global hydrological cycle and also affect the development of all living organisms on earth. Particularly over tropical regions, given the socio-economic conditions of many countries, the people basically depend on the rainfall and its variability (Kishtawal and Krishnamurti, 2001). This has led to extensive research to characterize rainfall variability on global as well as regional scales.

The study of variability of rainfall over short time scales, such as the diurnal cycle, has wide range of applications in meteorology, climatology and hydrology. Some of the applications are: to compare predictions of atmospheric models to real world atmospheric behaviour and to verify that rainfall estimates from low-altitude satellites are not biased because of infrequent observations of a given region (Bell and Reid, 1993), to evaluate evaporation on daily basis as the rainfall time of a day and successive sunshine duration affects the amount of daily evaporation (Oki and Musiake, 1994), to understand the physics of the atmosphere (Kishtawal and Krishnamurti, 2001), to invetigate the role of rainfall to fully understand the climate systems (Sorooshian et al., 2002), to understand the dynamics of precipitating systems in response to diurnally varying surface energy fluxes and wind profiles and to evaluate Numerical Weather Prediction (NWP) models and Global Circulation Model (GCM) simulations (Dejene, 2003), to understand the mechanisms of local weather (Vondou et al., 2009) etc.

The diurnal cycle of rainfall over land areas results from interactions between dynamic and radiative/solar forcings. When rainfall occurs regularly at particular time of the day, the atmospheric system is often characterized by physical processes that indicate strong convection during the favoured time (Sorooshian et al., 2002). Generally, a rise in land surface temperature leads to increased atmospheric instability and convection, reaching its maximum in the afternoon or early evening. During night time, due to radiational cooling of the land, there is a decrease in convection activity reaching its minimum in early morning. Night time cooling of cloud tops triggers atmospheric destabilization and results in a nocturnal secondary convection maximum. Moreover, such night time cooling might also result in maximum convection over water in early morning and decreasing convection throughout the day. However, the rainfall diurnal cycle is complicated over most areas owing to local forcings, prevailing wind directions and complex terrain leading to a complex pattern in diurnal cycle (Meisner and Arkin, 1987).

In the tropics, the rainfall diurnal cycle varies considerably from region to region (Bell and Reid, 1993). Spatio-temporal variability of rainfall plays an important role in hydrological processes like the rainfall-runoff response, estimation of probable maximum rainfall and erosion processes. Hence, understanding rainfall variability at relevant space and time scales is vital for proper agricultural planning and optimal management of water resources. However, rainfall variability is influenced by non-linear interactions between several factors and its accurate estimation is one of the major challenges in hydrometeorology (Haile et al., 2009b). This is particularly true in mountainous regions where in addition to the stochastic nature of rainfall, the rainfall pattern may be influenced by orographic factors. For instance, Buytaert et al. (2006) reported that large variability in elevation, slope and aspect may increase rainfall variability by means of processes such as rain shading and strong winds.

In recent decades, the diurnal cycle in tropical rainfall has been extensively studied by using data from different sources. However, in-situ observations of rainfall have been sparse in many areas. For areas where there is sparse and uneven distribution of ground based meteorological stations, recent progress in satellite remote sensing techniques, has made it possible to monitor diurnal cycle of rainfall from satellite data. The visible (VIS) and infrared (IR) observations from geosynchronous satellites have high temporal resolution (15-30 minutes), thus allowing to study diurnal cycles on intraday time-scales. The IR techniques, however, give indirect information on cloud top layers that only serves as a proxy variable to estimate rainfall (Adler and Negri, 1988). The microwave (MW) techniques have relatively good physical basis that give information on the distribution of hydrometeors within the cloud and provide a more direct signal from the cloud layer. However, the space platforms that carry such sensors overpass a given region intermittently and give only one or two samples of rainfall per day. A brief description on the VIS, IR and MW techniques for rainfall estimation is given in chapter 2, sections 2.1.1 and 2.1.2.

With the launch of the Tropical Rainfall Measuring Mission (TRMM) satellite having MW sensors on board, it provides physically direct measurements of rainfall and its vertical structure. This has added a new dimension to study rainfall variability at intraday time-scales. One of the priority science questions in the design of the TRMM satellite was "What is the diurnal cycle of tropical rainfall and how does it vary in space?" (Simpson et al., 1988). Many studies have shown that TRMM can provide sufficient observations at different local times to study the diurnal cycle of rainfall. Negri et al. (2002) used three years of TRMM microwave imager (TMI) and precipitation radar (PR) data to describe the rainfall diurnal cycle for 5^0 x 5^0 and 10^0 x 25^0 windows in the tropics. In addition, they also compared PR and TMI rain rate diurnal cycle estimates and found that over the land, TMI estimates tend to be higher than the PR. Kishtawal and Krishnamurti (2001) studied the diurnal cycle of rainfall using three months of TMI and PR observations for the entire Taiwan. They also validated their results with ground observations and showed that the diurnal patterns of rainfall estimates using TRMM match reasonably with the ground observations. Nesbitt and Zipser (2003) using three years of PR and TMI data and Wu (2004) using five years of PR and TMI data studied the diurnal cycle of rainfall tropics wide. In this study, TRMM-PR and TMI estimated rainfall is used to assess diurnal variability of rainfall in French Guiana and Upper Blue Nile basin. Moreover, TRMM diurnal cycle estimates are compared with ground observations. A brief over-view of the TRMM satellite and a review of literature on previous studies is given in chapter 2, sections 2.2 and 2.3 respectively.

1.2. Significance of the study

As discussed in the background section, tropical rainfall diurnal cycle studies have wide range of applications in various disciplines. This study aims at the assessment of rainfall diurnal cycle for French Guiana and the Upper Blue Nile basin. However, in these areas the lack of ground based rainfall data measured at the required time and space scales has limited the study of diurnal variability of rainfall. Around 90 % of the area of French Guiana is covered by tropical forest and is inaccessible to acquire ground observations. Moreover, in French Guiana, only few rain gauges are available that are located near the borders where there is human settlement. Similarly, in the Upper Blue Nile basin, in-situ observations of rainfall to study the diurnal cycle are sparse and unevenly located because of inaccessibility, remoteness and economic limitations. As such, in these areas, availability of ground based observations becomes the bottleneck for assessing diurnal variability of rainfall. As a result, so far, there are only few studies undertaken to assess the diurnal variability of rainfall in these areas. The recent advances in the technology of satellite rainfall estimation, however, have made it possible to study diurnal cycle of tropical rainfall in much improved detail at the required space and time-scales. This is also the premise of this study.

The livelihood of the north-eastern African countries is highly dependent on the water resources of the Nile basin. The Nile River has two major contributors of stream flow, the Blue Nile flows from Lake Tana in Ethiopia and the White Nile flows from Lake Victoria in Uganda. According to Yates and Strzepek (1998); UNESCO (2004); and (Conway, 2005), annually the Blue Nile River Basin contributes around 60 % of the flows to the Nile River. Water resources from the Upper Blue Nile basin are used for agriculture, tourism, recreation, domestic water supply and hydropower generation. The people in this basin and downstream of the Blue Nile River are heavily dependent on rainfall. The population in the basin is predominantly agrarian and the success of seasonal crops has large implications, such as the survival of the subsistence farmer and the countrywide economy. As the vast majority of agriculture in the basin is rainfed, rainfall plays a pivotal role. During the past century, shortage of rainfall and its space-time variability in the basin had led to recurrent and substantial shortfalls in agricultural production (Werkineh, 2002). Hence, information on the spatio-temporal distribution of rainfall is crucial in the region for various applications.

Recently, Alemseged et al. (2009b) studied the spatial and temporal patterns of rainfall variability over the Lake Tana basin using data from tipping bucket rain gauges and satellite based information on convective activity. However, despite its great importance, for the Upper Blue Nile basin where there are no sufficient hourly rainfall gauging stations, the diurnal cycle of rainfall and effects of orography have not yet been studied. With the launch of TRMM satellite, however, it has become possible to obtain physically direct estimates of rainfall on different hours of a day which allows the study of rainfall variability at intraday time-scales. Moreover, the satellite rainfall data can also be used to assess spatial rainfall distribution. Therefore, knowledge of the diurnal rainfall variability and spatial distribution of rainfall using satellite observations will help for meteorological, climate and hydrological studies, water resources planning and management and hydropower development in the region. Thus, remote sensing based rainfall variability studies are particularly important for countries like Ethiopia and French Guiana, where large parts have sparse and unevenly located ground based meteorological networks.

1.3. Objectives and research questions

1.3.1. General objective

The general objective of this study is to assess the diurnal cycle of rainfall in French Guiana and the Upper Blue Nile Basin using TRMM observations on seasonal basis.

1.3.2. Specific objectives

The following specific objectives are defined for this study:

- To assess the TRMM PR and TMI number of observations of the areas.
- To estimate the diurnal cycle of rainfall in terms of both rainfall occurrence and mean rain rate.
- To compare PR and TMI rainfall diurnal cycle estimates.
- To validate TRMM rainfall diurnal cycle estimates using ground observations.
- To assess effects of orography on the rainfall distribution.
- To estimate the seasonal rainfall depth from PR and TMI observations.

1.3.3. Research questions

Based on these objectives, the following research questions are formulated:

- What GIS/statistical functionalities can be used to determine the TRMM sampling, rainfall occurrence, and mean rain rate from TRMM overpasses?
- To what extent will the bias associated with the varying number of observations affect the TRMM diurnal cycle estimation?
- Can the spatial pattern in the diurnal cycle of rainfall be related to the topography in the Upper Blue Nile basin?
- Do the observations of non-rainy days influence the information from the diurnal cycle of unconditional mean rain rate?
- Which sensor's diurnal cycle estimation matches best with the ground observations?
- How does the rainfall distribution vary with respect to elevation and mountain orientation in the basin?
- Which TRMM sensor, PR or TMI, gives better estimates of the rainfall over the Upper Blue Nile basin?

In line with the previous studies of diurnal cycle of rainfall from satellite observations and its validation with ground observations, the following assumptions are considered:

- To assess the diurnal cycle of rainfall using TMI and PR rainfall estimates, the assumption is that the seasonal rainfall distribution shows a similar pattern.
- TRMM satellite retrieval errors have little effect on the estimated diurnal cycle of rainfall.
- The moving average point interpolation does not have much effect on the rain rate estimates from PR and TMI.

1.4. Outline of the thesis

Several studies have been conducted to characterize the diurnal variability of rainfall in many tropical regions. However, the availability of in-situ rainfall observations at the required space and time scales is an important limiting factor. This study focuses on the assessment of diurnal variability of rainfall using rainfall data from satellite observations for two sites, namely French Guiana and the Upper Blue Nile basin that are characterized by different climatic settings and located at different altitudinal ranges. This gives the possibility to investigate the application of TRMM rainfall data to study rainfall diurnal cycle at two different areas of the tropics. As discussed in the previous sections, the first chapter addresses the background, significance of the study, objectives and research questions.

Chapter two presents a literature review section and has three major parts. First, rainfall monitoring from space using IR, MW and combined IR-MW techniques is addressed. The second part contains a brief description of the TRMM satellite. Third, a review of previous studies related to the objectives of this study is presented.

General descriptions of French Guiana and the Upper Blue Nile basin and the climate and hydrology of the study areas are presented in chapter three.

Ground observations and satellite rainfall data are used in this study. The materials and methods sections which address the data sources, data processing and methodologies used to achieve the objectives of the study are in chapter four.

The results and discussion sections are presented in chapter five. The chapter discusses the results of TRMM satellite sampling of the study areas and rainfall diurnal cycle in terms of rainfall occurrence and mean rain rate for conditional and unconditional mean rain rates. Moreover, the comparison of PR and TMI, validation of TRMM diurnal cycle estimates and spatial variability of rainfall are addressed.

Finally, in chapter six, the conclusions as drawn from this study are presented. Moreover, some recommendations are given.

2. Literature review

In this chapter a review of literature on rainfall monitoring from space, a brief overview of the TRMM satellite and previous studies on diurnal rainfall variability are addressed.

2.1. Rainfall monitoring from space

Rainfall is recognized as one of the most principal variables of the global water cycle. Knowledge of rainfall and the underlying processes that affect rainfall are required for various research and application disciplines that have direct link to the global energy and water cycle. Some of the applications are: nowcasting, NWP, climate diagnostics and modelling, hydrological applications, flood forecasting, transportation, agro-meteorology, oceanography, and water resource management (ESA, 2004). To date, rainfall data are available from various in-situ and remote sensing observations (e.g. rain gauges, rain radars, MW, VIS or IR sensors) based on various platforms (mainly ground based, air-born or space-born). However, the fact that water cycle dynamics occurs at a wide-range of temporal and spatial scales makes the water cycle dynamics very challenging to observe, understand and predict. New emerging remote sensing technologies not only have their own merits but also have drawbacks with respect to spatial sampling and resolution, spatial coverage, temporal resolution, cost of operation, calibration, accuracy, consistency of retrievals, etc. (Schouppe and Ghazi, 2007).

There is an increasing demand for improved rainfall estimates from satellite systems at various scales in space and time, from global–climate down to local–instantaneous resolutions (Kidd et al., 2003). After the launch of the first meteorological satellites in the 1960's, methods for inferring rather than measuring rainfall rates from space were considered and improved from time to time (Levizzani and Mungnai, 2004). Since then, rainfall algorithms have emerged and provide a satisfactory quality level when rainfall products are averaged over suitable time and space scales. For instance, daily, monthly and yearly rainfall estimates have become increasingly vital inputs for climate studies. However, their quality deteriorates when the algorithms are applied to estimate instantaneous rain rates. New satellite rainfall estimation methods integrate the physical basics of rainfall formation and evolution to improve rainfall estimation.

The primary scope of satellite rainfall monitoring is to provide information on rainfall occurrence, amount and distribution over the globe for meteorological applications at all scales. A longstanding need of meteorological satellites is the improved identification and quantification of rainfall at time scales consistent with the nature and development of cloud systems (Levizzani et al., 2002). Meteorological satellites expand the coverage and time span of conventional ground based rainfall data for a number of applications. Ground based meteorological networks often have incomplete observations that commonly only are available at point scale and fixed intervals (Haile and Rientjes, 2007). Moreover, the uneven distribution of rain gauges and weather radars, and the relative lack of rainfall measurements over the oceans have constrained the use of global and local data.

Timely, accurate and comprehensive information about water resources is the basis for effective water resources management which requires adequate meteorological, hydrological and other related data. In areas where ground measurements are scarce, satellite observations can assist in enhancing the observation capabilities by providing additional data that complement ground observations (Maathuis et al., 2006). In this respect, for rainfall estimation from space, use has been made of orbiting and geostationary satellites using a range of spectral bands. As such, the Meteosat Second Generation (MSG-2) satellite that uses a 12-channel Spinning Enhanced Visible and Infrared Imager (SEVIRI) sensor can play a major role. Geostationary weather satellites with VIS and IR imagers provide a rapid temporal update cycle needed to capture the growth and decay of precipitating clouds to monitor rainfall at high temporal and spatial resolutions. MW sensors on board of the orbiting satellites, such as TRMM and Special Sensor Microwave Imager (SSM/I), acquire low temporal resolution images but with more direct observation on cloud profiles.

It is difficult to look at satellite rainfall estimates from a unified perspective encompassing all possible applications and considering all instrument-related aspects (Levizzani et al., 2002). Various rainfall estimation methods have tried to exploit VIS, IR, near infrared (NIR), water vapour (WV), and MW data. Remote sensing based rainfall estimation techniques are relatively complex and retrieval algorithms often have poor performance. This is because of the difficulties to capture spatio-temporal variability of rainfall formation and limitation of sensors to directly observe variables in the cloud system that govern rainfall formation (Haile and Rientjes, 2007). For rainfall retrieval, use is commonly made of the IR and MW bands of the electromagnetic spectrum. These bands provide complementary information for rainfall estimation that lead to the development of combined IR-MW based methods.

2.1.1. IR-based methods

Remote sensing based rainfall monitoring from IR-imagery of the geostationary satellites has a long history. To study the different cloud stages in detail, the geostationary satellites allow the observations at high temporal and spatial resolutions. Although the potential of these methods for the retrieval of rainfall when averaged over time has been proven, the accuracy of the instantaneous rainfall estimation is limited by the indirect retrieval schemes (Heinemann et al., 2002). In IR-based approaches, most algorithms are based on thresholds with a seasonal or regional dependence and the cloud top temperature is commonly used as a single indicator for inferring rainfall rates. As such, the temperature can only be considered as a proxy variable. The cloud top temperature for rainfall estimation is based on the assumption that relatively cold clouds are associated with high and thick clouds that are assumed to produce high rainfall rates. These approaches were the first to be conceived and are rather simple to apply while at the same time they show a relatively low degree of accuracy. They are mostly used in climatological applications over long time frames (Levizzani and Mungnai, 2004). Rainfall retrieval techniques that use cloud top temperature can be based on cloud indexing, bispectral analysis, cloud life history and cloud models (see Levizzani et al., 2002).

The meteorological community has benefited from the services of the current generation of the European geostationary meteorological satellites (METEOSAT). The advent of MSG is the most significant upgrade of the meteorological observing capabilities in geostationary orbit and offers many opportunities to improve cloud detection and characterization algorithms. The MSG system is

established under cooperation between the European Space Agency (ESA) and the European Organization for the Exploitation of Meteorological Satellites (EUMETSAT). The primary mission of MSG is the continuous observation of the earth's full disk using a 12-channel SEVIRI imaging radiometer. After the launch of MSG, it has continuously returned highly detailed imagery of Europe, the North Atlantic and Africa every 15 minutes, for operational use by meteorologists.

2.1.2. MW-based methods

Clouds are opaque in the VIS and IR spectral range and rainfall is inferred from cloud top structure. At passive MW frequencies precipitation particles are the main source of attenuation of the upwelling radiation. MW based approaches are based on the concept that emitted radiation in the MW frequencies is affected by atmospheric hydrometeors such as cloud and precipitation droplets. Therefore, MW radiometers can detect cloud structure and rain rate. MW techniques are thus physically more direct than those based on VIS/IR radiation. In MW based approaches, the brightness temperature is the proxy variable that has to been seen as an integrated variable over the cloud depth and as such the observations provide information on the entire cloud profile. Technical limitations, though, presently limit the launch of MW sensors to low earth orbiting satellites and hence images from these sensors have poor spatial and temporal resolutions. However, Levizzani et al. (2002) described that recent advancements will lead to the first MW sensor at the geostationary level. Technological developments of MW sensors on board of the orbiting satellites at the end of the 1990's, resulted in the launch of the TRMM satellite, which marked a breakthrough in the observational capabilities of the atmosphere-ocean system. Despite being physically more direct, the swath widths of the satellites in tropical orbit such as the TRMM and of sensors in polar orbits like the SSM/I series leave substantial gaps all over the globe.

2.1.3. Combined IR-MW methods

The higher spatial and temporal resolutions of geostationary satellite rainfall estimates on one hand and better physical insight of MW retrievals on the other hand are directing research efforts towards combined rainfall retrieval techniques. To overcome the shortcomings of rainfall estimation from a single data source, combination of measurements from different satellite sensors is a promising way. Combined IR-MW based approaches benefit from the availability of IR images at high temporal resolutions and from relatively direct information on cloud and rainfall characteristics from MW images. As a result, rainfall blending methods that combine rain rates as retrieved by MW sensors from orbiting satellites and brightness temperatures in the IR from geostationary sensors have recently come out (see Todd et al., 2001; Kidd et al., 2003). The idea is to make use of the superior performances of MW sensors that overpass intermittently a given area and to calibrate the IR temperatures of the geostationary imagery that is available at 15-30 minutes intervals.

From the perspective of combined methods, EUMETSAT realized the Multi-sensor Precipitation Estimator (MPE) in order to combine the advantages of high temporal and spatial resolutions of geostationary satellite sensors with the high accuracy in rain rate retrieval of MW sensors on polar orbiting satellites (Heinemann et al., 2002). The MPE was updated in July 2006 to utilize data from Meteosat-8 to generate the 0 degree product, replacing the previous service provided by the Meteosat-

7 satellite. The algorithm used for MPE is based on the combination of MW data from the SSM/I instrument on the US-Defense Meteorological Satellite Program (DMSP) satellites and images in the Meteosat IR-channel by a so-called blending technique. The end product consists of the rain rate in mm h^{-1} for each Meteosat image used in original pixel resolution. The assumption used is that cold clouds are more likely to produce rainfall than warmer clouds. In this way the method reproduces the average rain rates according to the MW measurements. The validation of MPE based on the comparison with other remote sensing methods in selected areas of Central and Eastern Europe and Central Africa showed that the MPE algorithm performed well (Heinemann and Kerényi, 2003). The method is well suited for the tropical and subtropical convection areas but can be used with its limitations also for higher latitudes.

The direct use of rainfall estimates in weather forecasts requires a high timeliness of data as well as a high temporal and spatial resolution which can only be obtained from geostationary satellites. In Europe, the dense ground-based radar-network assures the needs of the weather prediction community, but in large parts of Africa the situation is quite opposite. As such, almost no ground-based radar stations exist. In these areas the availability of satellite based rainfall data on an operational basis can be used for weather forecasting and is particularly essential for flood forecasting. EUMETSAT is co-operating with a number of African states in the frame of the Preparation for the Use of MSG in Africa (PUMA) project and offers satellite receiving stations and training on the application of satellite data to the National weather services of these countries. Therefore, for countries in Africa, where there are no dense ground-based rain gauge stations and no ground-based radar stations, the use of MSG is expected to have paramount importance for various meteorological applications.

Since IR observations from geostationary satellites such as MSG have a high temporal frequency, rainfall variability can be studied at intraday time-scales, though the IR techniques provide only indirect information about the rainfall. Moreover, as pointed out by Bell and Reid (1993), there is some concern that IR methods may overestimate rainfall and show a maxima in rainfall much later than actually observed at the ground. Hence to understand the tropical rainfall dynamics it requires more accurate rainfall estimations with time-space coverage that only satellites can provide. With the launch of the TRMM satellite, having TMI and PR on board of the satellite, it has become possible to obtain physically direct estimations of rainfall and its vertical structure. This capability has added a new dimension to the study of rainfall variability on intraday time-scales. Moreover, one of the highest priorities of TRMM satellite is to understand the diurnal cycle of tropical rainfall and its variation in space.

2.2. TRMM satellite overview

The launch of the TRMM satellite was motivated by considering the basic importance of rainfall in the Earth's climate system, to overcome the issue of inadequate network of surface rainfall measurements over much of the Earth, and by the vital role of tropical rainfall in global climate dynamics and the global hydrologic cycle. TRMM was launched on November 27, 1997 as a joint space project between the National Aeronautics and Space Administration (NASA) of the United States and the Japan Aerospace Exploration Agency (JAXA) of Japan. The space segment of TRMM is a satellite in a 350 km circular orbit with a 35^0 inclination angle. According to Kummerow et al.

(1998), originally, TRMM was designed for a 3 to 5 years lifetime. Based on TRMM's excellent performance and promise, NASA and JAXA decided in 2001 to extend the mission. Various options were studied for extending the mission lifetime, and the decision was made to boost the operating altitude from 350 km to 402.5 km to reduce drag and conserve fuel (Bilanow and Slojkowski, 2006; Committee on the Future of the Tropical Rainfall Measuring Mission, 2006). The primary TRMM instruments' swath width, ground resolution and orbital period before and after the change of the satellite average operating altitude are given in table 2.1. The time period before August 7, 2001 is referred to as pre-boost and the time period after August 24, 2001 is referred to as post-boost.

Table 2-1 TRMM rainfall measurement sensors' overview (source: http://trmm.gsfc.nasa.gov/)

TRMM Instrument	Pre-boost	Post-boost	Pre-boost	Post-boost	Pre-boost	Post-boost
	Swath width (km)		Ground resolution (km)		Orbital period (minutes)	
PR	215	247	4.3	5		
TMI	760	878	4.4	5.1	91.5	92.5
			(at 85 GHz)	(at 85 GHz)		
VIRS	720	833	2.2	2.4		

Compared to polar orbiting environmental satellites, the orbital characteristics of the TRMM satellite (low altitude (402.5 km), 35-degree inclination and non-sun-synchronous orbit) provide multiple benefits with regard to the space and time of sampling. The low-altitude orbit provides rapid updating and high spatial resolution in the tropical belt (Simpson et al., 1988 ;Committee on the Future of the Tropical Rainfall Measuring Mission, 2006). The inclined nature of the orbit allows the satellite to overpass a given location at different time every day and enables the sampling of the diurnal variation of tropical rainfall (Simpson et al., 1988; Kummerow et al., 2000). In its rainfall measurement package, TRMM has the PR, the TMI, and the Visible and Infrared Radiometer System (VIRS). Due to its complementary suite of active and passive sensors, TRMM satellite has been called a "flying rain gauge" by the Committee on the Future of the Tropical Rainfall Measuring Mission (2006). In addition, the TRMM satellite carries two related Earth Observing System instruments: the Lightning Imaging Sensor (LIS) designed to investigate the global incidence of lightening and the Cloud and the Earth's Radiant Energy System (CERES) especially designed to measure reflected and emitted radiative energy from the earth's surface and the atmosphere.

As described by Simpson et al. (1988); Kummerow et al. (1998); and Kummerow et al. (2000), the main scientific goals of TRMM are to determine the distribution and variability of rainfall and energy (latent heat of condensation) exchange of tropical and subtropical regions to advance knowledge of the global energy and water cycles. This is important for applications of improving short-term climate models, GCM and in understanding the hydrological cycle, particularly as it is highly affected by tropical rainfall and its variability (Simpson et al., 1988). Since 1998, TRMM has provided data for a wide range of applications in the scientific community. These include applications in increasing the basic scientific knowledge (e.g., descriptive and diagnostic studies) as well as operational applications such as monitoring weather features, notably tropical cyclone activity, NWP, climate monitoring and climate model development, and model assimilation of TRMM data in forecast operations (see Committee on the Future of the Tropical Rainfall Measuring Mission, 2006).

2.2.1. Precipitation Radar (PR)

PR is the key TRMM instrument and the first rain radar in space that scans right to left in the cross-track direction. PR is an active instrument that emits radar pulses towards the ground at frequency of 13.8 GHz with horizontal polarization and measures the strength of the return signal (Kummerow et al., 1998; Kummerow et al., 2000). This strength of return signal is related to volume of falling water and the high frequency ensures to get the three dimensional rainfall distributions. Kummerow et al. (1998), summarized the key goals of PR as: providing three dimensional structure of rainfall and rainfall type, obtaining quantitative rainfall measurements over land and ocean and improving the overall TRMM rainfall retreival accuracy by combined use of active PR, passive TMI and VIRS sensor data. PR has a unique feature which allows the measurement of rain over land where passive microwave channels have more difficulty.

PR can provide the vertical profiles of rain and snow up to 20 km above the surface. The minimum sensitivity of PR is around 20 dB before the boost which can detect fairly light rain rates of about 0.5-0.7 mm h^{-1} (Iguchi et al., 2000; Kummerow et al., 1998) with a decrease in sensitivity of about 1.2 dB after the boost (Nesbitt et al., 2004). With its range resolution, PR is also able to separate rain echoes for vertical sample sizes of about 250 m. The estimates of heat released into the atmosphere at different heights based on PR's measurements can be used to improve models of the global atmospheric circulation. The rain-profiling algorithm for PR that provides rain rate and vertical rainfall profiles designated as 2A25 by the TRMM project is described in detail by Iguchi et al. (2000). The algorithm corrects for the rain attenuation in measured radar reflectivity and estimates the instantaneous three-dimensional distribution of rain from the PR data.

2.2.2. TRMM Microwave Imager (TMI)

TMI is a multichannel, dual-polarized (except for 21.3 GHz), conically scanning passive microwave sensor. It measures atmospheric and surface brightness temperatures at 5 frequencies: 10.7, 19.4, 21.3, 37.0, and 85.5 GHz and nine channels. These frequencies are similar to that of SSM/I except the addition of a pair of 10.7 GHz channels to provide a linear response for high rainfall rates and frequency change of the water vapour channel from 22.235 to 21.3 GHz (Kummerow et al., 1998). TMI is designed to provide quantitative estimates of rainfall, water vapour, cloud water content, and sea surface temperature over a wide swath by measuring the minute amounts of microwave energy emitted from Earth and its atmosphere. TMI is referred to as the "workhorse" of TRMM's sensors by the Committee on the Future of the Tropical Rainfall Measuring Mission (2006) because of its wide swath, relatively small size, low power consumption, and good quantitative information.

Measuring rainfall accurately with MW sensors from space is a difficult task and requires some complex equations. Land surfaces are different from oceans and emit about 90 % of the absorbed radiation, so there is very little contrast between the temperature of land surfaces and rain drops. Over the land surface, the TMI rain algorithm makes use of rain information only from the two 85.5 GHz ice-scattering channels. This high frequency channels measure the brightness temperature depression associated with the reduction in received radiation by the satellite due to ice-scattering processes. Using statistically determined empirical relations, the ice scattering signal is matched to a rain rate. The lower frequency channels detect the precipitable water more directly at the lower regions of the

cloud. However, these cloud properties have to be differentiated from upwelling MW emissions from the earth's surface. Commonly, these channels become contaminated because of the highly varying emissions from the surface (i.e. non-homogeneous background) and cannot be used to determine rain rates over the land surface. The TRMM-TMI 2A12 algorithm for rainfall estimation from passive microwave sensors knows as the Goddard profiling Algorithm (GPROF) is described in detail by Kummerow et al (2001).

2.2.3. Visible and Infrared Scanner (VIRS)

VIRS is a five-channel imaging spectrometer which senses radiation emitted from Earth in five spectral regions ranging from visible to infrared (0.6 to 12 µm). It uses a rotating mirror that scans cross-track direction. The VIRS is very similar in many ways to the Advanced Very High Resolution Radiometer (AVHRR). Kummerow et al. (1998) described that VIRS is included in the TRMM sensor package for two reasons: the first is to delineate rainfall (gives a very indirect observation of rainfall and as such it provides very high resolution information on cloud coverage, type and cloud top temperatures) and the second is to provide a link between derived rainfall and similar data from low earth orbiting sensors and continuous coverage by geostationary meteorological satellites.

2.2.4. TRMM PR-2A25 and TMI-2A12 retrieval algorithms

The PR operates at a frequency of 13.8 GHz, which suffers significantly from rain attenuation. Hence, the rain-attenuation correction is one of the major tasks of the PR algorithm. When rain rate is weak, an iteration method is applied to correct for the rain attenuation. When rain is intense and the rain attenuation is high, a surface reference technique is applied. The algorithm also applies a beam-filling correction as the rain may not be horizontally uniform with in the radar beam. Reflectivity-rain-rate (Z-R) relationship is a key issue for rain estimation from PR. The TRMM PR-2A25 algorithm performs the process of inverting the PR's measured reflectivity to attenuation-corrected reflectivity factor (Z_e) and rain rate. The algorithm uses 1C21 (measured radar profiles and rain height information), 2A21 (provides estimate of path attenuation) and 2A23 (provides rain type, measured brightband heights and climatological surface temperature data) which are used to estimate the heights of liquid, mixed-phase, and frozen hydrometeors using the convective–stratiform separation algorithm. The algorithm makes use of these information as well as horizontal reflectivity gradients to correct for non-uniform beam filling to constrain a globally assumed attenuation and reflectivity-rain-rate (Z-R) relationship on a pixel by pixel basis. Factors that add uncertainty to the PR retrievals of rain rate include its global drop size distribution assumptions and Z-R inversion technique. Considering all these variables, the rain rate estimates are calculated from Z_e profiles using a power law. A detailed description of the 2A25 algorithm can be found in Iguchi et al. (2000).

The TMI-2A12 algorithm also called the GPROF is designed to provide rain rate estimates, vertical structure of rainfall and the associated latent heating. Brightness temperature determined using radiative transfer calculations is used to estimate the rain rate given the vertical distribution of hydrometeors. The algorithm uses a Bayesian statistical method to match the observed brightness temperature from a pixel with those from a database of simulated hydrometeor profiles from cloud resolving model profiles coupled with a microwave radiative transfer model (Kummerow et al., 2001;

Nesbitt et al., 2004). Using the results of a cumulus ensemble model, brightness temperatures for each TMI channel are calculated and the most appropriate precipitation structure is determined by a Bayesian technique from the measured brightness temperatures. The physics of the algorithm depends both on emission and scattering-based retrieval techniques. Thus, over ocean, the usefulness of both the emission and scattering channels enables the efficient use of a Bayesian method to select hydrometeor profiles in the database from the full suite of brightness temperatures. Over land surfaces, however, only scattering frequencies are useful for rain rate estimation which yields little information to use a Bayesian profile selection technique in GPROF because of the high and variable MW emissivity of land surfaces. In general, ice-scattering methods have a major limitation in that they are inherently empirical because of the unknown phase, density, size distribution, shape, and orientation of the ice particles in the sample volume as well as the empirical relationship used to relate the ice-scattering optical depth and the rain rate underlying the ice layer. A detailed description of the TMI-2A12 algorithm can be found in Kummerow et al.(2001).

2.3. Previous studies

The diurnal cycle and variability of tropical rainfall largely affects the global rainfall. In the past few decades, a number of researches were devoted to study the diurnal rainfall variability at global and regional scales. For instance, at global scale, Dai (2001) studied the diurnal variability of rainfall using 3-hourly weather data. At regional scale such variability was studied by, Walther (2009) and Bielec-Bakowska (2009) over Europe; Oki and Musiake over Japan and Malaysia; and Kousky (1980) over the tropics using ground based observations. During recent decades and with the advancement in satellite remote sensing, IR and MW data have been used for rainfall diurnal cycle studies. For example, Kishtawal and Krishnamurti (2001), Negri et al. (2002), Dejene (2003), Nesbitt and Zipser, Wu (2004) used TRMM observations for diurnal cycle studies in various regions of the tropics. Using a convective index from MSG-2 and hourly rainfall data from rain gauges, Haile et al. (2009b) studied the spatio-temporal rainfall variability of the Lake Tana basin. Vondou et al. (2009) investigated the diurnal cycle of convective activity using data from Meteosat 7 for a period of five years.

Using 3-hourly weather data from nearly 15,000 stations around the globe (50^0S-70^0N), Dai (2001) studied the diurnal variation in frequency of precipitation occurrence and thunderstorms. The analysis was made on seasonal basis for June-August and December-February. It was reported that over most land areas, strong late afternoon (1500-1900LST) maximum precipitation occurrence and thunderstorms were observed in both summer and winter seasons. Moreover, over most of the land areas the diurnal (first harmonic) dominates while the semidiurnal (second harmonic) is significant over the oceans. Over most of the land areas, the diurnal harmonic explains 60-70 % of the daily variance of rainfall. Over many oceanic areas adjacent to the continents, precipitation is most frequent in the morning (around 0600LST).

From ground based hourly observations Walther et al. (2009) studied the diurnal cycle of rainfall amount and frequency in Sweden on a seasonal basis. A clear diurnal rainfall cycle was observed during summer and the majority of the stations showed a rainfall maximum in the afternoon (1200-1800LST). Exceptions to this were the coastal part of central Sweden with an early-morning maximum (0000-0600 LST) and the east coast of southern Sweden with a morning maximum (0600-1200 LST). However, afternoon maximum were observed during winter along the east-coast and

central south Sweden and morning maximum over most of the other parts of the country. Nonetheless, the amplitude of the diurnal cycle was much weaker compared to that in summer. Bielec-Bakowska and Lupikasza, (2009) studied the daily precipitation variability in Poland from ground observations and the results showed that both the amount and the frequency of precipitation were maximum around midday, especially during the warm seasons of the year.

For northeast Brazil, Kousky (1980), studied the diurnal variation of rainfall by using surface observations from recording rain gauges. It was found that most coastal areas experience nocturnal maximum rainfall occurrence (2100-0900LST). It was argued that this could be attributed to the convergence between the mean onshore flow and the offshore land breeze. However, the inland areas experience day time maximum (1400-1600LST), associated with the development and inland advance of the see breeze. Oki and Musiake (1994) studied the diurnal cycle in Japan and Malaysia using more than 10 years of ground based observations. Based on their results, the diurnal cycle of precipitation in Japan can be classified into three groups. The coastal regions have a rainfall maximum in the morning. In the inland region both morning and afternoon maximum were found during the rainy season related to the southwest Asian monsoon. In the third group, a comparatively strong evening maximum was observed. For Malaysia, the inland region has a pronounced maximum of rainfall at 1600 LST. The morning maximum of rainfall is observed during the southwest monsoon on the west coast and during the northeast monsoon season on the east coast.

Haile et al. (2009b), used hourly rainfall data from recording rain gauges and a convective index based on IR images from MSG-2 SEVIRI sensor to study the spatio-temporal rainfall variability of the Lake Tana basin. It was reported that the rainfall showed a spatially varying diurnal cycle. Over the southern shore of Lake Tana the nocturnal rainfall occurrence was higher than in the mountainous areas further from the Lake in the south direction. Moreover, over Gilgel Abbay, Ribb and Gumera catchments the maximum convection occurred between 1600-1700LST while for Lake Tana and Megech catchments it was between 2200-2300LST. For areas over the west of central Africa, Vondou et al. (2009), studied the diurnal cycle of convective activity using data from Meteosat 7 for a period of five years. It was found that over the land, convective activity exhibits a diurnal cycle characterized by an afternoon maximum convection, while over the sea a weak diurnal cycle with maximum convective activity around noon was observed.

Using observations from TRMM and ground based data, Kishtawal and Krishnamurti (2001), studied the diurnal rainfall variability of Taiwan. Based on their results TRMM observations of July-August showed a bimodal nature of the diurnal rainfall variability. The morning rain rate maximum varied between 0300 and 0600LST and the time of afternoon maximum was around 1600LST. They also used the PR sensor and revealed a diurnal cycle of convective and stratiform rainfall. The convective activity increases during the late afternoon over the entire Taiwan. Moreover, the pattern of TRMM diurnal cycle estimates match reasonably with those from ground observations.

Negri et al. (2002) used three years of observations from PR and TMI to examine the temporal sampling and diurnal cycle of rainfall for selected grid boxes in the Amazon basin and the Atlantic ocean. They concluded that for three years data, the optimum period of accumulation required to eliminate hourly variations (errors) in sampling pattern is 4 hours. In their result, over land, the diurnal cycle of rain rate for a 5^0x5^0 grid box (5^0-10^0S, 65^0-70^0W) in the Amazon basin showed an

afternoon maximum at 1600 LST. For a grid box of the same size (5^0-10^0N, 30^0-35^0W) in the Atlantic ocean, morning rain rate maximum was observed at 0600LST. Using TRMM PR data, Dejene (2003) studied the spatial and diurnal rainfall variability and vertical profile of rainfall systems over selected areas in Africa. His assessment based on one month of data (July) revealed a bimodal pattern in the diurnal cycle of surface rain rate for the Sahel and Ethiopian highland regions. For both regions, in the afternoon the convective activity was maximum between 1800-2100LST while the morning maximum occurred between 0900-1200LST.

Nesbitt and Zipser (2003) combined TRMM satellite observations from the PR and TMI to yield a comprehensive 3-years dataset of rainfall for the tropics (between 36^0 north and south). They found that rainfall over land areas showed a diurnal cycle with a marked minimum in the mid-morning hours and a rainfall maximum in the afternoon which slowly decreases through midnight. However, the oceans revealed a diurnal cycle with an early morning maximum rainfall, with a minimum in the late afternoon. Wu (2004) used five years of PR and TMI data averaged over two hour intervals to study the diurnal cycle of tropical rainfall (between 30^0 north and south). Based on the results, in most oceanic regions the maximum rain rate was observed between 0400-0700LST. Over the islands, the rain rate is maximum between 0700-0800LST. Over continents with heavy total rain, a maximum rain rate was observed between 1400-1500LST, while over continents with lesser total rain the maximum rain rate was observed between 1900-2100LST.

The over-view of similar studies presented above related to the objectives of this study are summarized in table 2.2.

Table 2-2 Summary of previous studies

Author(s)	Study area	Data source	Result
Dai (2001)	Global scale between 50^0S-70^0N	Ground observations	Maximum precipitation occurrence was observed in the afternoon (1500- 1900LST) over most land areas and in the morning (0600LST) over the oceans. Moreover, over most of the land areas the diurnal (first harmonic) dominates while the semidiurnal (second harmonic) is significant over the oceans.
Walther et al. (2009)	Sweden	Ground observations	The majority of the stations showed a maximum rainfall amount and frequency in the afternoon (1200-1800LST) except the costal parts that showed morning (around 0600LST) maximum rainfall.
Lupikasaza (2009)	Poland, Krakow	Ground observations	Maximum amount and frequency of precipitation was observed around midday during the warm season.
Kousky (1980)	Northeast Brazil	Ground observations	Nocturnal maximum rainfall occurrence (2100-0900LST) over most coastal areas while the inland areas experience day time (1400-1600LST) maximum rainfall.

Oki and Musiake (1994)	Japan and Malaysia	Ground observations	Over Japan, the coastal areas showed a rainfall maximum in the morning. In the inland region both morning and afternoon maximum were observed during the rainy season. For Malaysia, maximum rainfall was observed at 1600LST the inland areas while morning maximum of rainfall was observed over the costal areas.
Haile et al. (2009)	Lake Tana basin	Ground observations and a convective index from IR images	The rainfall showed spatially varying diurnal cycle. Over Gilgel Abay, Rib and Gumera sub-basins an afternoon maximum convection was observed. Over Lake Tana and Megech sub-basin night time maximum convection was observed.
Vondou et al. (2009)	West of central Africa	Convective activity from Meteosat-7	Over the land areas, an afternoon maximum convective activity was observed, while over the sea the maximum convective activity was observed around noon.
Kishtawal and Krishnamurti (2001)	Taiwan	TRMM-PR and TMI observations	The diurnal rainfall variability showed bimodal nature with morning (0300-0600LST) and afternoon (around 1600LST) rain rate maximum.
Negri et al. (2002)	Amazon basin (5^0-10^0S, 65^0-70^0W) and Atlantic ocean (5^0-10^0N, 30^0-35^0W)	TRMM-PR and TMI observations	An afternoon (1600LST) and morning (0600LST) rain rate maximum was observed over the Amazon basin and Atlantic ocean respectively. Moreover, over the land TMI rain rate estimates are higher than PR.
Dejene (2003)	Selected areas in Africa	TRMM-PR	A bimodal pattern in the diurnal cycle of surface rain rate was observed for the Sahel and Ethiopian highland regions.
Nesbitt and Zipser (2003)	Over the tropics (between 36^0 north and south)	TRMM-PR and TMI observations	Over the land areas a maximum rainfall was observed in the afternoon while over the oceans the rainfall was maximum during early morning.
Wu (2004)	Over the tropics (between 30^0 north and south)	TRMM-PR and TMI observations	In most oceanic regions the maximum rain rate was observed between 0400-0700LST. Over continents a maximum rain rate was observed between 1400-1500LST, and between 1900-2100LST.

3. Description of the study areas

In this study two areas, French Guiana and Upper Blue Nile basin, are selected for assessing the diurnal variability of rainfall. These areas are found in the tropical region and are characterized by different climatic and topographic conditions. The first is part of the Amazonian forest and receives high amounts of rainfall while the Upper Blue Nile basin is characterized by a more complex topography. As such, considering these areas gives the possibility to assess the diurnal variability of rainfall for areas with different climatic and topographic settings and different latitudinal locations.
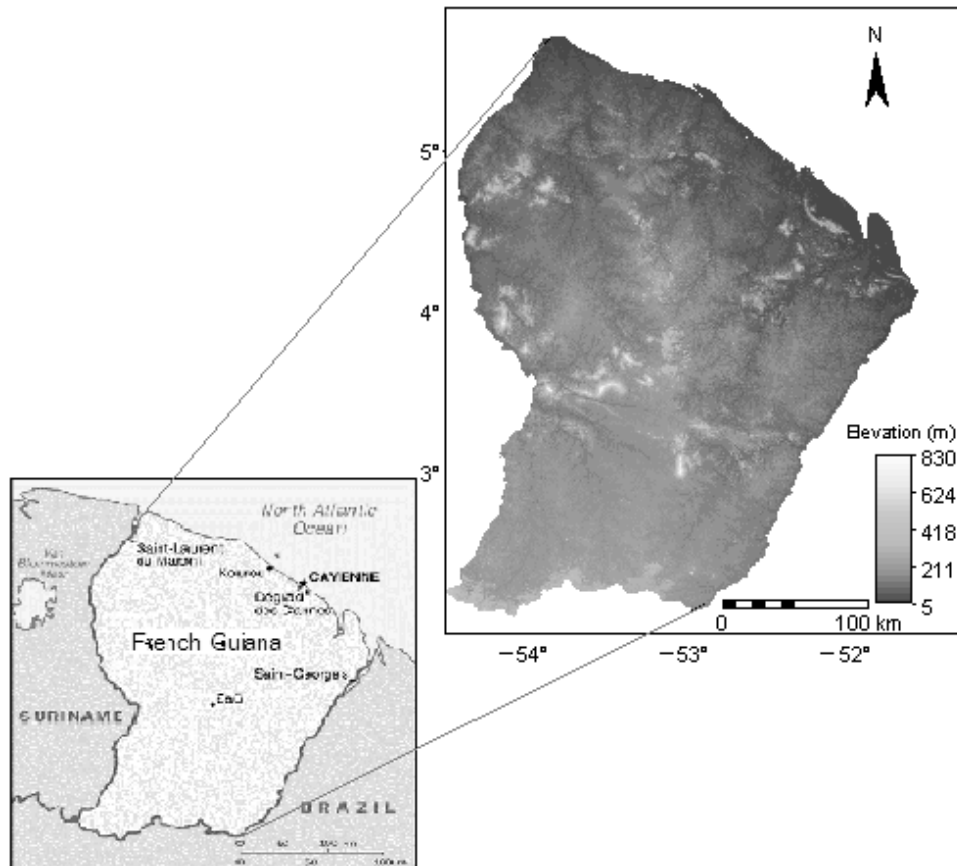
3.1. French Guiana

3.1.1. General

French Guiana is one of the outer most regions of the European Union and has a surface area of 82,845 km². It is located in the North-Eastern part of South America and has frontiers with Surinam in the West and Brazil in the South. The country is bounded by the Maroni River in the West, the Oyapock in the East and the Tumuc Humac mountains in the South. In the north, a narrow costal strip fronts the Atlantic Ocean coast line. It consists of two main geographical regions that are a coastal strip where the majority of the people live and a dense, inaccessible rainforest which gradually rises to the modest peaks of the Tumuc-Humac Mountains along the Brazilian frontier. As shown in the Digital Elevation Model (DEM) as extracted from Shuttle Radar Topography Mission (SRTM), the altitude ranges from 5 to 830 m (see figure 3.1). The SRTM is of 90 m resolution. The latitude ranges from 2°06'42''N to 5°44'11''N and its longitude from 51°37'13''W to 54°33'58''W. The land starts to gently rise in the central regions of the country. Some 90 % of the country is covered by dense tropical forests; that is part of the Amazon rain forest. Apart from a few airfields navigable rivers are the only means of access to the interior. Most economic development is concentrated along the coastal plain. The European satellite launching center (also known as the Guiana Space Centre, or GSC) is located at Kourou.

3.1.2. Climate and hydrology

French Guinea is a land of rivers that many flow north from the southern mountains. Major rivers are the Maroni and Lawa, forming its border with Suriname; the Oyapok, forming a long natural border with Brazil, and the Approuaque, Camopi, Mana and Tompok. French Guiana has a typical wet equatorial warm and humid climate, driven mainly by the seasonal meridional migration of the Intertropical Convergence Zone (ITCZ). In its southern position, the ITCZ causes northeast trade winds from January to July while, for the rest of the year when it is in its northern situation, the country experiences southeast trade winds. There are two periods of high rainfall, April - July (the principal one) and January- February (secondary). The dry season lasts from July to December when stable south-eastern trade winds are dominant. The pattern of flow of the rivers of French Guiana varies with that of the rainfall pattern. Maximum flows are in April-July while minimum flows are

generally in November. The country is characterized by having little change in temperatures during the year with annual average of 27 °C. The average annual rainfall ranges between 2500-3000 mm (after Artigas et al., 2003). There are four main seasons in French Guiana:

- the long dry season, from August to November,
- the short rainy season from December to February,
- the short dry season also known as the 'little March summer' from February to March,
- the long rainy season from April to July.

Figure 3.1 DEM of French Guiana extracted from SRTM (Projection: UTM-zone 22N, Datum: WGS1984, Ellipsoid: WGS84)

3.2. Upper Blue Nile Basin

3.2.1. General

The Upper Blue Nile Basin is the source region of the Blue Nile River and drains a large area of the central and south-western Ethiopian Highlands. It is the largest river basin in Ethiopia in terms of volume of discharge and provides a vital source of freshwater to the downstream users, Sudan and Egypt. The basin is characterized by complex topography consisting of rolling ridges and flat grassland areas with twisting streams that waterfall over vertical sides of the gorge. The grades are steepest in the highland region and become flatter along the lowlands. Much of the highland areas

have elevations above 1500 m and with maximum of around 4200 m in the Choke Mountain. The total drainage area of the basin is about 175,000 km^2 as extracted from 90 m resolution SRTM (see fig 3.2). The area is located between $7^0 44'32''$ to $12^0 45'19''$ north latitude and $34^0 29'20''$ to $39^0 48'17''$ east longitude. The livelihood of the people in the basin is heavily dependent on rainfed agriculture and small scale irrigation schemes.
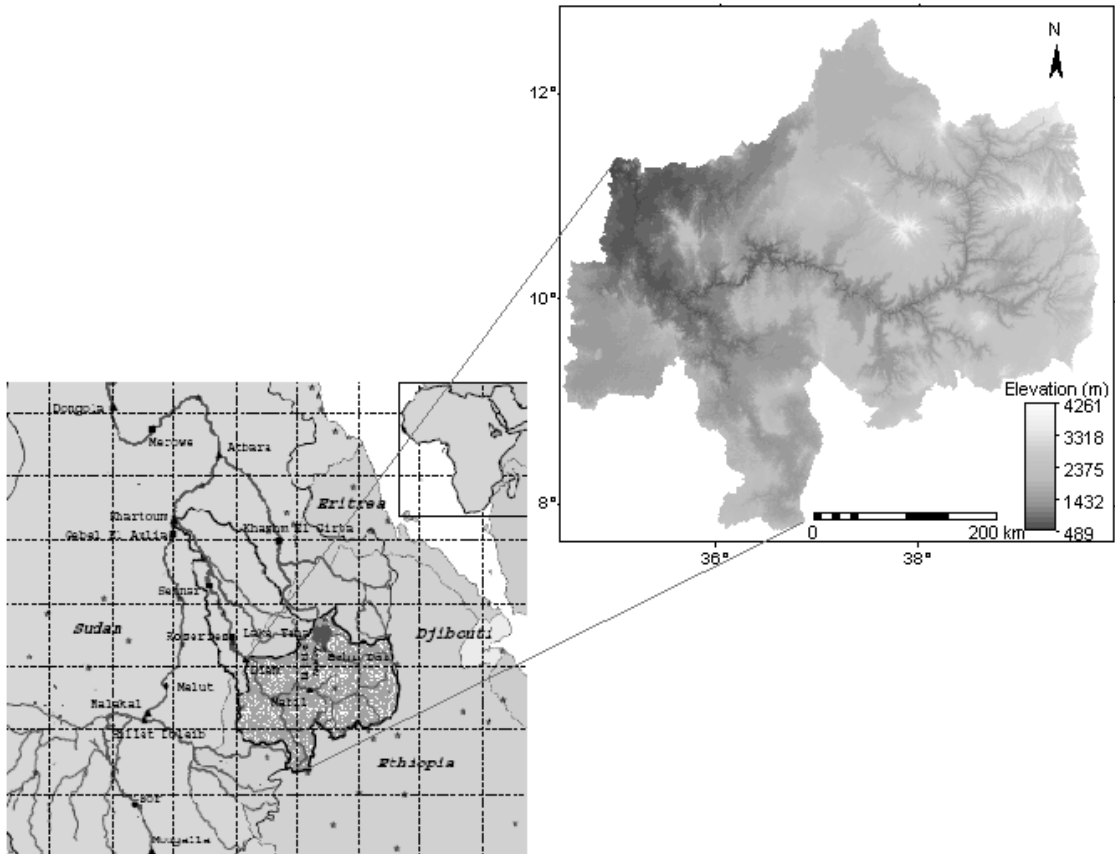
Figure 3.2 DEM of the Upper Blue Nile Basin extracted from SRTM (Projection: UTM-zone 37N, Datum: WGS1984, Ellipsoid: WGS84)

The Blue Nile River runs from its origin, Lake Tana, to the Sudanese border and meets the White Nile River at Khartoum, Sudan. The river has cut a deep and twisty route through the central Ethiopian Highlands and in some places its gorge is around 1 km deep. The river flows about 900 km from Lake Tana until it leaves Ethiopia and crosses into the very large plain areas of Sudan with an elevation difference of 1300 m. More than 85 % of the Nile River flows originate from the Ethiopian highlands and among the tributaries to the main stream of the Nile River, the Blue Nile River is the major tributary contributing about 60 % of the flow. The major tributaries of the Blue Nile River in Ethiopia are Gilgel Abay, Megech, Ribb, Gumera, Beshilo, Wolaka, Jemma, Muger, Guder, Fincha, Didessa, Anger, Dabus and Belles (see figure 3.3). The river basin is composed mainly of volcanic and Pre-Cambrian periodment rocks with small areas of sedimentary rocks. The soils generally consist of latosols on gentle slopes and deep vertisols in flatter areas which are subjected to waterlogging (after Conway, 2000).
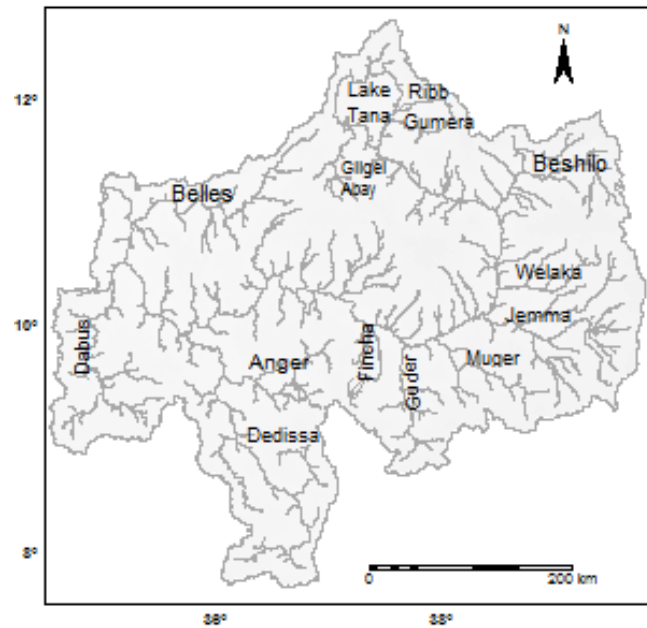
Figure 3.3 Major tributaries of the Upper Blue Nile Basin

3.2.2. Climate and hydrology

The climate of the basin varies from humid to semi-arid. Because of widely varying topography of the basin, elevation strongly influences the climate and human activities (Kim et al., 2008). In this basin the wet season is from June through September with 70 % of the annual rainfall (Conway, 2000). The dry season is from November through April while October and May are transitional months from the wet season to the dry season and from the dry season to the wet season respectively. Based on the Ethiopian classification of climate, that also takes elevation into account, there are three zones: Kolla (below 1800 m) with mean annual temperature of 20-28 ^{0}C, Woyina Dega (between 1800-2400 m) with mean annual temperature of 16-20 ^{0}C and Dega (above 2400 m) with mean annual temperature of 6-16^{0}C. Depending on the method, the period and stations used in prior studies, the estimated annual rainfall ranges from 1200 mm to 1600 mm (Kim and Kaluarachchi, 2008; UNESCO, 2004). The annual rainfall has an increasing trend from northeast to southwest. Based on 32 rainfall stations with varying length of record, Abtew et al. (2008) reported that the mean annual rainfall of the basin is 1423 mm (1960-2002) with standard deviation of 125 mm. There are three mechanisms that influence the rainfall characteristics of Ethiopia (Conway, 2000; Kim et al., 2008). These are the ITCZ that drives the summer monsoon during the wet season, the Saharan anticyclone that generates dry warm north-easterly winds during the dry season, and the Arabian highs that produce thermal lows during the mild season. Conway (2000) reported that there is wide range of seasonal rainfall distribution in the basin. In addition, particularly during the wet season, there is high spatial heterogeneity in rainfall (Kim et al., 2008). The seasonal distribution of runoff in the basin varies significantly due to differences in catchment physiography and seasonality of rainfall. The rivers in the south and south-western parts (e.g. Dabus, Anger and Didessa) have longer flow periods and larger dry season flows. These runoff patterns suggest the spatial variability of rainfall distribution in the basin with longer wet season in the south-west and shorter wet season in the north and northeast.

Camberlin (1997), studied large scale circulation features over the source region of the Nile and during the rainy season a general south-westerly monsoon flow can be noticed. He also described that in the whole of eastern Africa, wind flows are distinctly channelled by topographic features. Topography is the most important factor that regionally modifies the general circulation pattern (Camberlin, 2009). Mountain ranges also set up their own circulation and generate their own climate. In East Africa, large water bodies such as lakes, also tend to develop their own circulation, in the form of lake breezes induced by the diurnal temperature variations of the lakes compared to the surrounding areas. As such, daytime breezes diverge from lakes to the warmer surrounding land, and night-time land breezes converging to the warmer middle part of the lakes (Camberlin, 2009).

4. Materials and methods

4.1. Data source

A number of studies reported on the diurnal cycle of rainfall using data from remote sensing and ground observations (see section 2.3 of this thesis). For this study, PR and TMI rainfall data from the TRMM satellite and ground observations from rain gauges are used to assess the diurnal variability of rainfall. For both PR (2A25) and TMI (2A12) orbital data is used and the processing steps are discussed in section 4.3. Ground observations from rain gauges are used to validate the diurnal cycle estimate from the TRMM observations.
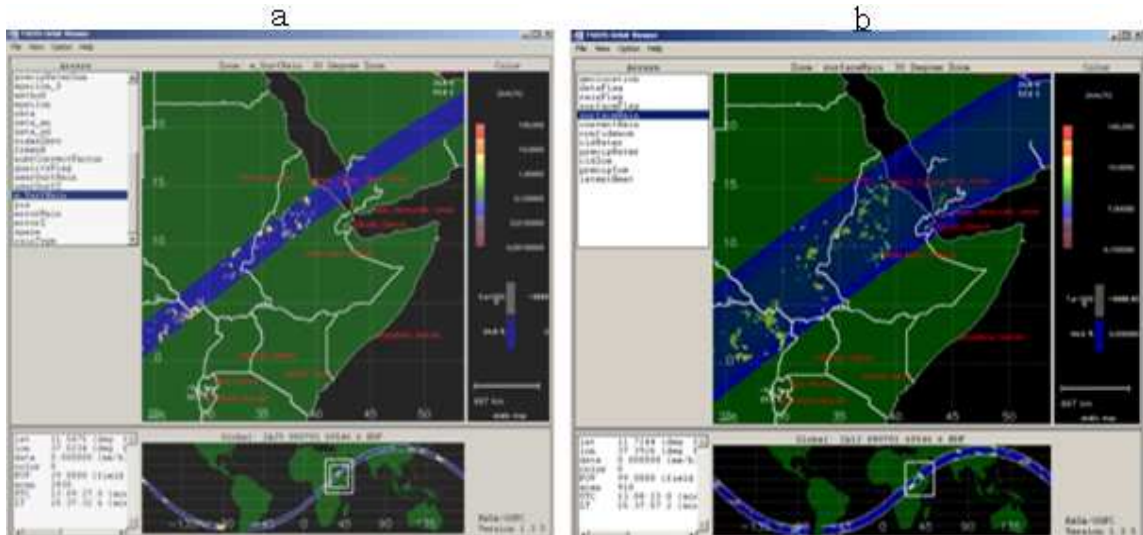
4.1.1. Remote sensing data

Real-time processing and post-processing of the TRMM satellite data are performed by the TRMM Science Data and Information System (TSDIS). This system has a number of rainfall data depending on the combination of instruments and spatial and temporal scales. In this study one year of level-2 TMI data (2A12) for April, May, June and July (AMJJ) for the year 2005 is used for French Guiana and seven years of level-2 TMI (2A12) and PR (2A25) data for June, July, August, September (JJAS) for the years 2002 to 2008 are used for the Upper Blue Nile basin. Around 200 TMI images for French Guiana and more than 1100 PR and 1600 TMI images for the Upper Blue Nile basin of both ascending and descending orbits are processed for this study.

For PR, three rainfall products are available. These are: the average, near surface and estimated surface rain rates. The average rain rate is the average of the observations between two bin heights of 2 and 4 km. The near surface rain rate is the one observed from bins close to the surface which indicates that this rain rate is at some height above the ground surface. The estimated surface rain is the rain rate (mm h^{-1}) at the true (detected) surface bin. Hence, for this study, from PR rainfall products the estimated surface rain is used. From TMI two types of rainfall data are available, the convective surface rain and the surface rain rate data. Here, the surface rain data which is the estimated rain rate (mm h^{-1}) at the surface is used. More information on the description of the products is available at the link: http://pps.gsfc.nasa.gov/tsdis/Documents/ICSVol4.

TRMM data is available free of charge at the link: (http://disc.sci.gsfc.nasa.gov/data/datapool). For French Guiana, the data is downloaded for a grid box of size 2^{0}N to 6^{0}N latitude and 51^{0}W to 55^{0}W longitude while a grid box of size 7^{0}N to 13^{0}N latitude to 34^{0}E to 40^{0}E longitude is used for the Upper Blue Nile Basin. Both PR and TMI rainfall data are available in Hierarchical Data Files (HDF) format. For both PR and TMI, rain rate data (in mm h^{-1}) are selected using the Orbit Viewer. The Orbit Viewer for TRMM data was developed by TSDIS and is used to display the HDF data. The software shows the satellite overpass line over the study area and serves to identify the satellite overpass time for which there is an observation and to export the geolocation and rain rate data to

ASCII table format. Figure 4.1 (a) and (b) show the sample TRMM PR and TMI overpasses respectively over Upper Blue Nile Basin at 1309UTC for July 1, 2008.

Figure 4.1 Orbit Viewer showing the TRMM overpasses over the Upper Blue Nile basin

In addition to satellite rainfall data, remote sensing data from SRTM is used to extract the DEMs of the study areas. DEMs are used to delineate the boundaries and tributaries of the study areas. In addition, the DEM is used to assess the effect of topographical characteristics such as elevation on the spatial distribution of rainfall in the Upper Blue Nile Basin. SRTM provides a freely available data set of global elevations. The processed SRTM 90 m digital elevation model (DEM) for the entire globe was compiled by Consultative Group for International Agriculture Research Consortium for Spatial Information and is made available to the public via internet mapping interface. SRTM data can be downloaded following the link: http://srtm.csi.cgiar.org/SELECTION/inputCoord.asp.

4.1.2. Ground observation

Rainfall estimates from satellites have substantial errors (Wu, 2004) and therefore require validation using ground based rainfall observations. Three-hourly accumulated rainfall data for French Guiana from Saint-Georges, Rochambeau, and Maripasoula stations is collected for the year 2005. The data represents the rainfall depth accumulated for the preceding three hours period. The data for these three stations is collected by order from the National Climatic Data Center (NCDC) following the link: http://www.ncdc.noaa.gov/oa/ncdc.html. The data for the period of AMJJ is used for validation of the diurnal cycle estimates from TMI observation. For the Upper Blue Nile Basin, hourly rain intensity data for the period of JJAS from Mekane-selam, Shawura and Fiche stations for the years 2002 to 2005 is used. The latitudinal and longitudinal locations of the stations and the corresponding elevations are given in table 4.1.

Table 4-1 Latitude and longitude of the stations and corresponding elevations

French Guiana station name	Latitude	Longitude	Elevation (m)
Saint-Georges	$3^0$53' N	$51^0$53' W	7
Rochambeau	$4^0$50' N	$52^0$22' W	9
Maripasoula	$3^0$38' N	$54^0$2' W	106
Upper Blue Nile station name			
Mekane-selam	$10^0$45'N	$38^0$45'E	2600
Shawura	$11^0$56'N	$36^0$52'E	2232
Fiche	$9^0$48'N	$38^0$42'E	2750

The locations of the ground observations for French Guiana and the Upper Blue Nile basin are shown in figure 4.2.
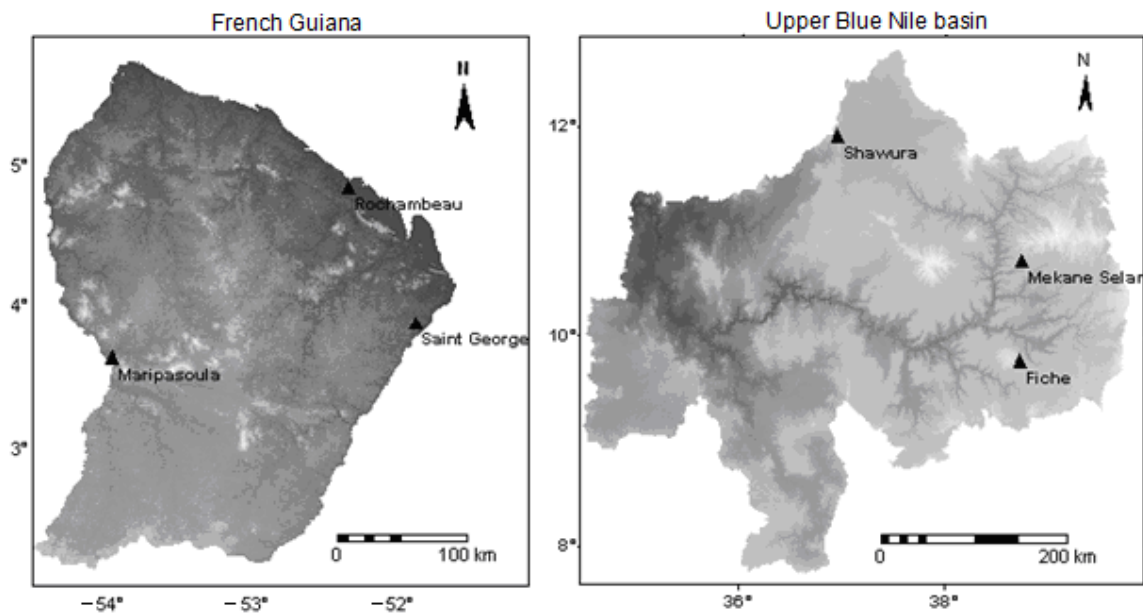
Figure 4.2 The locations of rain gauges in French Guiana and the Upper Blue Nile Basin

4.2. TRMM Data processing and methodology

TRMM level-2 data sets (PR-2A25 and TMI-2A12) for the satellite overpass time are extracted and converted to ASCII table format using the Orbit Viewer. Each data set has two ASCII files that contain the geolocation and the rainfall rate. The resulting data is imported to the Integrated Land and Water Information System (ILWIS) software (www.itc.nl) as table format for further processing. After the geolocation and rain rate files are imported as a table, the next step is joining the rain rate column with the corresponding geolocation data and converting the resulting table into a point map. Since the TRMM satellite is orbiting the earth with an inclination of 35^0 to the equator, the data is available following the orbit path. Therefore, it is necessary to arrange the data in WGS84LatLon coordinate system with Universal Traverse Mercator (UTM) projection system for the study areas with their respective UTM zones. Moreover, even though the products represent pixel values they are

provided as point data representing a pixel size of nearly 5×5 km resolution for PR and 5×12 km for TMI. Therefore, in ILWIS, point interpolation is applied to create raster maps from the point data. The raster maps are then stratified by LST and map lists are created to determine TRMM sampling of the study areas (number of observations), rainfall occurrence and average rain rate using map list statistics in ILWIS. See figure 4.3 for the simplified flow chart of the procedures.
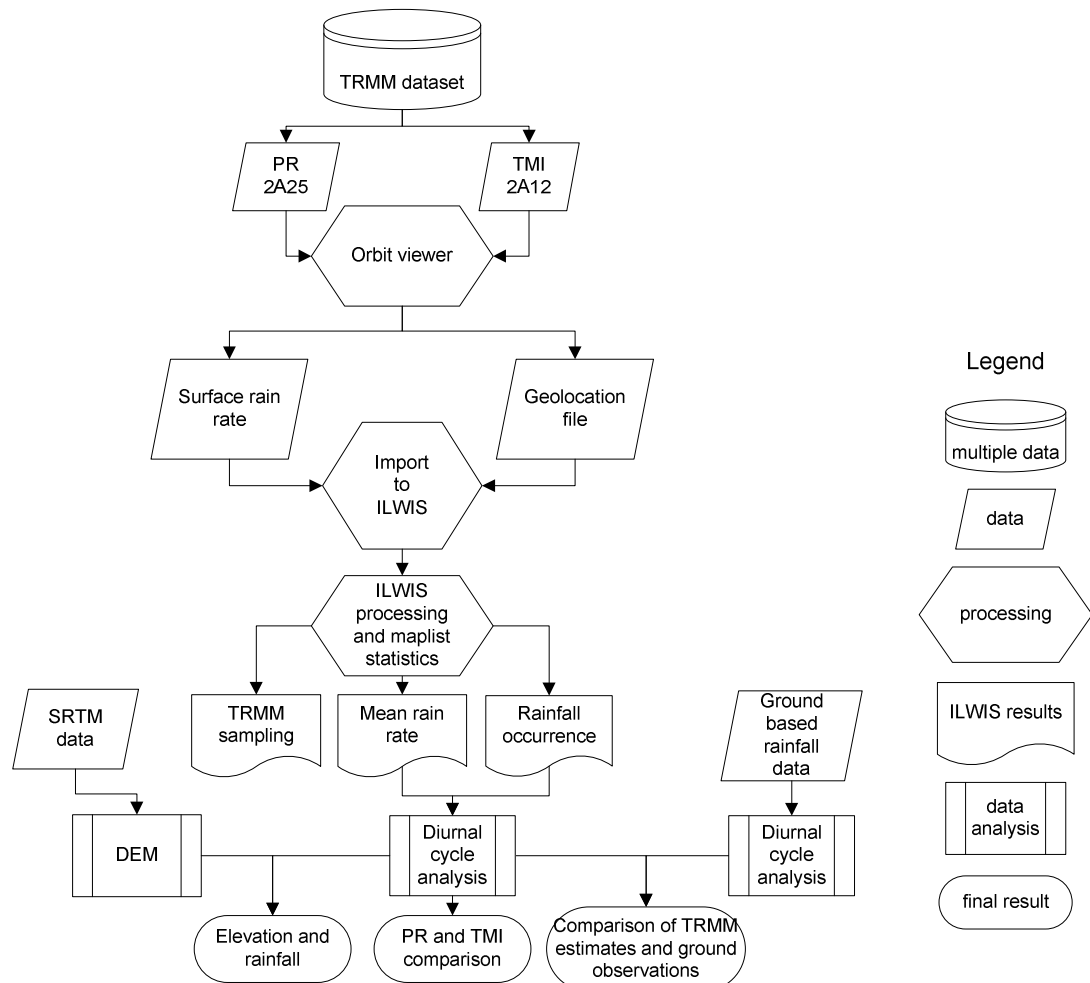
Figure 4.3 Flow chart showing the procedures followed in the methodology

4.2.1. Point interpolation

In ILWIS point interpolation, the input map is a point map with a value domain while the output of a point interpolation is a raster map. To convert the point data to raster maps, moving average point interpolation with inverse distance weighting is used. Moving average assigns to pixels weighted averaged point values. The weight function is the variable that defines the exponential rate of decrease of the influence of neighbouring points. Increasing the weight function will decrease the relative influence of more distant neighbours and it ensures that points close to an output pixel obtain larger weights than points which are farther away. The limiting distance is the maximum search radius to find the points which will be taken into account during the calculation of an output pixel value. See equation 4.1 for the simplest form of inverse distance weighted interpolation. For each output pixel,

not all the points R_i are used to estimate the interpolated value R_0, but only the values of the points which fall within the limiting distance are used.

$$R_0 = \frac{\sum_{i=1}^{n} R_i w_i}{\sum_{i=1}^{n} w_i} \qquad [4.1]$$

$$w_i = \frac{1}{d_i^{\lambda}} \qquad [4.2]$$

where: d_i = the limiting distance, w_i = the weight, λ = the weight function, and n = the number of points with in the limiting distance. For the TRMM-PR and TMI data with a horizontal resolution of 5 km, moving average point interpolation is done using the inverse distance weighting method with power 2. Interpolation is done for a grid element size of 5×5 km. For the moving average interpolation, limiting distances of 7.5 km (8 points) and 18 km (12 points) are specified for PR and TMI respectively to make sure that a rainfall rate is assigned to each 5×5 km pixel.

4.2.2. Statistics for diurnal cycle

Statistics of count, sum, average and standard deviation are applied to analyze the diurnal cycle. These statistics are estimated at 1-hourly and 2-hourly periods to analyze TRMM sampling, frequency of rainfall occurrence and mean rain rate. The TRMM sampling of the study areas is defined by 'count' from the map lists stratified by LST using map list statistics as this gives the TRMM-PR and TMI total number of observations (samples) on pixel basis. After the number of TRMM observations is determined, the uniformity of sampling is assessed. To see the uniformity in the TRMM sampling pattern, the coefficient of variations (Cv), sigma/mean (i.e. standard deviation (σ) divided by the mean (μ)) of the number of observations are calculated on pixel basis. This ratio quantifies the uniformity of each pixel, where lower numbers indicate a more uniform sampling.

$$Cv = \frac{\sigma}{\mu} \qquad [4.3]$$

For rain occurrence and mean rain rate calculations, rainfall is defined using a threshold of 1 mm h^{-1}. This threshold is used based on the fact that TRMM rain rate estimates are more reliable for rain rate of 1 mm h^{-1} and higher (Kummerow et al., 1998; Nesbitt and Zipser, 2003; Haile et al., 2009a). The frequency of rainfall occurrence is commonly used to study rainfall diurnal variability and for this study it is defined as the number of observations with rainfall values greater or equal to 1 mm h^{-1} divided by the total number of observations. To calculate the rainfall occurrence first the raster maps are defined in such a way that the pixels with values greater or equal to 1 mm h^{-1} will have a value of '1', or otherwise '?' is assigned. From these maps 'count' is performed using map list statistics to know the number of observations with a rain rate value greater or equal to 1 mm h^{-1} (N_1). The results are then divided by the corresponding total number of observations or TRMM sampling (TN) for each LST (see eqn. 4.4).

$$Rain\ occurrence\ (\%) = \frac{N_1}{TN} \times 100 \qquad [4.4]$$

The mean rain rate is calculated for unconditional and conditional rainfall. The unconditional mean rain rate is calculated taking the total number of observations including non-rainy observations. However, the conditional mean rain rate excludes non-rainy observations by use of a certain threshold for the calculation of the mean rain rate. This eliminates the effect of non-rainy observations on the mean rain rate. Like the rainfall occurrence, also here, a threshold of 1 mm h^{-1} is used. For calculating the mean rain rate, raster maps are defined so that pixels with values greater or equal to 1 will maintain their original values, or otherwise '0' is assigned. From the resulting raster maps 'sum' is calculated using map list statistics for each LST. To get the unconditional mean rain rate, the 'sum' map at each LST is divided by the corresponding total number of observations TN (see eqn. 4.5)

$$Unconditional\ mean\ rain\ rate\ (mm\ h^{-1}) = \frac{\sum rain\ rate\ images}{TN} \qquad [4.5]$$

For the conditional mean rain rate as conditioned by the rainfall occurrence, a similar approach with that of unconditional rain rate is used except that in the denominator the count map calculated using 1 mm h^{-1} threshold is used instead of count map for total number of observations. This accounts only for the rainy hours (greater or equal to 1 mm h^{-1}) so as to eliminate the effect of the non-rainy hours on the statistics (see eqn. 4.6).

$$Conditional\ mean\ rain\ rate\ (mm\ h^{-1}) = \frac{\sum rain\ rate\ images}{N_1} \qquad [4.6]$$

4.2.3. PR and TMI mean rain rate comparison

Rain rate estimates from TRMM PR (2A25) and TMI (2A12) algorithms show differences due to various factors associated with the sensors characteristics and surface properties. Some of the factors include the differences in the physics of the retrieval approaches (active vs passive MW retrievals and their inherent assumptions), the differences in sensitivity of the sensors, type of surface, type of rain, etc. (Nesbitt et al., 2004). To understand the regional characteristics of the disagreement between PR and TMI rain rates, Ikai and Nakamura (2003) used global ratio maps of PR and TMI rain rates. For the mean rain rate comparison, the assumption is that the difference in swath widths between PR and TMI has little effect on the conditional mean rain rate. In this study, to compare the mean rain rate estimated from PR and TMI for the Upper Blue Nile basin, conditional mean rain rate difference maps are calculated on pixel basis for selected LST. This is done by deducting the PR conditional mean rain rate map from the corresponding TMI conditional mean rain rate map. Then the resulting map is classified and the percentage of the areas where the PR and TMI estimates show similar estimations and differences are calculated to see which sensor overestimates or underestimates the rain rate over the Upper Blue Nile basin.

4.2.4. Comparison of PR and TMI estimates with ground observations

Comparing rainfall observations from satellite and ground based gauging stations is not straightforward. Satellite based microwave sensors like PR and TMI rely on instantaneous measurements of microwave radiances from the cloud system to make an estimate of rainfall rates. On the other hand, satellites provide spatial data with a given pixel size while rain gauges provide point measurements of the amount of accumulated rainfall over the observation time. Moreover, rainfall

shows large variability over space and time. Assuming that the variability of rainfall within the pixel size of the satellite is little, a comparison between the rainfall diurnal cycle from TRMM observations and ground truth is performed. For French Guiana the ground data are available in the form of accumulated rainfall depth on three hourly periods. Hence, the comparison with ground truth is done only for rainfall occurrence. However, for the Upper Blue Nile basin, rain rate data is available from the ground observations. Therefore, the comparison is done for rainfall occurrence and mean rain rate. For this purpose rainfall occurrence and conditional mean rain rate from the TRMM observations are selected for those pixels that overlay with the locations of the rain gauges. Since the threshold applied for the TRMM satellite data is 1 mm h^{-1}, the same threshold is used for ground observations. For the ground observations of the Upper Blue Nile basin the assumption is that the seasonal average of the observations from 2002-2005 is representative for the entire period of the satellite observations (2002-2008). The comparison of the rainfall diurnal cycle estimates from TMI for French Guiana and PR and TMI for the Upper Blue Nile basin with that of the ground observations is assessed in terms of the pattern of the rainfall diurnal cycle. The approach used here is using bar graphs to see the general pattern of the diurnal cycle. Moreover, the correlation between the satellite and ground observations is examined.

4.2.5. Harmonic Analysis

The nature of the diurnal cycle of rainfall occurrence and mean rain rate is examined using harmonic analysis which gives information about the amplitude and phase (timing) of the peak. The procedure used here is the method described by Dai (2001); Haile et al.(2009b) and (Vondou et al., 2009). Accordingly, the diurnal cycle is expressed by the following form of Fourier series expansion:

$$F(t) = m + S_1 + S_2 + ... + S_n \qquad [4.7]$$

Where $F(t)$ = the fitted series, m = the mean value of the diurnal cycle and S_n = the nth harmonic of the diurnal cycle. Commonly, in rainfall studies, we are interested on the first two harmonics that are applied to examine the diurnal and semi diurnal cycles (see Dai, 2001; Haile et al., 2009b; Lim and Suh, 2000). The first and second harmonics of the series are expressed as follows:

$$S_1 = a_1 \cos(\omega t - \phi_1) \qquad [4.8]$$
$$S_2 = a_2 \cos(2\omega t - \phi_2) \qquad [4.9]$$

Where a and ϕ are the amplitude and phase angle of the cosine function, ω equals $2\pi/24$ since the number of hours in a day is 24. The variance explained by each harmonic can be determined from the fraction of variance of each harmonic (σ_i^2) and standard deviation of the observations (σ).

$$Variance\ exp\mathit{lained} = \sigma_i^2 / \sigma^2 \qquad [4.10]$$

Where σ_i^2 can be determined from $a_i / 2$.

The harmonic analysis is applied for the TRMM-PR and TMI estimates that overlay with the ground observations. Moreover, for the Upper Blue Nile basin, the harmonic analysis is applied for areal average TRMM-PR observations for selected sub-basins. Considering the spatial variability of the diurnal cycle of rainfall in the entire basin, Lake Tana, Belles, Beshilo, Dabus, Jemma, Gilgel Abbay

and Muger sub-basins are selected arbitrarily. Moreover, the analysis is also applied to see the spatial variability of rainfall along the Blue Nile river gorge. For this the pixel values at the intersection points between the main river line and the transects are considered (see figure 4.4 for the layout of the transects).

4.2.6. Spatial variability of rainfall

The Upper Blue Nile basin is characterized by complex topography ranging from lowlands with elevation around 500 m up to mountainous areas of more than 4000 m elevation above mean sea level. Rainfall distribution in mountainous areas and plain areas differ by effects of topography and local climatic settings. In mountainous areas, weather systems interact with topography and result in highly non-uniform rainfall (Arora et al., 2006). As such, the Upper Blue Nile basin is suitable to examine the relation between elevation and rainfall. To assess the spatial pattern of the diurnal cycle of rainfall in the basin and the effect of terrain elevation on rainfall distribution, transects are taken that cross the lowland areas, Lake Tana, mountainous areas, and the Blue Nile gorge. Figure 4.4 shows the layout of transects XX' and YY' across the Upper Blue Nile basin. Transect XX' enables us to assess the diurnal variability in the lowland areas of the southwest part, Blue Nile gorge, Choke mountain, and ridges in the northeast. Transect YY' crosses Lake Tana, Choke mountain, and Blue Nile gorge. Moreover, the transects are taken in such a way that they cross the gorge at different locations so as to assess the diurnal cycle of rainfall in the upstream and downstream of the river. The pattern in time and space of the diurnal cycle of rainfall along the two transects is assessed for a 24-hours period. In addition, results are shown graphically for selected LST to see the effect of elevation on rainfall.
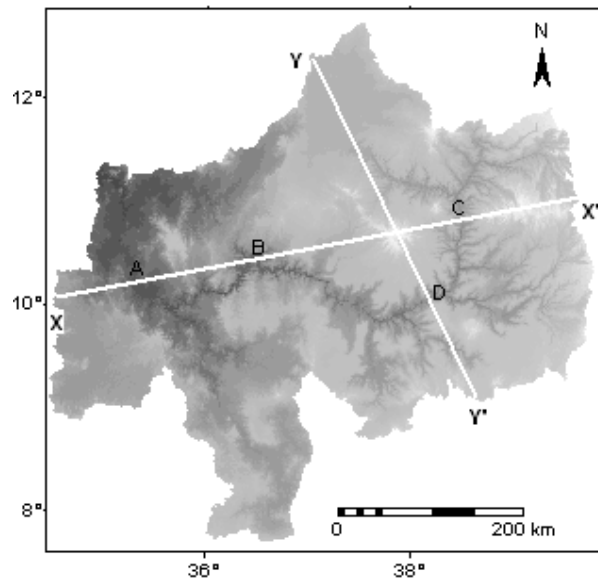
Figure 4.4 Transects XX' and YY' across the Upper Blue Nile Basin

4.2.7. Estimation of rainfall depth

For the Upper Blue Nile basin, from the mean hourly rain rate (RR) and rainfall occurrence (RO) maps of PR and TMI observations the mean of daily accumulated rainfall depth (RD) is estimated for the rainy season (JJAS). The RR and RO maps are on hourly period from seven years of observations.

The RR and RO mean values for one day are calculated from the hourly maps using map list statistics in ILWIS. Assuming that the calculated RR and RO are representative for the entire rainy season, the rainfall depth for the rainy season can be determined using the following relation.

$$RD = 24 \times RR \times RO \times TD \qquad \text{[4.11]}$$

Where: 24 is the number of hours with in a day, and *TD* is the total number of days during the rainy season (120 days).

5. Results and discussion

5.1. TRMM satellite number of observations

The TRMM satellite number of observations from PR and TMI is assessed to examine the total number of samples used to assess the diurnal cycle of rainfall for the study areas. This helps to evaluate the varying number of observations at different times of the day on pixel basis. The total number of observations is used in the calculations of rainfall occurrence and mean rain rate. Hence, the varying number of observations for each LST introduces a bias into the TRMM estimated rainfall and affects the estimated rainfall diurnal cycle.

5.1.1. French Guiana, TMI

The number of TMI observations for French Guiana as aggregated on three-hourly periods for both ascending and descending orbits for the period of AMJJ of the year 2005 is shown in figure 5.1. The number of TMI observations ranges from 15 to 21 with a mean of 18.
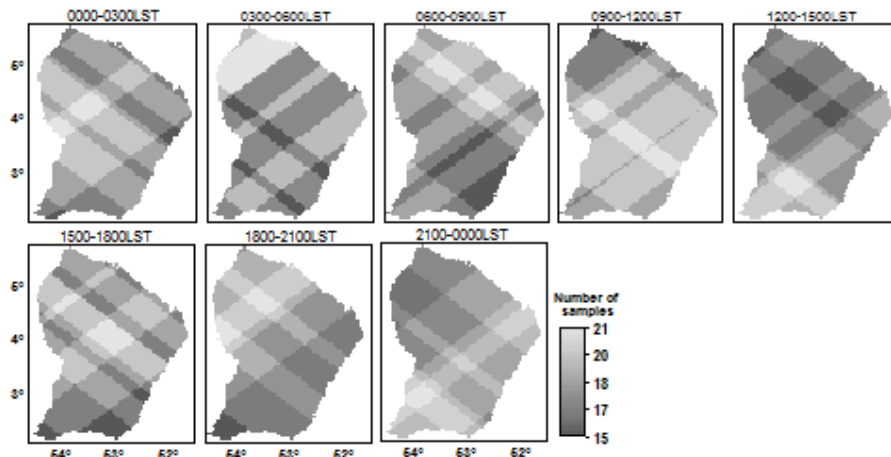
Figure 5.1 Number of TMI observations for French Guiana on 3-hourly periods

To assess the uniformity of the number of observations of each pixel, the coefficient of variation (standard deviation divided by mean) of the number of observations is mapped in figure 5.2. The coefficient of variation ranges from 7 to 15%. As such there is a bias by the varying number of observations at each LST. Hence, the bias in the estimated diurnal cycle as a result of the variation in the number of observations is proportional to the coefficient of variation (Negri et al., 2002). Since the number of observations is aggregated on a three-hourly periods, the map for the coefficient of variation depicts a relatively uniform sampling and hence has low bias associated with the varying number of observations.
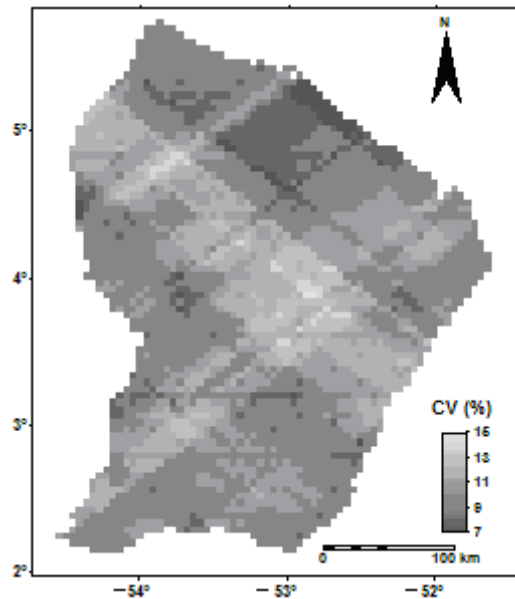
Figure 5.2 Coefficient of variation of the number of observations of TMI data

5.1.2. Upper Blue Nile Basin, PR

Figure 5.3 shows the number of TRMM-PR observations on a 1-hourly period for the period of JJAS from 2002-2008 for the Upper Blue Nile Basin. The number of observations is stratified by LST for both ascending and descending orbits. The number of PR observations ranges from 8 to 20 with a mean of 13. As shown in the number of observation map of TRMM-PR, for most of the LSTs and in most parts of the basin the number of observations is nearly uniform.

The narrow swath width of the PR data leads to only lower number of observations on a daily period (Negri et al., 2002; Nesbitt and Zipser, 2003). This causes biases in the averages due to varying number of observations at different LSTs. Hence, to sample a complete diurnal cycle at a particular location, it is necessary to aggregate the data over time. Therefore, the TRMM-PR number of observations accumulated over a 2-hourly periods is examined. Appendix I shows the number of TRMM-PR overpasses on a 2-hourly periods for both ascending and descending orbits in the period of JJAS from 2002-2008 for the basin. The number of PR samples ranges from 19 to 31 with a mean of 26. As shown in the figure in the appendix, a more uniform sampling is obtained when the data is aggregated on a 2-hourly periods.

To see the effect of accumulating the data at a 1-hourly and 2-hourly periods on the TRMM-PR sampling, the coefficient of variation (Cv) is mapped in figure 5.4 (a) for 1-hourly and (b) for 2-hourly. The Cv shows the uniformity of number of observations of each pixel. The coefficient of variation ranges from 12 to 23 % (figure 5.4a) for 1-hourly period and from 5 to 13 % (figure 5.4b) for 2-hourly periods. Thus, accumulating the data on 2-hourly periods increases the uniformity in sampling nearly by a factor 2. The range of values for coefficient of variation on a 2-hourly periods shows more uniformity in the number of observations as compared to the one examined by Negri et al. (2002) which was 8 to 22 % for PR over a 4-hourly periods using 3 years of data for a land area of size $5^0 \times 5^0$. Moreover, this shows that the bias in the estimated diurnal cycle associated with the

varying number of observations is low for both 1-hourly and 2-hourly periods and hence the PR data are suited to show the rainfall diurnal cycle.
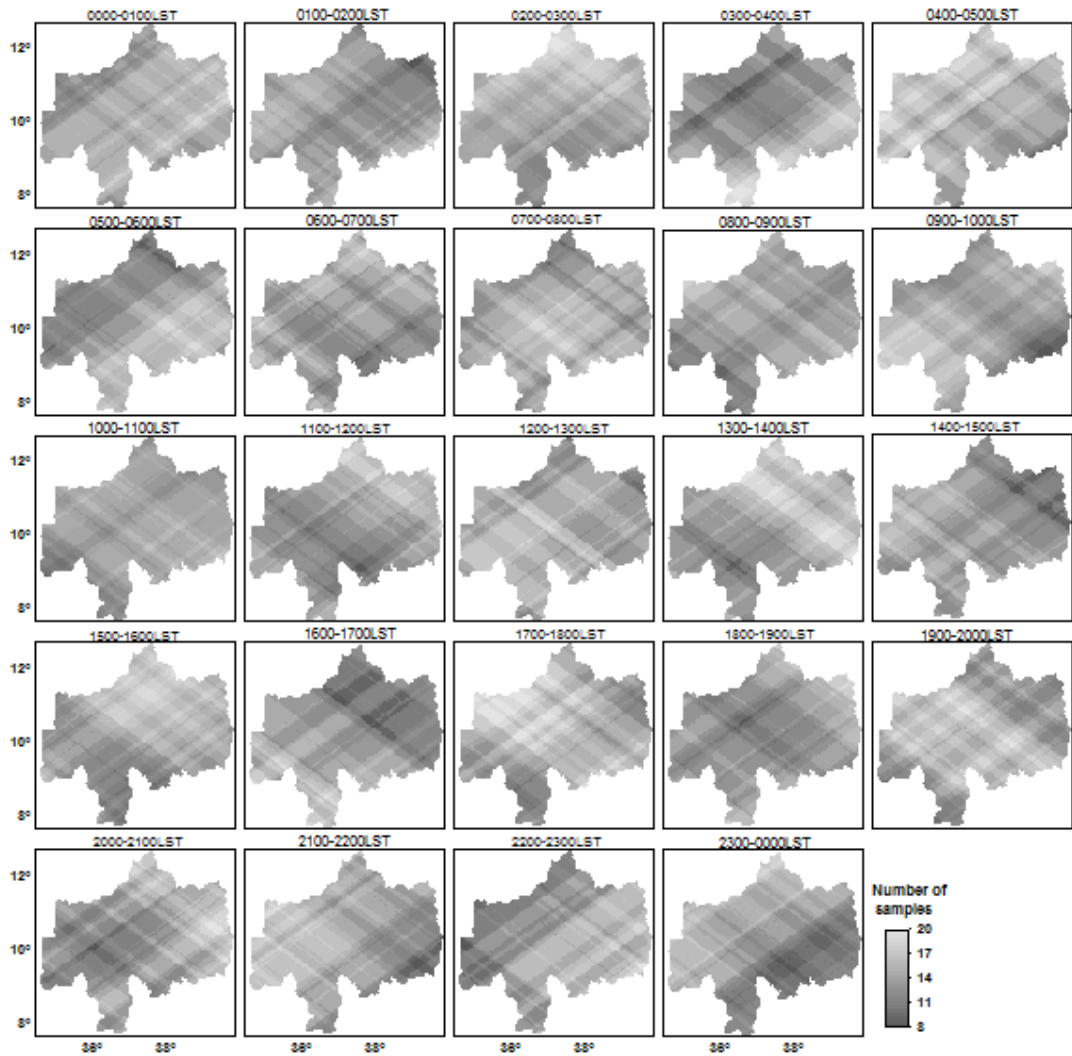

Figure 5.3 Number of PR observations for the Upper Blue Nile Basin on 1-hourly period
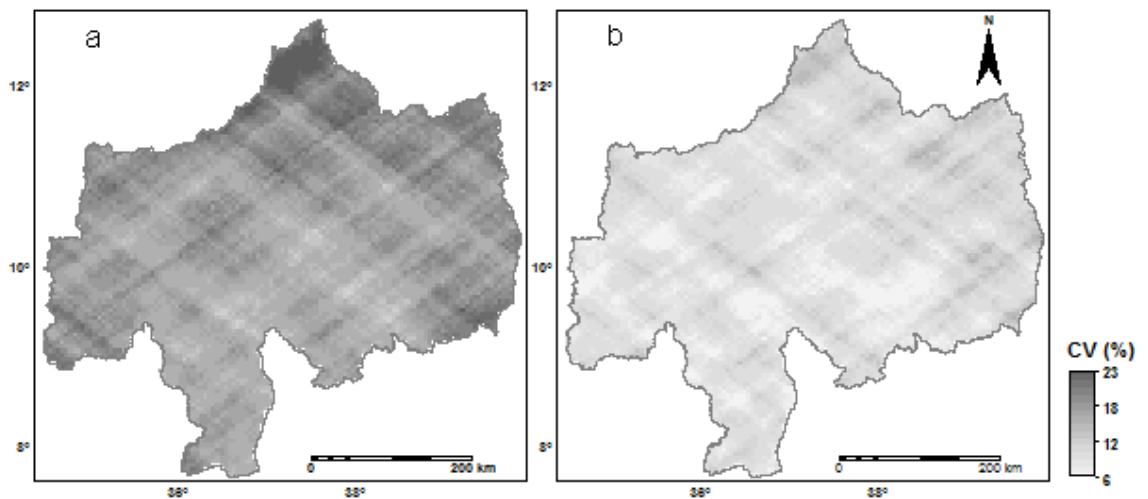
Figure 5.4 Coefficient of variation of the number of observations of PR data

5.1.3. Upper Blue Nile Basin, TMI

The number of TMI observations for the Upper Blue Nile Basin for the period of JJAS from 2002-2008 on a 1-hourly period is shown on figure 5.5. The number of observations is stratified by LST for both ascending and descending orbits. The pattern in the number of observations is similar with that of the PR, but with greater number of observations because of the wider TMI swath width (878 km) as compared to the PR (247 km). The number of TMI samples ranges from 37 to 50 with a mean of 43.
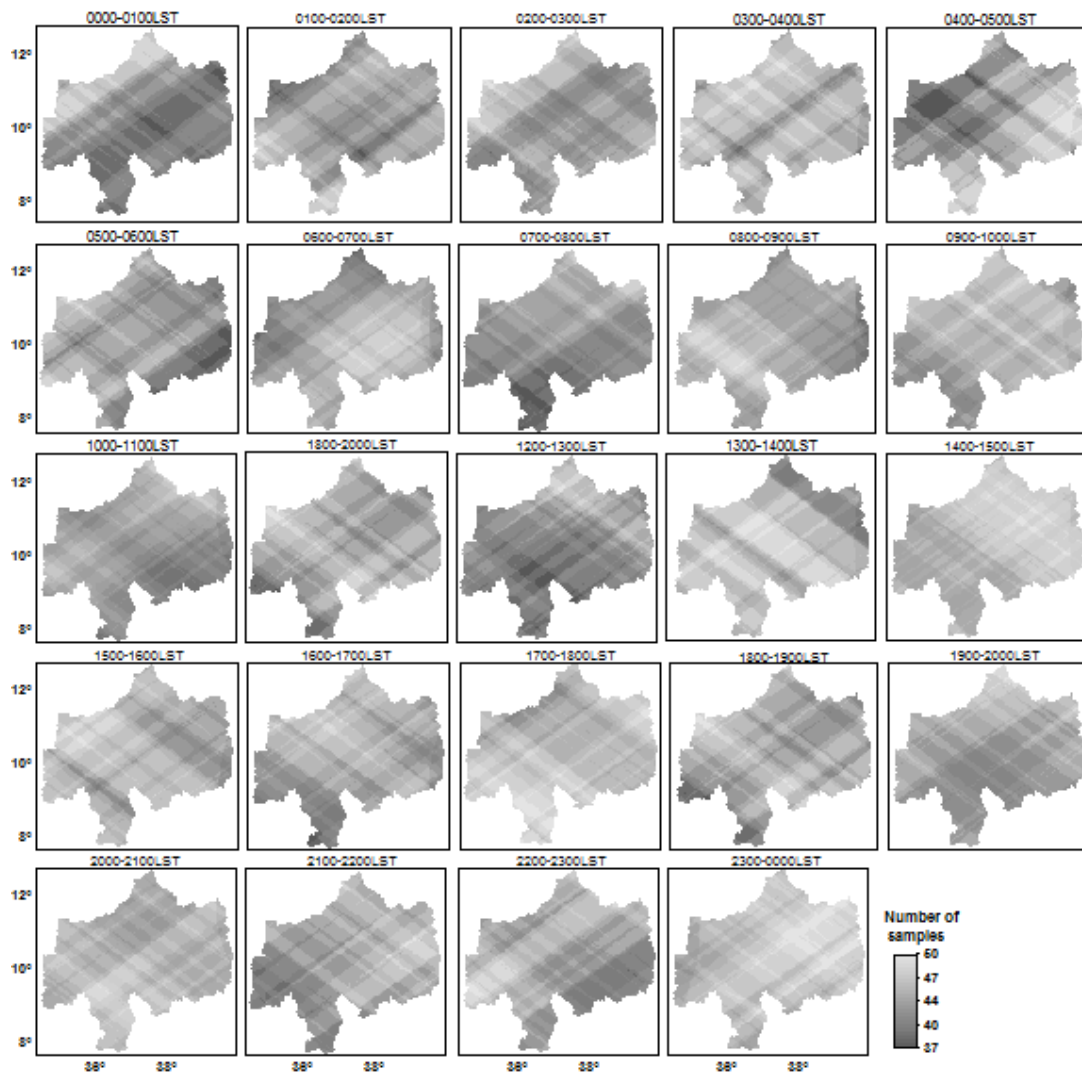
Figure 5.5 Number of TMI observations for Upper Blue Nile Basin on 1-hourly period

The coefficient of variation of the number of TMI observations is calculated and mapped in figure 5.6 to see the uniformity of number of observations. The value ranges from 5 to 9 %. This shows the effect of the wider swath width where a more uniform sampling is obtained from TMI as compared to PR. Therefore, the rainfall estimates from TMI are less biased by the higher observation frequency as compared to that of the PR estimates. As such, by the number of observations, the TMI estimates are assumed to be more reliable than estimates by PR.
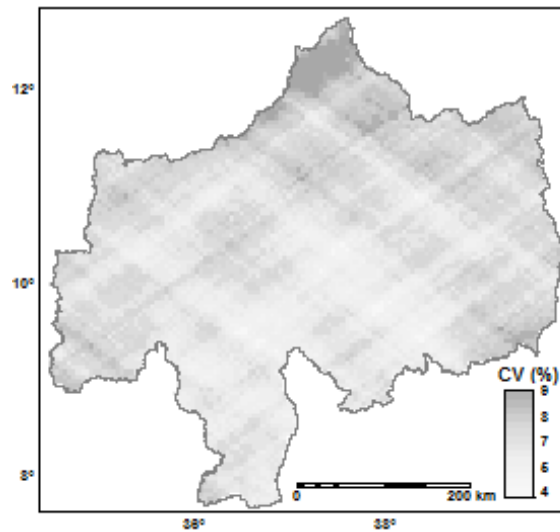
Figure 5.6 Coefficient of variation of the number of observations of TMI data

5.2. Rainfall diurnal cycle

The rainfall diurnal cycle is assessed for both French Guiana and Upper Blue Nile basin in terms of rainfall occurrence and mean rain rate.

5.2.1. French Guiana, TMI

The diurnal distribution of rainfall occurrence analysed on a 3-hourly periods is shown in figure 5.7. The maximum rainfall occurrence varied between 24 % and 50 %. Between mid-night and mid-day (0000-1200LST), minimum rainfall occurrence is observed over most parts of French Guiana. The rainfall occurrence starts to increase from 1200-1500LST in the central part of the country and attains its maximum value over most parts of the country during mid to late afternoon (1500-1800LST). Between 1800-2100LST, the rainfall occurrence is maximum over the south-western parts and decreases afterwards, from 2100-0000LST.
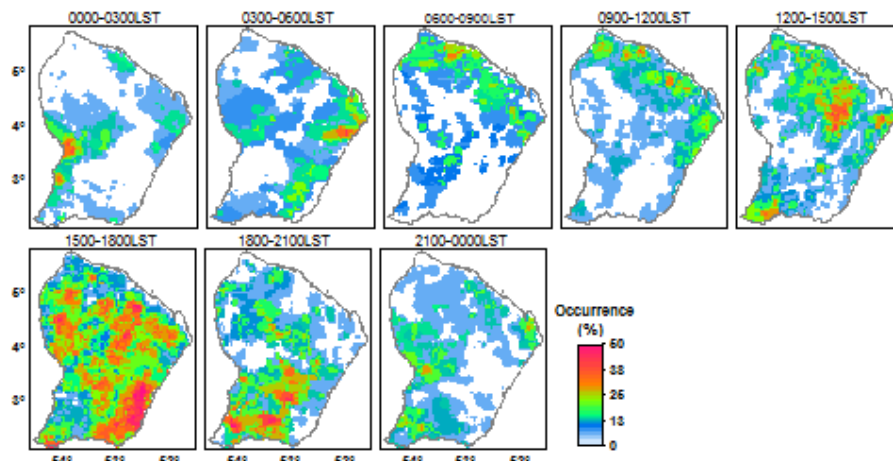
Figure 5.7 Diurnal cycle of rainfall occurrence using TMI data on 3-hourly periods

The diurnal cycle of conditional mean rain rate averaged over a three hourly periods is also assessed and is shown in figure 5.8. The results show a similar patter with that of the rainfall occurrence. The maximum rain rate varies between 10 mm h^{-1} and 20 mm h^{-1}. The rain rate is low over most parts of the country between 0000-1200LST and starts to increase in the afternoon. Over most parts of the country, the maximum rain rate is observed in the afternoon between 1500-1800LST and starts to decrease from 1800-0000LST. Over the northern parts of South America and the Amazon, Sorooshian et al. (2002), found similar results with maximum convection from 1600-1800LST that was linked to afternoon heating and leading to maximum rainfall.
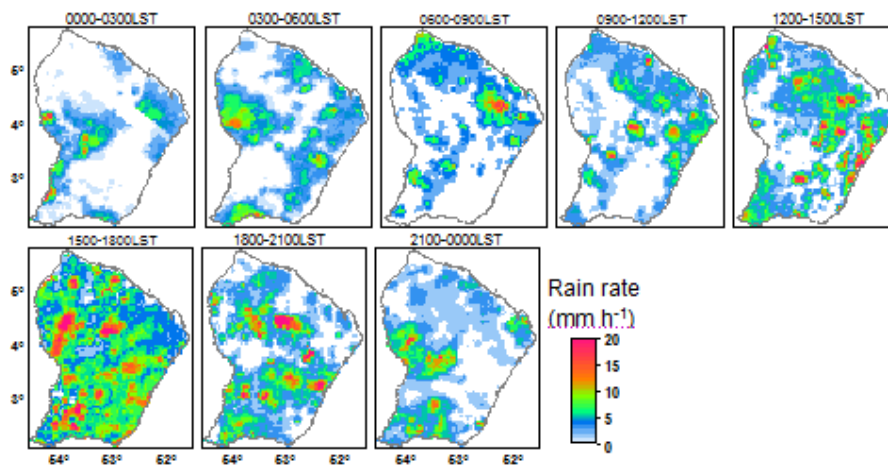
Figure 5.8 Diurnal cycle of conditional mean rain rate using TMI data on 3-hourly periods

5.2.2. Upper Blue Nile Basin, PR

Figure 5.9 shows the diurnal distribution of hourly rainfall occurrence over the entire Upper Blue Nile basin for JJAS. The maximum rainfall occurrence varies between 36 % and 50 %. From mid-night till afternoon (0000-1500LST), the rainfall occurrence is minimum over most parts of the basin. However, the northern parts of Didessa, Dabus, Jemma and Muger subbasins show a maximum rainfall occurrence between midnight and early morning. The diurnal distribution shows highest rainfall occurrence of 50 % in the mid to late afternoon (1500-1800LST) over land except for areas following the Blue Nile River gorge (shown by the thin dark gray line). It is observed that the areas along the Blue Nile River gorge show different patterns and the rain occurrence in these areas is maximum during the night time between 2000-2300LST. Over Lake Tana and around Fincha reservoir, maximum rainfall occurrence is observed during mid-night periods between 2200-0000LST. Moreover, the southern shore of the lake is characterized by higher rainfall occurrence than the other sides of the lake. Similar results over the southern shore of Lake Tana were found by Haile et al. (2009b) using rainfall data from rain gauges and a convective index from MSG-2 IR images. Moreover, they also found mid to late afternoon maximum rainfall occurrence and convective activity around the ridges of Gilgel Abbay sub-basin. This is in agreement with the results of this study in which late afternoon (1600-1800LST) maximum rainfall occurrence is observed around the ridges of Gilgel Abbay.
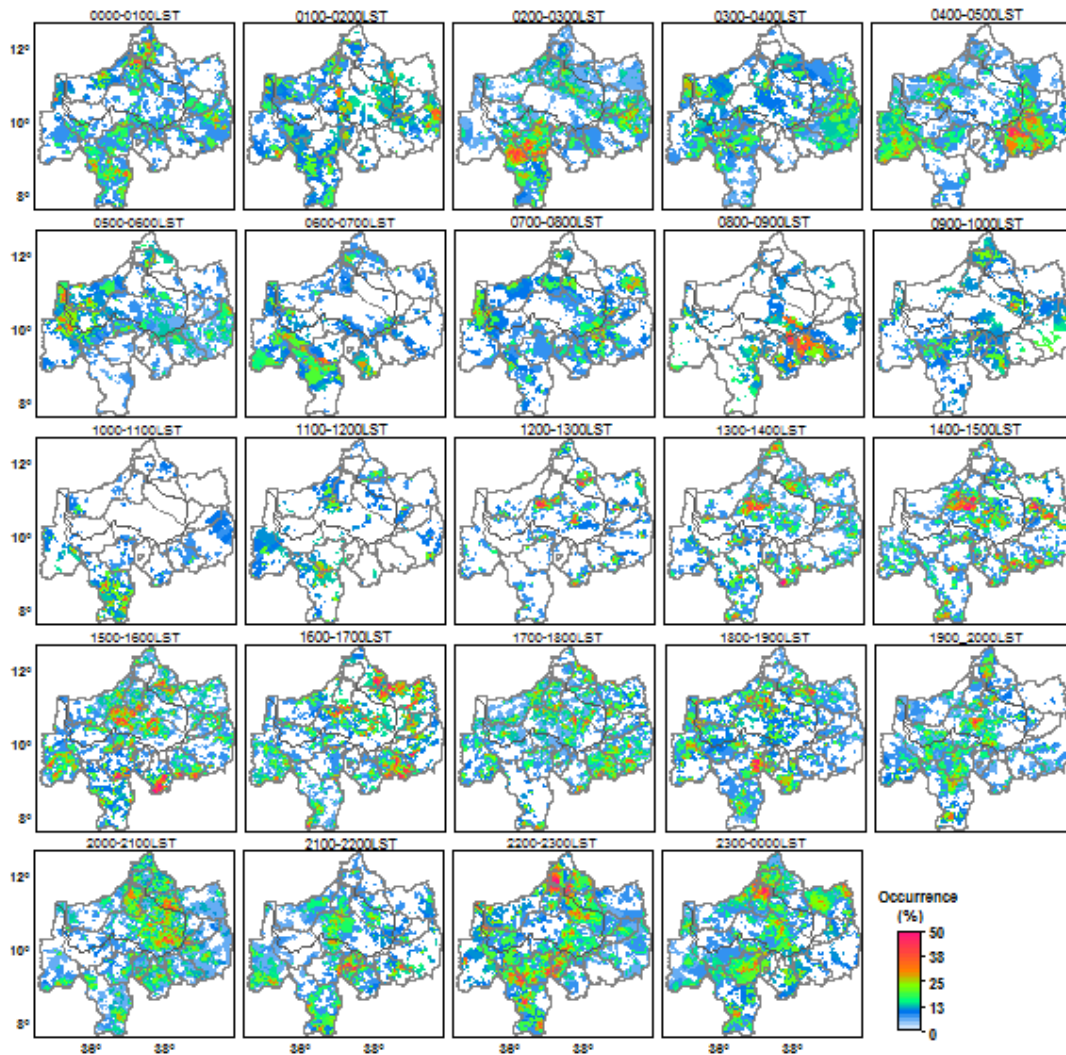
Figure 5.9 Diurnal cycle of rainfall occurrence using PR data on 1-houry period

To minimize the effect of varying number of observations on the analysis of the diurnal cycle of rainfall occurrence, the analysis is repeated for the PR observations accumulated on 2-hourly periods. The result is shown in Appendix II and it depicts almost a similar pattern of the rainfall diurnal cycle with that of the hourly distribution. The maximum rainfall occurrence varies between 30 and 46 %.

The results of the diurnal distribution of conditional mean rain rate on 1-hourly period (see figure 5.10) are closely related to those of the rainfall occurrence. Over most areas of the basin, the mean rain rate is low between 0000-1500LST. However, like the rainfall occurrence, exceptions to this are the Didessa, Dabus, Jemma and Muger sub-basins which are characterized by maximum conditional mean rain rate observed between midnight to early morning. Most areas of the basin show a mid to late afternoon maximum conditional mean rain rate between 1500-1800LST. Over Lake Tana, night time maximum mean rain rate is observed. For the areas along the Blue Nile River a night time maximum rain rate is observed between 2000-2300LST. Barros et al. (2004), found similar results over the valley in the Aravalli range with maximum rain rate observed during midnight and they associated the midnight maximum rain rate in the valley with the effect of complex topography.
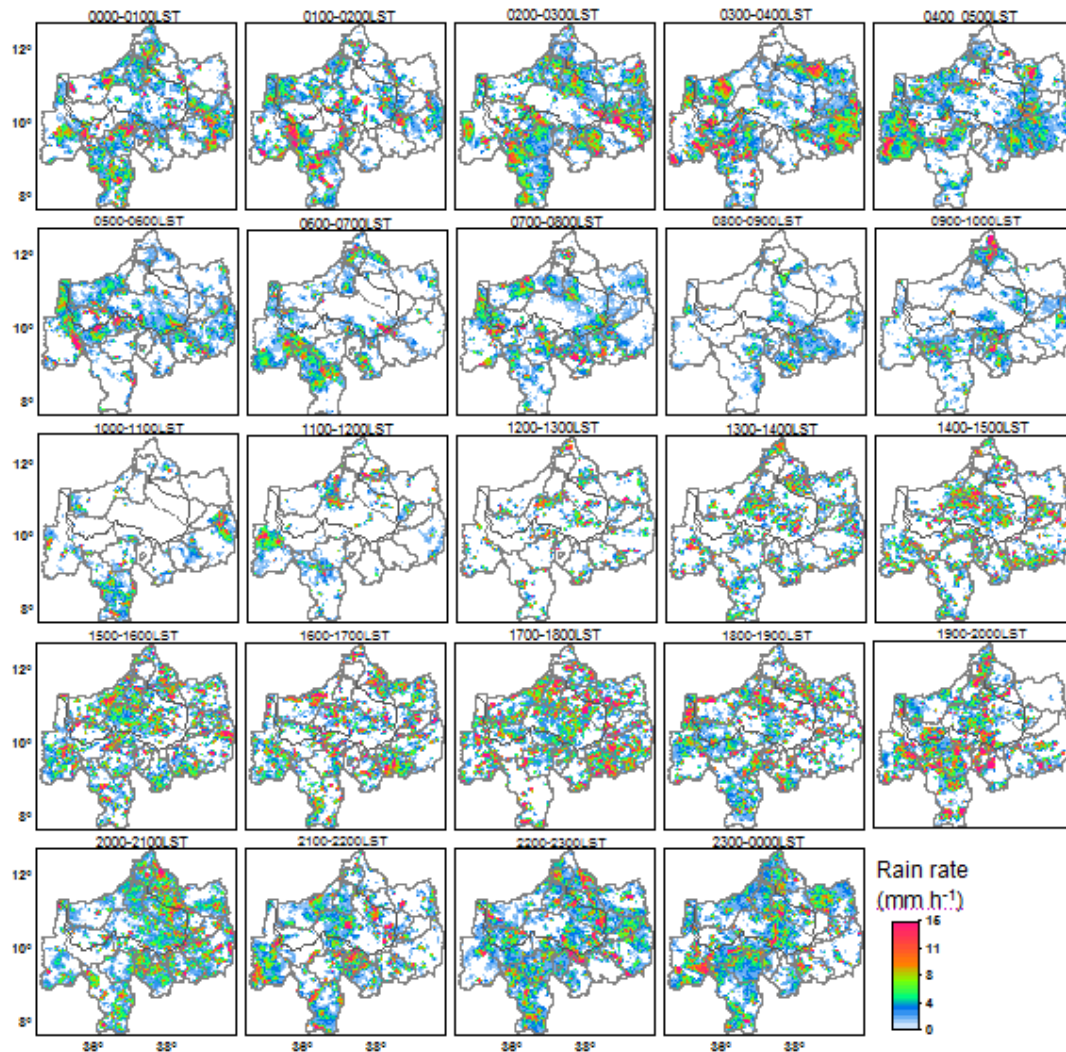
Figure 5.10 Diurnal cycle of conditional mean rain rate using PR data on 1-hourly period

In the same way as the rainfall occurrence, to minimize the effect of varying number of observations at different LSTs, the diurnal cycle of conditional mean rain rate is also assessed for PR observations aggregated on 2-hourly periods. The result is shown in appendix II and the diurnal cycle of conditional mean rain rate aggregated on 2-hourly periods depicts a similar pattern with that of the PR observations on 1-hourly period.

To see the effect of non-rainy days on the mean rain rate, the diurnal cycle of rainfall is also assessed for unconditional mean rain rate. The diurnal cycle of unconditional mean rain rate is shown in figure 5.11. This value is less by a factor of 3 from the conditional mean rain rate and this is due to the inclusion of non-rainy observations in the calculation of the unconditional mean rain rate which lowers the value of mean rain rate. The pattern of diurnal cycle of unconditional mean rain rate over the basin is similar to that of the conditional mean rain rate. However, because of the averaging effects of the non-rainy observations the information is not as clear as the conditional mean rain rate diurnal cycle. The patterns observed from the rainfall occurrence diurnal cycle are also evident in both the unconditional and conditional rain rate diurnal cycle.
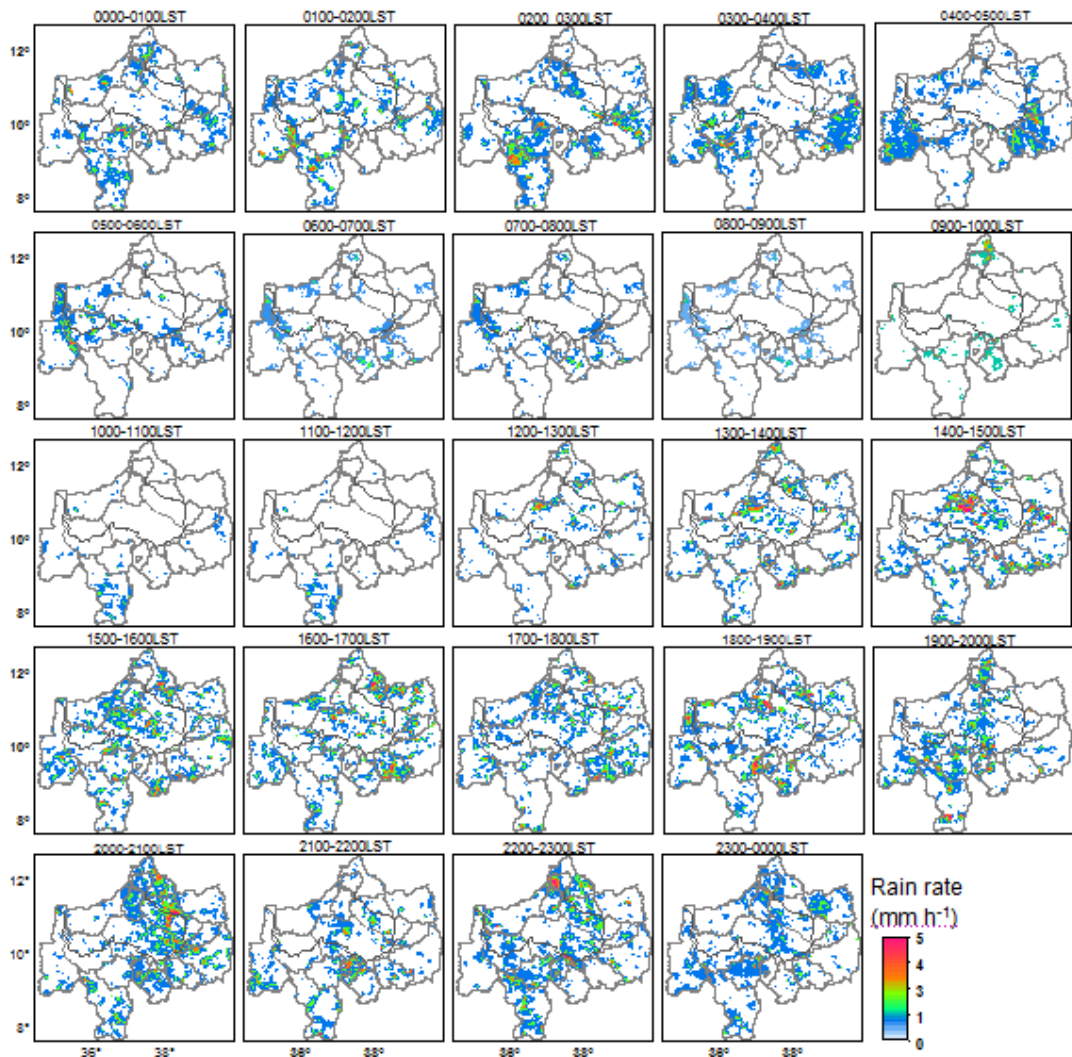
Figure 5.11 Diurnal cycle of unconditional mean rain rate using PR data on 1-hourly period

5.2.3.   Upper Blue Nile Basin, TMI

The diurnal cycle of rainfall distribution in terms of rainfall occurrence and conditional mean rain rate for the Upper Blue Nile Basin is assessed using TMI data. Figure 5.12 shows the diurnal cycle of rainfall occurrence on 1-hourly period. The results show a similar diurnal cycle distribution with that of the analysis using PR data. However, the maximum rainfall occurrence varies between 32 % and 60 %. From the diurnal cycle of rainfall occurrence it is evident that from 0000-1500LST the rainfall occurrence is minimum over most parts of the basin. However, in the south-western parts of the basin (Dabus and Didessa sub-basins) night time to early morning (0100-0600LST) maximum rainfall occurrence is observed. Over most parts of the basin the rainfall occurrence is maximum during mid to late afternoon between 1500-1800LST. In the areas along the Blue Nile gorge, Lake Tana and Fincha reservoir, night time maximum rainfall occurrence is observed from 2200-0000LST. Over Lake Tana, the rainfall occurrence in the southern shore of the lake is higher than the other sides and this suggests the spatial variability of rainfall over the lake.
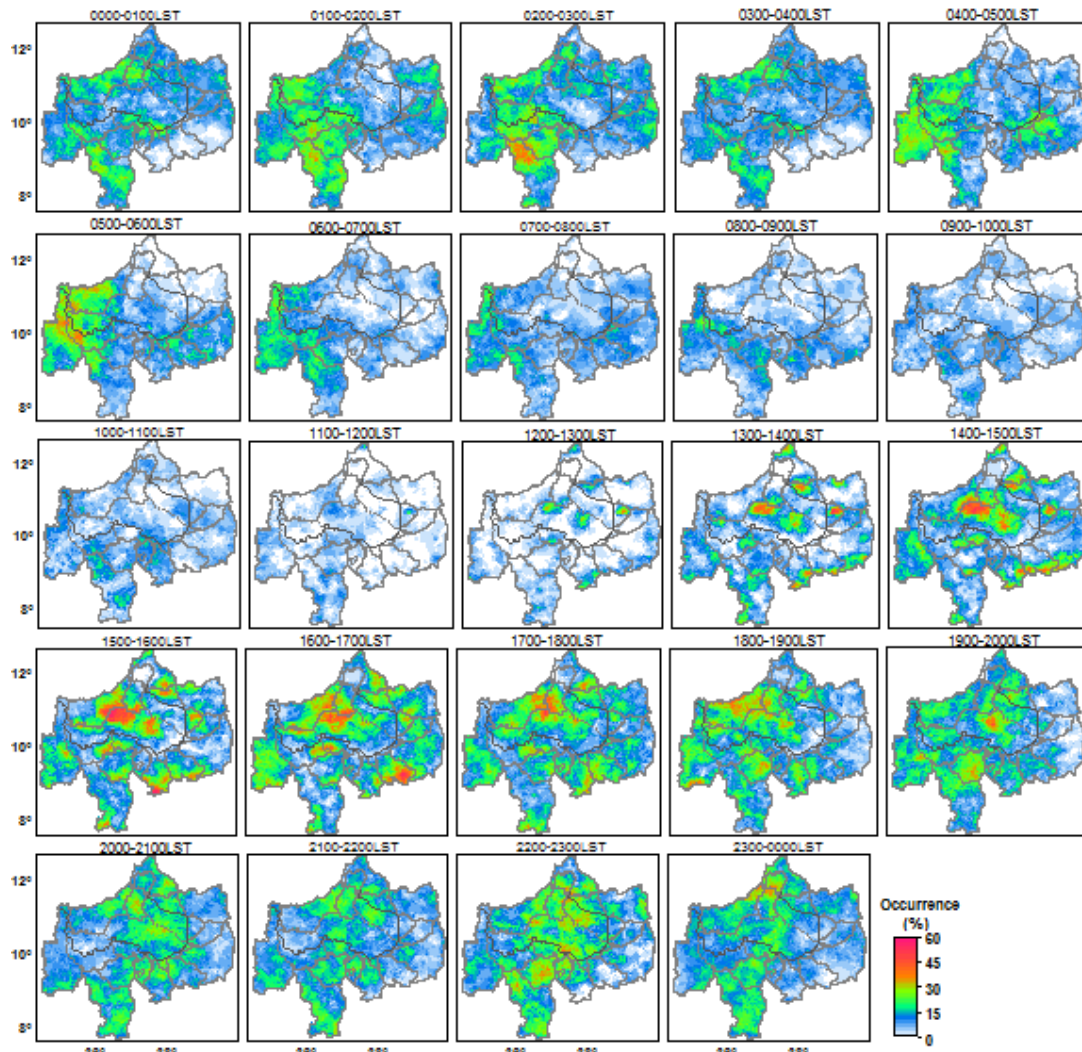
Figure 5.12 Diurnal cycle of rainfall occurrence using TMI data on 1-hourly period

The information from the diurnal cycle of unconditional mean rain rate from PR observations is influenced by the averaging effect of the non-rainy observations. As such, the magnitude of the unconditional mean rain rate is lower than the conditional mean rain rate. Therefore, the assessment of the diurnal cycle of the unconditional mean rain rate is not repeated for TMI observations. The diurnal cycle of conditional mean rain rate on 1-hourly period is assessed and the results are shown in figure 5.13. The result shows a similar pattern with that of the diurnal cycle of rainfall occurrence. Over most areas of the basin, the conditional mean rain rate is minimum between midnight and the afternoon (0000-1500LST). Most areas of the basin show a mid to late afternoon maximum conditional mean rain rate between 1500-1800LST. Over Lake Tana a night time maximum conditional mean rain rate is observed. For the areas along the Blue Nile River maximum rain rate is observed around mid night from 2200-0000LST.
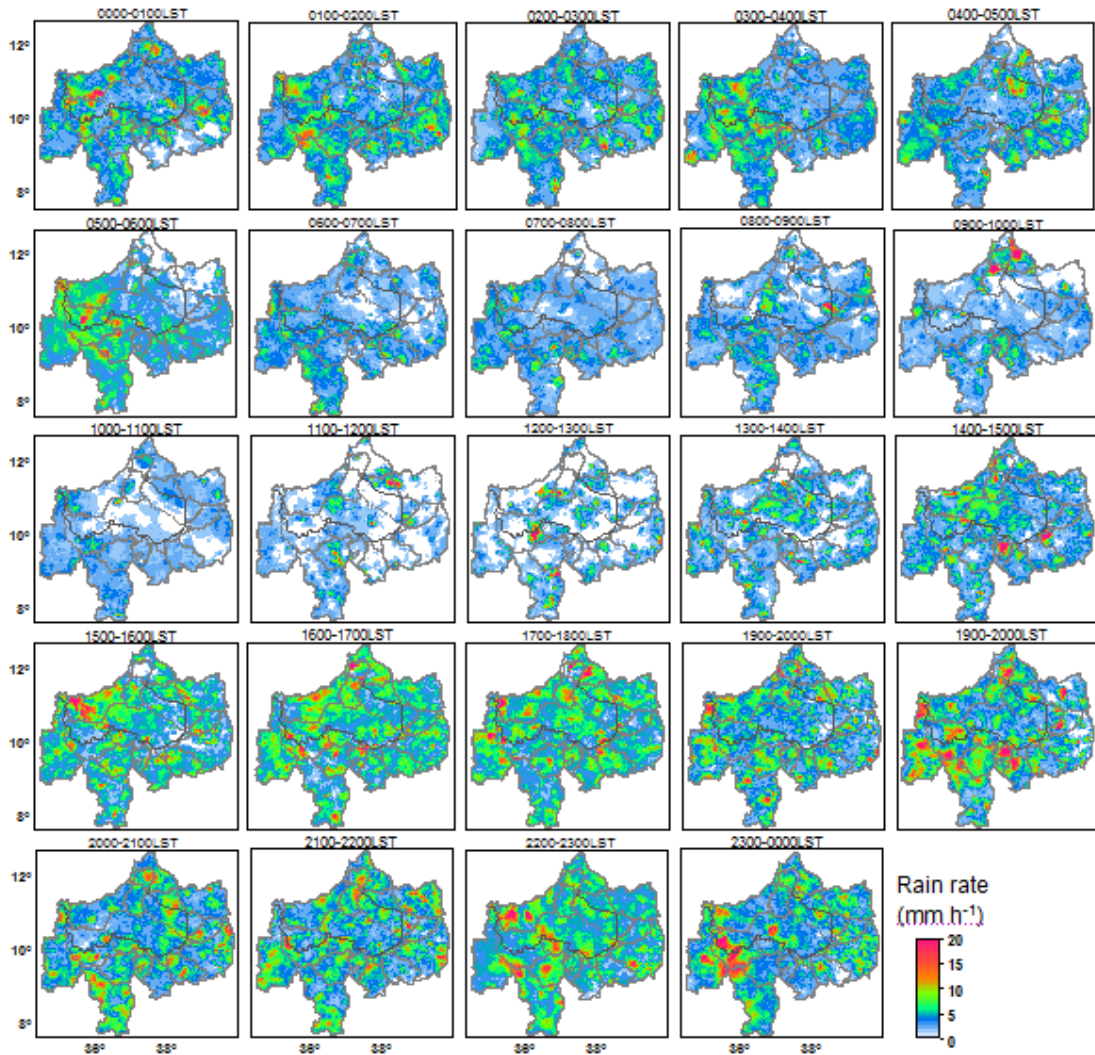
Figure 5.13 Diurnal cycle of conditional mean rain rate using TMI data on 1-hourly period

5.2.4. Mean rain rate comparison of PR and TMI estimates

To compare the conditional mean rain rate estimations from the PR and TMI sensors, the difference between the rain rate estimates of the two sensors is calculated and the resulting map is classified into three classes as: PR>TMI, PR=TMI and PR < TMI (see figure 5.14). This is done for selected LSTs. The LSTs are selected at 6 hour interval so that the assessment is done for the morning, midday, afternoon, and midnight times. Hence, the selected LSTs are 0500-0600LST, 1100-1200LST, 1700-1800LST and 2300-0000LST. Table 5.1 shows the percentage of the areas of each class for the selected LSTs.

Table 5-1 The percentage of areas of each class for the selected LSTs

	0500-0600LST	1100-1200LST	1700-1800LST	2300-0000LST
PR > TMI	23	14	27	25
PR = TMI	35	62	22	26
PR < TMI	42	24	51	48

Table 5.1 and figure 5.14 indicate that the PR and TMI observations have similar rain rate estimates over most parts of the basin during midday (1100-1200LST). This covers around 62% of the total area of the basin. This could be because during the midday over most of the areas of the basin there is no rainfall observed. However, for the rest of the LSTs selected, the TMI rain rate estimates are higher than that of the PR over most of the areas of the basin. This suggests that the rain rates estimated from the PR and TMI sensors are dependent on local time as reported by Furuzawa and Nakamura (2005). They reported that over land areas during the day time between 0600-1800LST the PR rain rates are higher than TMI. However, in this study, for the selected LSTs over most areas of the basin the TMI rain rate estimates are higher than PR. Over the land surface, the general overestimation of the TMI rain rate is also confirmed by Kummerow et al. (2000); Negri et al. (2002); and Nesbitt et al. (2004). Over the mountainous areas of the basin, the PR estimates are higher particularly during the afternoon and midnight. Using three months (JJA) TMI (2A12) and PR (2A25) rain rates averaged over a grid box of 0.50x0.50, Ikai and Nakamura (2003) reported that PR-rain rate is higher than TMI-rain rate in mountainous regions over land, for instance, the Rockies, the Andes, and the Himalayas. The general difference between the PR and TMI rain rate estimates can be attributed to the combination of ambiguity in estimating the profile from TMI, ambiguity of the attenuation correction for PR in heavy rainfall around the tropical areas, and the algorithmic bias in the conversion from brightness temperature to rain rate in the TMI algorithm. Over land surface, TMI overestimates the rain rate and Nesbitt et al. (2004) attributed this disagreement with the PR to the biases associated with the empirically derived 85 GHz ice-scattering rain rate relationship of TMI. They also suggested that PR overestimation could likely be due to the bias in the relationship between attenuation corrected reflectivity factor and rain rate or an erroneous attenuation correction for intense convection.
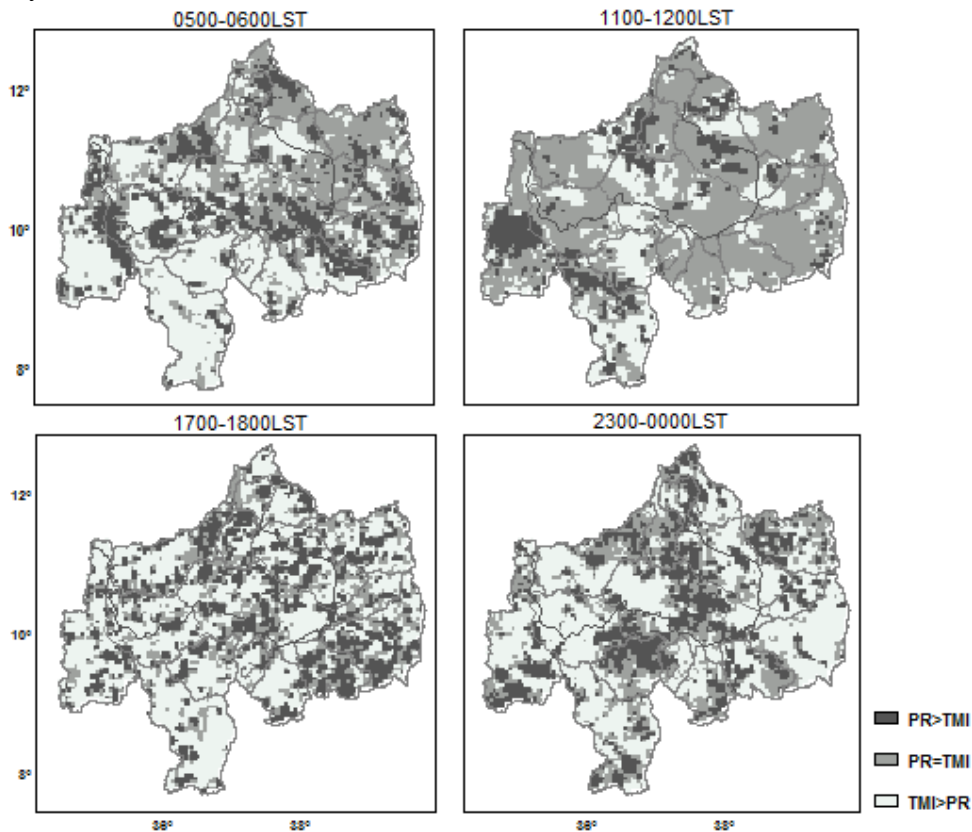
Figure 5.14 Mean rain rate difference between PR and TMI observations for selected LST

5.2.5.   Validation of PR and TMI estimates using ground observations

The graphical approach used here to compare the TRMM satellite diurnal cycle estimates with the ground observation in French Guiana and Upper Blue Nile basin is the one used by Kishtawal and Krishnamurti (2001). As such the bar graphs show the pattern of the diurnal cycle from the TRMM and ground observations. Figure 5.15 depicts the diurnal cycle of rainfall occurrence for the three stations in French Guiana and TMI observations. For Saint Georges and Mariposoula the highest rainfall occurrence is in the afternoon (1500-1800LST) from the satellite and ground observations while an early morning (0300-0600LST) maximum is observed in Rochambeau. In general, it is observed that the pattern of the diurnal cycle of rainfall occurrence from TMI observations matches with that of the ground truth. However, in most of the LSTs the rainfall occurrence from ground truth is higher than TMI observations. The correlation analysis between the rainfall occurrence from the TMI observations and ground truth shows a significant correlation at 95 % confidence level. The Pearson correlation coefficients for Saint Georges, Rochambeau and Mariposoula are 0.73, 0.72 and 0.78 respectively. This suggests that despite the difference in magnitude the diurnal cycle of rainfall occurrence estimates from the TMI observations as aggregated on three-hourly periods for French Guiana are representative of the actual cycle. The differences in the magnitude of the rainfall occurrence could be attributed to the difference in the type of data. As such, the ground observations are accumulated rainfall depth while the TMI estimates are mean rain rate. Moreover, the ground truth represents point rainfall data whereas TMI represents spatial rainfall observations
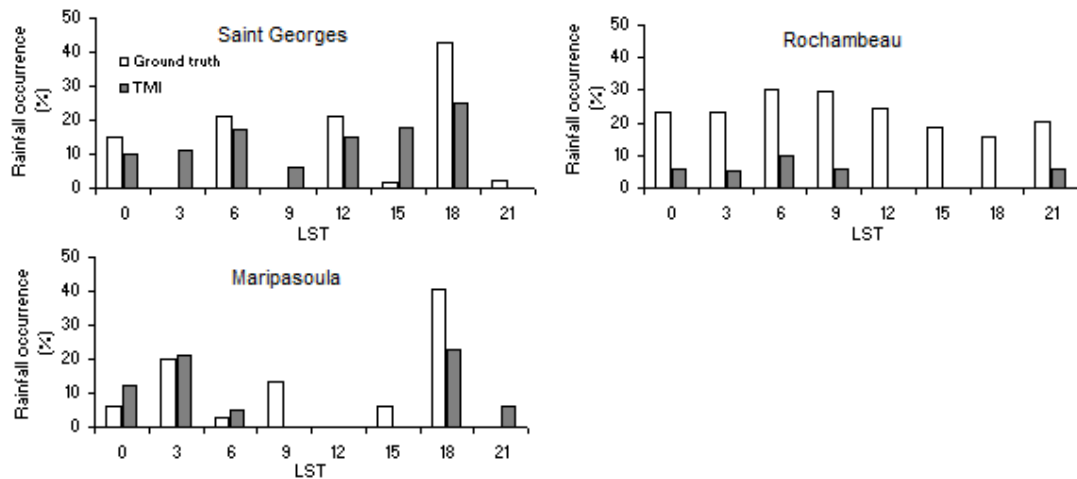
Figure 5.15 Diurnal cycle of rainfall occurrence from TMI and ground observations

Figure 5.16 depicts the diurnal cycle of rainfall occurrence for the three stations in the Upper Blue Nile basin, PR and TMI observations. The observed rainfall occurrences are highest in the early morning, afternoon and midnight from the three observations in Fiche, Mekane-selam and Shawura. In general, it is observed that the pattern of the diurnal cycle of rainfall occurrence from PR and TMI observations matches with the ground truth. For each station a correlation matrix is analysed and is shown in table 5.2. The correlation analysis between the rainfall occurrence from PR and TMI estimates and the ground truth shows that both PR and TMI estimates depict comparable correlations with the ground observations in Fiche with R^2=0.72 and 0.78 respectively. The diurnal cycle estimates from PR are more correlated with the ground observations in Mekane-selam (R^2=0.75) and Shawura

(R^2=0.73) than the TMI. Overall, the analysis shows there is significant correlation between the satellite estimated diurnal cycle of rainfall occurrence and the ground observations for the three stations at 95 % significance level. Moreover, a significant correlation is observed between the PR and TMI estimated diurnal cycle in all the station sites. However, the rainfall occurrence estimations from TMI are higher than PR and ground observations in most of the LSTs.
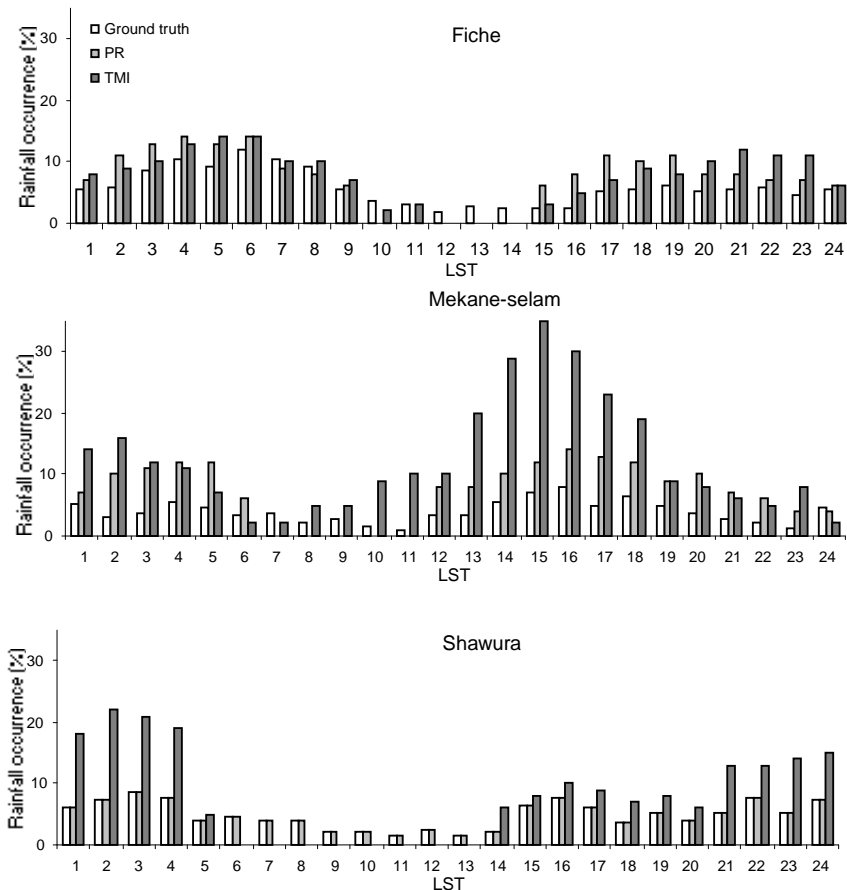
Figure 5.16 Diurnal cycle of rainfall occurrence from PR, TMI and ground observations

Figure 5.17 shows the diurnal cycle of the PR and TMI conditional mean rain rate estimates with ground observations from Fiche station. This station is chosen as it shows relatively better correlation compared to the other stations. Unlike the rainfall occurrence, the patterns of the diurnal cycle of conditional mean rain rate observed from the PR and TMI do not show reasonable match with the ground truth over the three station sites (not shown for Mekane-selam and Shawura).
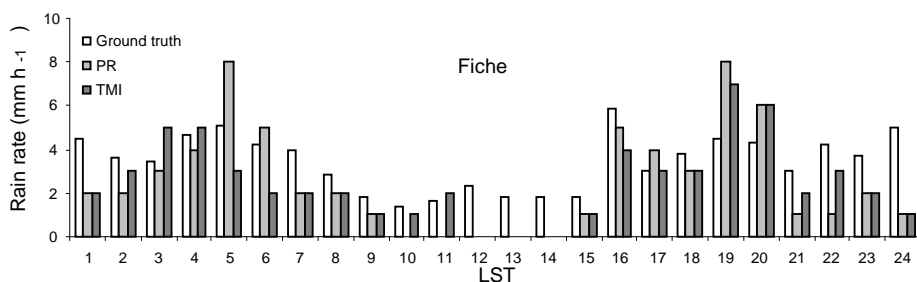
Figure 5.17 Diurnal cycle of conditional mean rain rate from PR, TMI and ground observations

In table 5.2 it is shown that there is no significant correlation between the satellite estimated and the ground observed diurnal cycle of mean rain rate particularly at Mekane-selam and Shawura stations. However, the correlation shows that the PR estimates are more correlated to the ground observations than the TMI estimates in all the three stations. The correlation matrix also depicts that in the station sites there is a significant correlation between the PR and TMI mean rain rate estimates at 95 % significance level.

Table 5-2 Correlation matrix for the three station sites

		Rainfall occurrence			Rain rate		
		Fiche					
		GT	PR	TMI	GT	PR	TMI
Fiche	GT	1			1		
	PR	0.72*	1		0.53*	1	
	TMI	0.78*	0.81*	1	0.44	0.73*	1
		Mekane-selam					
		GT	PR	TMI	GT	PR	TMI
Mekane-selam	GT	1			1		
	PR	0.75*	1		0.47	1	
	TMI	0.66*	0.63*	1	0.22	0.64*	1
		Shawura					
		GT	PR	TMI	GT	PR	TMI
Shawura	GT	1			1		
	PR	0.73*	1		0.3	1	
	TMI	0.61*	0.81*	1	0.21	0.66*	1

* Correlation is significant at the 0.05 level

As it is observed from the rainfall occurrence and mean rain rate diurnal cycles from the TRMM satellite and ground observations, the estimations from PR are closer to the ground observations than TMI. Using eight years of TMI and PR estimates, Ji (2006) made a comparison of mean rainfall and diurnal cycles between TRMM satellite and ground observations over Florida and Darwin sites. He reported that the diurnal cycles from PR and TMI estimates are similar to the gauge observations and amplitudes of diurnal cycle between PR and gauge data are close, while TMI observations showed larger amplitudes of diurnal cycle. Over land surface, the higher reliability of PR rain rate estimates compared to TMI is also reported by Furuzawa and Nakamura (2005). They attributed this to PR's superior vertical and horizontal resolution that allows the PR to observe smaller scale precipitation features that cannot be unambiguously resolved by the TMI. However TMI rain estimations are more accurate over the oceans due to the homogeneous surface background emissions that can be more clearly distinguished from atmospheric emissions associated with clouds and precipitation (Furuzawa and Nakamura, 2005).

5.2.6. Diurnal cycle using Harmonic analysis

The Fourier series expansion of the form in equations 4.7-4.9 was applied to the rainfall occurrence and conditional mean rain rate for the ground truth, PR and TMI observations at the station sites. In addition, the correlation analysis from the previous section shows that PR estimates are closer to the ground observations than TMI. Hence, the harmonic analysis is applied for areal average rainfall occurrence and conditional mean rain rate estimated from PR for the selected sub-basins. This analysis is used to determine the diurnal (first harmonic) and semi-diurnal (second harmonic) rainfall occurrence and mean rain rate variations. As described by Dai (2001) and Haile et al. (2009b), the percentage of the total daily variance explained by the sum of the first two harmonics is a measure for the representativeness of the diurnal variations. Thus, the variance explained by the first two harmonics is also assessed to represent the observed variations.

The sum of the two harmonics fitted to the ground truth, PR and TMI observations of rainfall occurrence and mean rain rate are shown in figure 5.18. The variance of the observed rainfall occurrence for ground truth, PR and TMI at the three station sites ranges from 65-89 % (see table 5.3). Except for Mekane-selam, the first harmonics explains most of the variance. The mean of the diurnal cycle ranges from 4-12 % with the highest mean observed from TMI in Mekane-selam while the amplitude ranges from 1-9 %. In Fiche, the time of the amplitude occurs in the early morning (0600LST) for the ground truth which shows a delay of 1-hour from the PR and TMI observations. However, the amplitude occurs in the afternoon (at 1600LST) for ground truth and PR observations and at 1500LST for TMI in Mekane-selam. The time of the amplitude occurs during night but at different LSTs for the three observations in Shawura. As such it is observed that there are inter and intra-site differences in the mean, amplitude and time to the amplitude of the rainfall occurrence diurnal cycle observations.
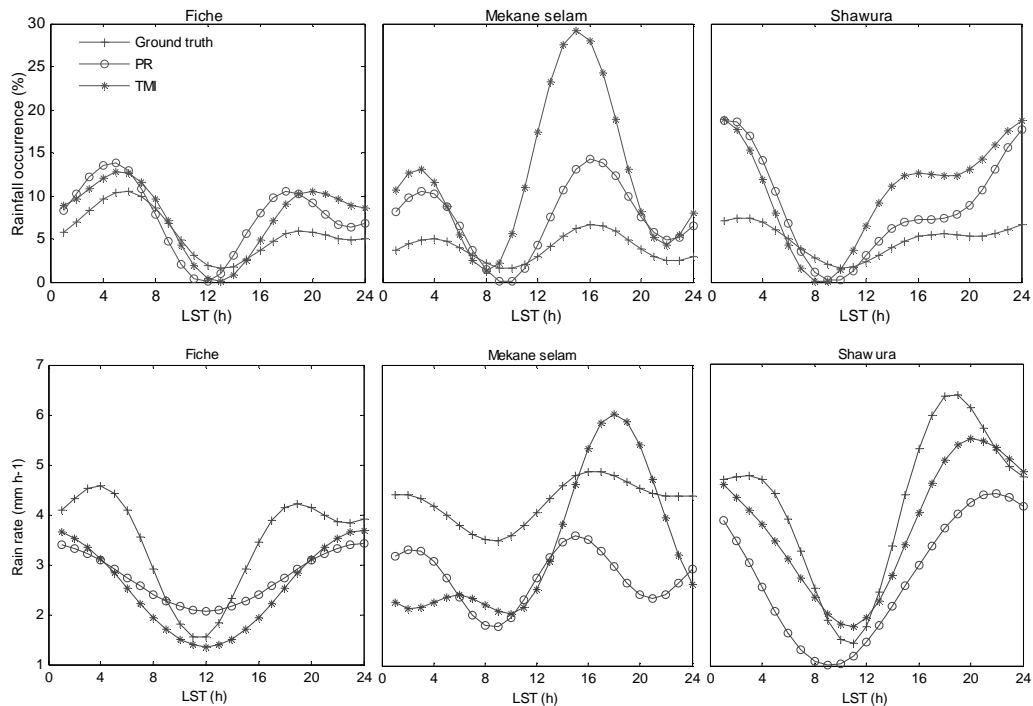
Figure 5.18 Fitted sum of the first two harmonics for the three station sites

Compared to the rainfall occurrence, the variance explained by the sum of the two harmonics for the conditional mean rain rate reveals a weak diurnal variation (variance explained ranging from 31-66 % see table 5.3) except for Shawura where a strong diurnal cycle is observed. The mean diurnal cycle of the rain rate ranges from 2-5 mm h^{-1} with the highest observed in Shawura from ground truth while the range of the amplitude is from 1-2 mm h^{-1}. The time of the amplitude is at 0400LST for the ground truth at Fiche and it shows a delay by 3-hours from the satellite observations. Similarly, the mean of the diurnal cycle, amplitude and the time of the amplitude show differences among the observations in Mekane-selam and Shawura. In table 5.3, the mean of the diurnal cycle and the amplitude are in (%) and (mm h^{-1}) for the rainfall occurrence and mean rain rate respectively.

Table 5-3 Results from the harmonic analysis for the three station sites

Rainfall occurrence						
		Variance explained (%)		Mean of the diurnal		LST of the amplitude
Station	Observation	First harmonic	Second harmonic	cycle	Amplitude	(h)
	Ground truth	55	34	6	3	0600
Fiche	PR	32	45	8	4	0500
	TMI	52	29	8	4	0500
	Ground truth	14	57	4	1	1600
Mekane-selam	PR	22	56	7	3	1600
	TMI	39	45	12	8	1500
	Ground truth	48	17	5	2	0300
Shawura	PR	49	12	8	6	0200
	TMI	50	15	11	9	0100
Rain rate						
	Ground truth	42	17	3	2	0400
Fiche	PR	4	37	3	2	0100
	TMI	20	27	3	1	0100
	Ground truth	23	8	3	2	1600
Mekane-selam	PR	43	9	3	2	1500
	TMI	9	45	2	1	1800
	Ground truth	52	14	5	1	1800
Shawura	PR	63	0	2	2	2200
	TMI	51	2	3	2	2000

The areas of the sub-basins that are arbitrarily selected for the harmonic analysis of the areal average rainfall occurrence and mean rain rate are shown in table 5.4.

Table 5-4 Areas of the sub-basins selected

	Sub-basin						
	Belles	Beshilo	Gilgel abbay	Dabus	Jemma	Muger	Lake Tana
Area (km^2)	13700	12250	4525	18075	15500	7400	3000

The sum of the first two harmonics fitted to the areal average rainfall occurrence, mean rain rate, and to the pixel values selected along the Blue Nile River are shown in figure 5.19. The grouping of the sub-basins is based on their time of maximum observation.
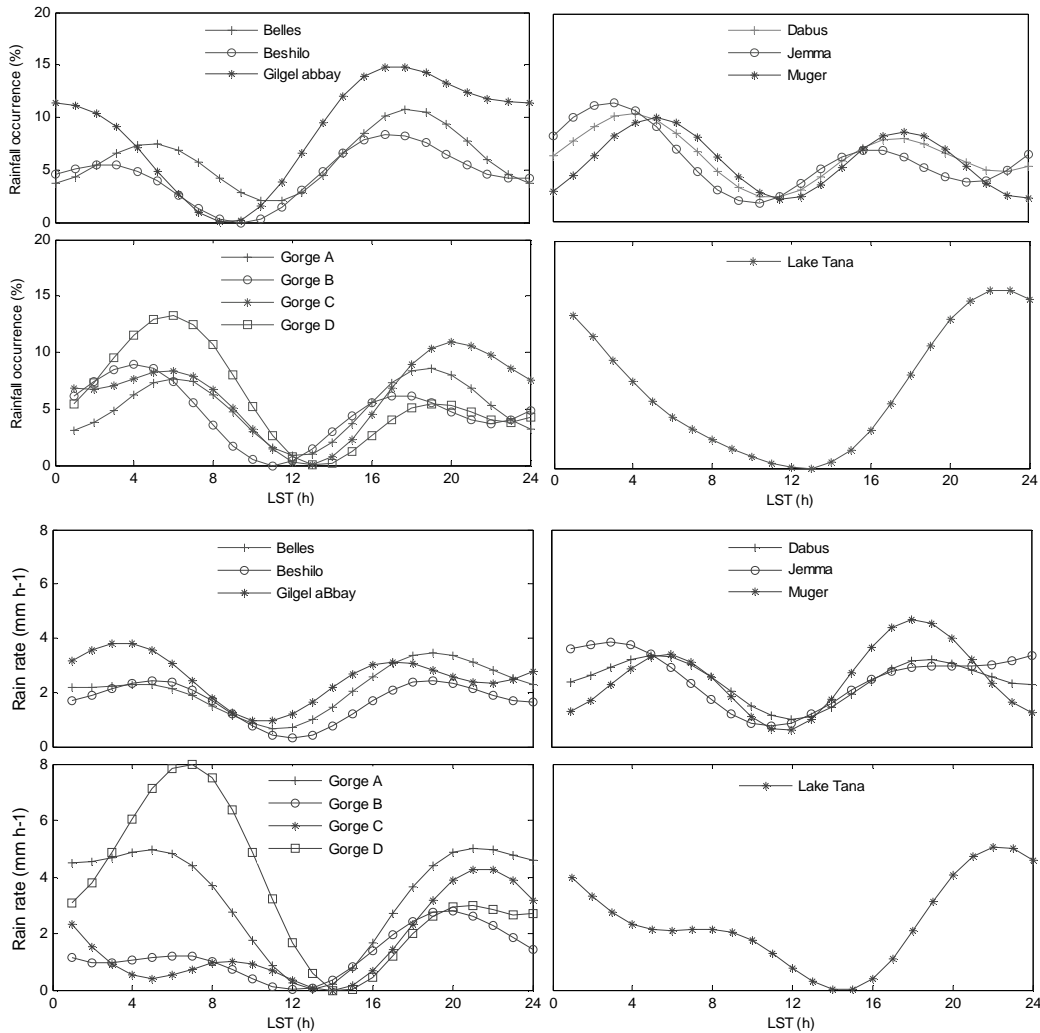
Figure 5.19 Fitted sum of the first two harmonics for the selected sub-basins

For Belles, Beshilo and Gilgel Abbay sub-basins, the mean daily variation of the rainfall occurrence explained by the sum of the first two harmonics ranges from 53-61 % (see table 5.5). The semi-diurnal variation predominates in the Belles sub-basin while the diurnal variation explains higher percentages in the Beshilo and Gilgel Abbay sub-basins. The mean of the diurnal cycle and the amplitude ranges between 4-9 % and 3-6 % respectively, while the time to the amplitude for the three sub-basins is between 1600-1700LST. For Dabus, Jemma and Muger sub-basins the daily mean rainfall occurrence variation explained by the first two harmonics is between 42-81 %. The semi-diurnal variation accounts for most of the daily variance in Dabus and Muger, but the diurnal variation is predominant in Jemma sub-basin. For these sub-basins, the mean diurnal cycle is between 6-8 % with amplitude ranging from 3-5 % that is observed in the early morning (between 0400-0600LST). Over Lake Tana, the diurnal variation predominates with the first harmonics explaining 59 % of the variation while the semi-diurnal variation is very weak (only 2 %). The mean of the diurnal variation and the amplitude are equal (7 %). The time of the amplitude is at 2200LST. For the points taken along the Blue Nile

River, the first two harmonics explain 13-30 % of the mean daily variation in rainfall occurrence. As such, the daily mean variation of the rainfall occurrence explained by the two harmonics is low at the points considered. Moreover, differences in the mean of the diurnal cycle, the amplitude and the times of the amplitude are observed for the four points along the river. This suggests that there is variation in the rainfall diurnal cycle along the river.

**Table 5-5** Results from the harmonic analysis

Rainfall occurrence					
Sub-basin/ gorge	Variance explained (%)		Mean of the diurnal cycle	Amplitude	LST of the amplitude (h)
	First harmonic	Second harmonic			
Belles	14	39	6	3	1700
Beshilo	31	23	4	3	1600
Gilgel Abbay	51	10	9	6	1600
Dabus	14	39	6	3	0500
Jemma	50	31	8	5	0400
Muger	1	31	6	3	0600
Lake Tana	59	2	7	7	2200
Gorge A	2	11	6	2	1900
Gorge B	18	11	5	2	0400
Gorge C	11	7	6	4	2000
Gorge D	19	11	6	4	0600
Rain rate					
Belles	35	15	2	1	1900
Beshilo	14	16	2	1	1900
Gilgel Abay	10	13	3	2	0400
Dabus	19	28	2	1	0500
Jemma	40	9	3	1	0300
Muger	9	41	3	2	1800
Lake Tana	53	16	2	2	2200
Gorge A	56	13	2	1	2100
Gorge B	9	4	1	1	2000
Gorge C	21	9	2	2	2100
Gorge D	16	6	4	3	0700

The two harmonics explain 50 % of the variance in the daily variation of the mean rain rate in Belles sub-basin. However, only 23 and 30 % of the variance is explained in Gilgel Abbay and Beshilo sub-basins respectively. The time of the amplitude is at night (1900LST) for Belles and Beshilo and early morning (0400LST) for Gilgel Abbay sub-basin. As such, a phase shift is observed between the rainfall occurrence and the mean rain rate diurnal cycles in these sub-basins. The sum of the two harmonics explains 47 and 49 % of the daily rain rate variation in Dabus and Jemma sub-basins with the time of the amplitude of 0500 and 0300LST respectively. Over Muger sub-basin, like the rainfall occurrence, most of the variation of the rain rate is explained by the second harmonics (41%) and as

such the semi-diurnal variation predominates. Over Lake Tana, the diurnal variation accounts for 53 % of the daily variation with a weak semi-diurnal cycle which accounts for only 16 %. The variation in the mean rain rate over Lake Tana is in phase with the rainfall occurrence and the time of the amplitude is during night time at 2200LST. Except for Gorge A which shows a dominant diurnal cycle explaining 56 % of the variance, the diurnal and semi-diurnal variations of the mean rain rate are weak for the rest of the points along the river. However, for most of the points, the time to the amplitude is observed during night time between 2000-2100LST. In general, from the three station sites, the selected sub-basins and the points along the Blue Nile River the mean of the diurnal cycle, the amplitude and time of the amplitude of the rainfall occurrence and conditional mean rain rate show spatially varying diurnal cycle over the basin.

### 5.2.7. Diurnal variability with terrain elevation

There is high variation of terrain elevation in the Upper Blue Nile basin along the transects XX' and YY' (see figure 5.20). The distances along the transects are measured starting from X to X' and from Y to Y' (see figure 4.4 for the layout of the transects). The elevation along the transects ranges from around 500 m in the gorge to more than 4000 m in the mountainous areas. Therefore, from these transects, it is possible to assess the relation between terrain elevation and rainfall and the effect of mountain orientation on rainfall distribution. For this purpose, the rainfall occurrence and conditional mean rain rate estimated from both PR and TMI are used. As such, it is also possible to compare the diurnal cycle estimates of PR and TMI along the transects.
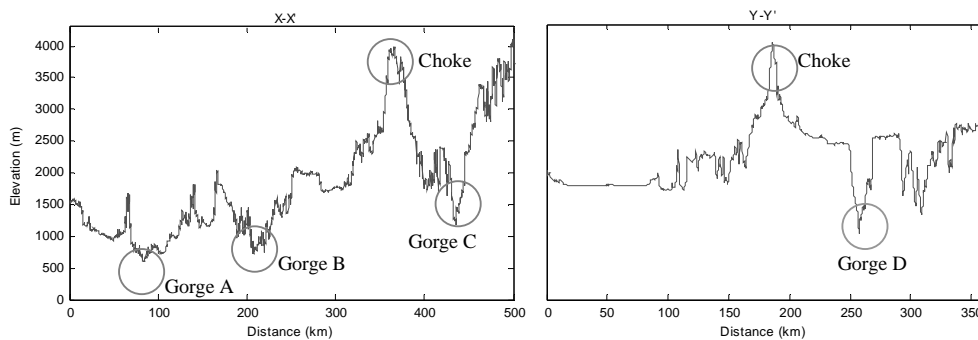
**Figure 5.20** Variation of elevation along the transects

To assess the pattern of the 24-hour diurnal cycle of rainfall along transect XX' and YY', the rainfall occurrence and conditional mean rain rate are mapped for each LST along the transects. Figure 5.21 shows the diurnal cycle of rainfall occurrence along transect XX'. The rainfall occurrence ranges from 0 to 40% with maximum occurrence observed in the mountainous areas for both PR and TMI. Over the South-western parts of the mountainous areas, an afternoon to midnight maximum rainfall occurrence is observed. However, over the North-eastern part, an afternoon maximum is observed but with relatively lower magnitude. This suggests the existence of orographic influences in the area that leads to rain shadow effect in the mountainous areas facing the Northeast. As described in section 3.2.2, the general air circulation pattern in the Blue Nile basin is characterized by south-westerly flow and hence the mountainous areas in the north, northeast and northwest can be influenced by orographic effects. As such, the windward side receives more rainfall than the leeward side. In the northeast mountainous areas of gorge C, maximum occurrence is observed only in the afternoon. Along the transect between gorges A and B, where there is high topographic variation, a relatively

high variation in rainfall occurrence is observed. However, in the Blue Nile gorge relatively different conditions prevail. Though it is not highly pronounced, a night time to early morning maximum is observed in gorges A and B while in gorge C the highest occurrence is during night time. This indicates that there is variability in rainfall occurrence along the gorge. It is also observed that along the transect the estimated rainfall occurrence from TMI is higher than that of PR.
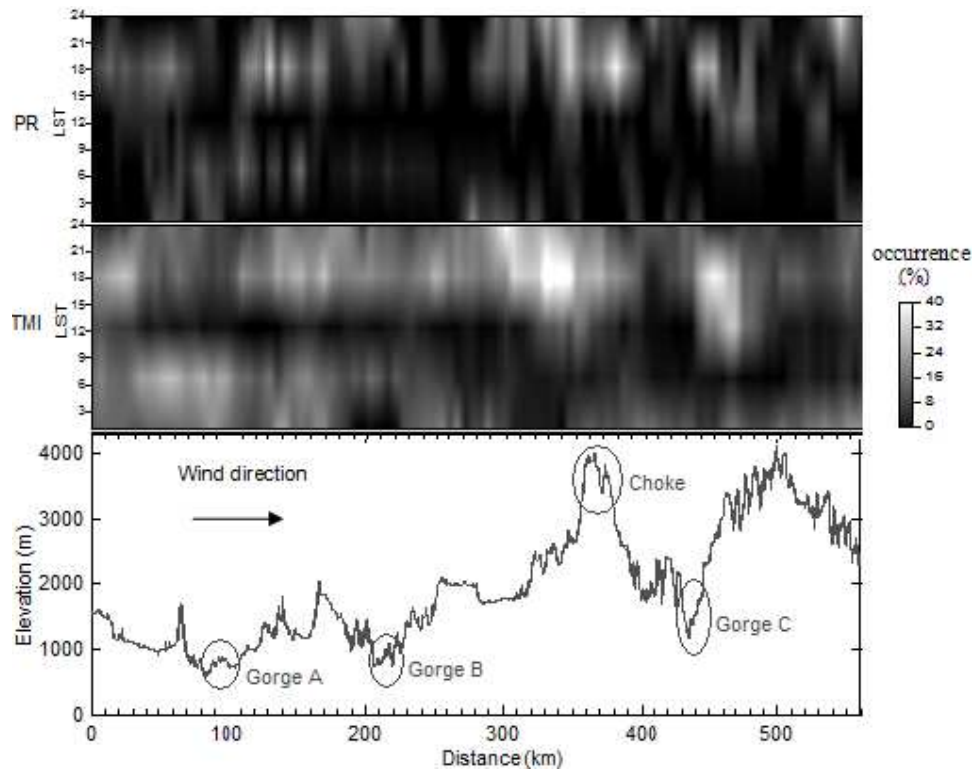
Figure 5.21 Diurnal cycle of rainfall occurrence along transect XX'

Along transect YY', which crosses Lake Tana, Choke mountain and Blue Nile gorge, the rainfall occurrence is maximum around midnight over Lake Tana (see figure 5.22). Around Choke mountain, an afternoon maximum rainfall occurrence is observed; however, the magnitude is relatively lower compared to the one observed in transect XX'. This could be due to the effect of the orientation of the mountain on rainfall distribution indicating the existence of orographic effects in the area in which the mountainous areas facing the southwest are characterized by high frequency of rainfall occurrence. In the Blue Nile gorge at point D, an early morning maximum rainfall occurrence is observed from both the PR and TMI observations particularly with PR showing a higher rainfall occurrence than TMI. For the areas in the southeast of gorge D, midnight to early morning maximum rainfall occurrence is observed from the PR observation while the TMI does not show a pronounced maximum. However, as we go further to the southeast an afternoon maximum is observed from both PR and TMI observations. Along the transect there exists a rugged topography between Lake Tana and Choke mountain and correspondingly high variability in rainfall occurrence is observed in these areas. In general, it is observed that there is variability in the magnitude and in the time of maximum rainfall occurrence along the transects that suggests spatial variability of rainfall occurrence in the basin. Differences in the rainfall occurrence estimations from the PR and TMI observations are also revealed along the transects.
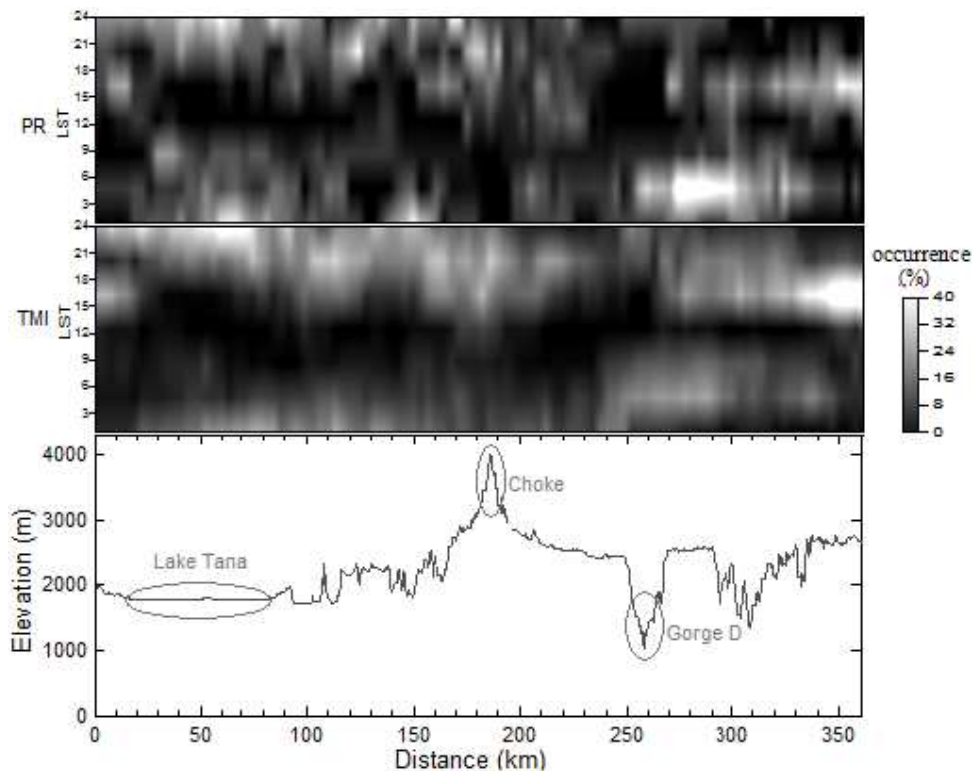
Figure 5.22 Diurnal cycle of rainfall occurrence along transect YY'

The diurnal cycle of conditional mean rain rate along transect XX' is shown in figure 5.23. In the lowland areas to the southwest of gorge A, an afternoon mean rain rate maximum is observed. In gorge A, the mean rain rate attains its maximum during the night time, but for gorges B and C a pronounced maximum mean rain rate is not observed. This indicates variability in the mean rain rate along the gorge. In the south-western part of Choke mountain, an afternoon maximum mean rain rate is observed from TMI while the PR observations reveal late afternoon to midnight maximum. The mean rain rate in the opposite side of the Choke mountain (north-eastern part) is lower than the areas in the southwest of the mountain which can be attributed to the rain shadow effect. Along the transect over most of the LSTs with an exception of some localized points, the mean rain rate estimated from TMI is higher than PR.

Along transect YY', the pattern of conditional mean rain rate (see figure 5.24) shows night time maximum over Lake Tana from both PR and TMI observations. Moreover, the mean rain rate in the southern part of the lake is higher than the northern part. This is in agreement with Alemseged et al. (2009b) as they found maximum night time convection over the southern shore of the lake. Over the Blue Nile gorge at point D, the highest mean rain rate is observed in the early morning from the PR observations while no pronounced maximum is observed from TMI observations. Over the north of Choke Mountain and over the areas southeast of gorge D the maximum mean rain rate is observed in the afternoon from PR observations. From TMI observations, however, night time to early morning maximum mean rain rate is observed in the areas north of Choke Mountain. In general, along the transect it is shown that there is spatial variability in the magnitude of the mean rain rate and its time of maximum. Moreover, the differences in the PR and TMI mean rain rate estimates are also evident from the observations along this transect.
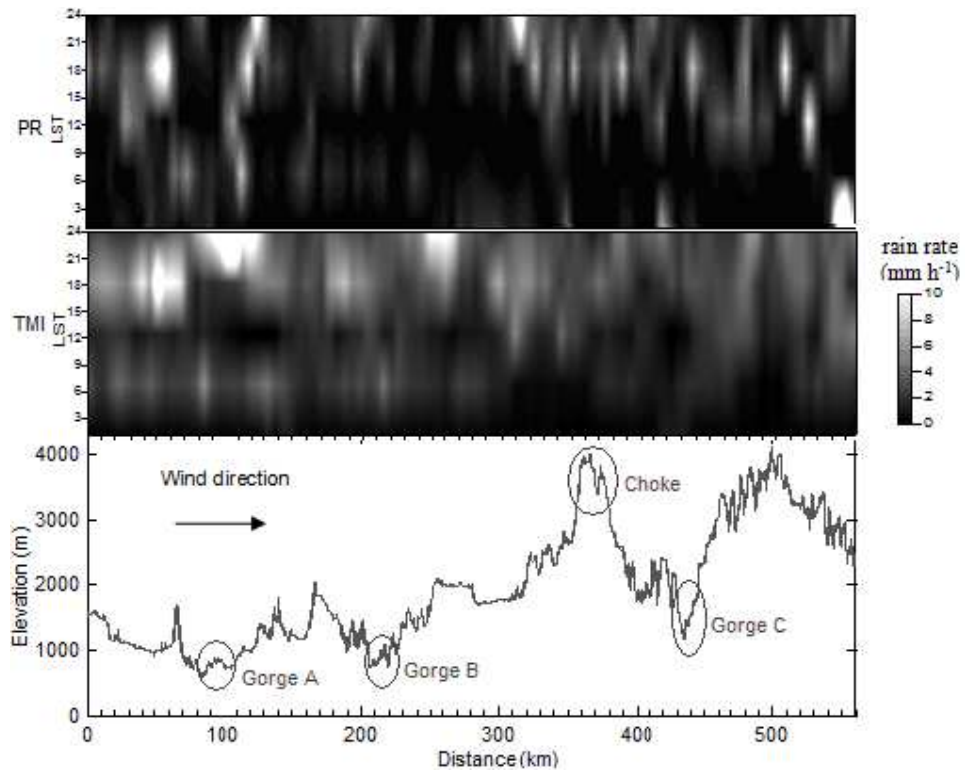
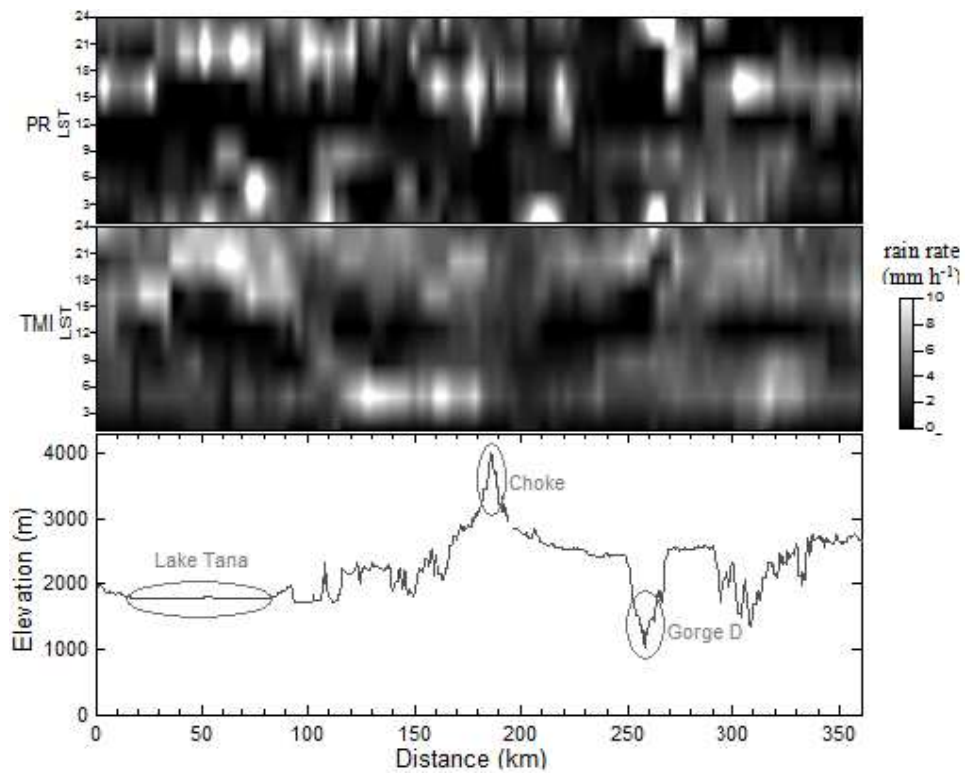**Figure 5.23** Diurnal cycle of mean rain rate along transect XX'

**Figure 5.24** Diurnal cycle of rainfall occurrence along transect YY'

Kuraji et al. (2001) argued that it is not the rainfall intensity, but the rainfall occurrence that can show pronounced differences with altitudinal increments. Therefore, here the patterns of rainfall occurrence along the transects are assessed for selected LSTs to further investigate the effect of terrain elevation in rainfall distribution and compare PR and TMI rainfall occurrence estimates. The LST is selected at 6-hour interval and as such the assessment is done for morning, midday, afternoon, and midnight times. Therefore, the same LSTs selected for the PR and TMI comparison are also used here. Figure 5.25 shows the variation of elevation and the pattern of rainfall occurrence along the transect XX'.
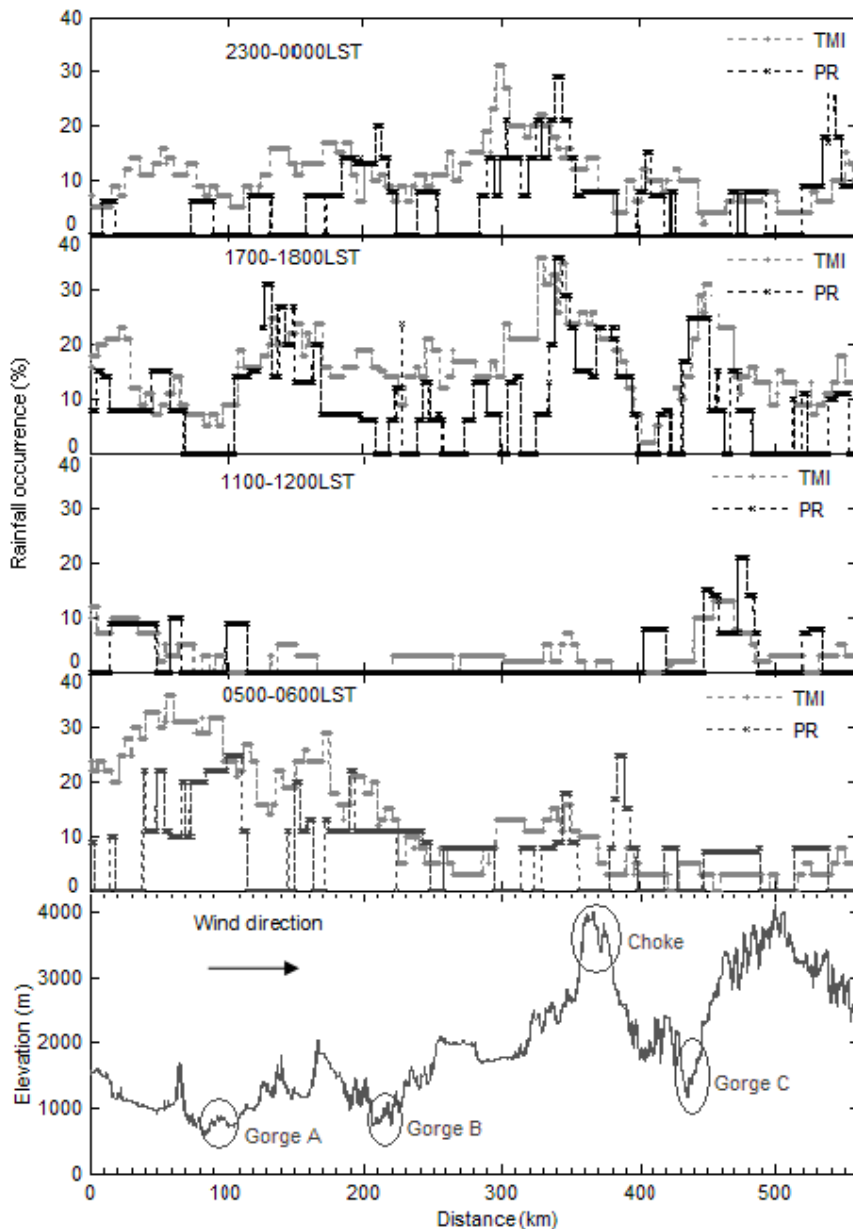
Figure 5.25 Variation of rainfall occurrence along transect XX' for selected LSTs

From the result, it is observed that there is a clear increasing trend of rainfall occurrence with terrain elevation particularly for 1700-1800LST. Haile et al (2009b) found a direct relation between convective index and elevation on 1500 and 1800LST for a transect across the ridges of Gilgel Abbay catchment. Arora et al. (2006) reported that, in general, in mountainous areas orographic precipitation

occurrences increase with an increase in elevation. However, in this study, almost an inverse relation is observed during early morning between 0500-0600LST. Sen and Habib (2000) reported that, in general, rainfall increases with elevation but sometimes inverse cases occur due to orographic and meteorological features of the area. Haile et al. (2009b) also found an inverse relation of convective index with elevation in early night hours. Since the rainfall occurrence is quite low between 1100-1200LST, no clear trend is observed during this period. Though it is not much pronounced, a direct relation between rainfall occurrence and terrain elevation is also observed between 2300-0000LST. Moreover, almost for all the selected LSTs, the estimated rainfall occurrence from TMI is higher than the PR. A direct relation between rainfall occurrence and terrain elevation is also evident from transect YY' for 1700-1800LST (see figure 5.26). However, for the other LSTs, there is not as such a clear trend that shows the relation between rainfall occurrence and terrain elevation. In most of the observations, the TMI estimates are higher than the PR.
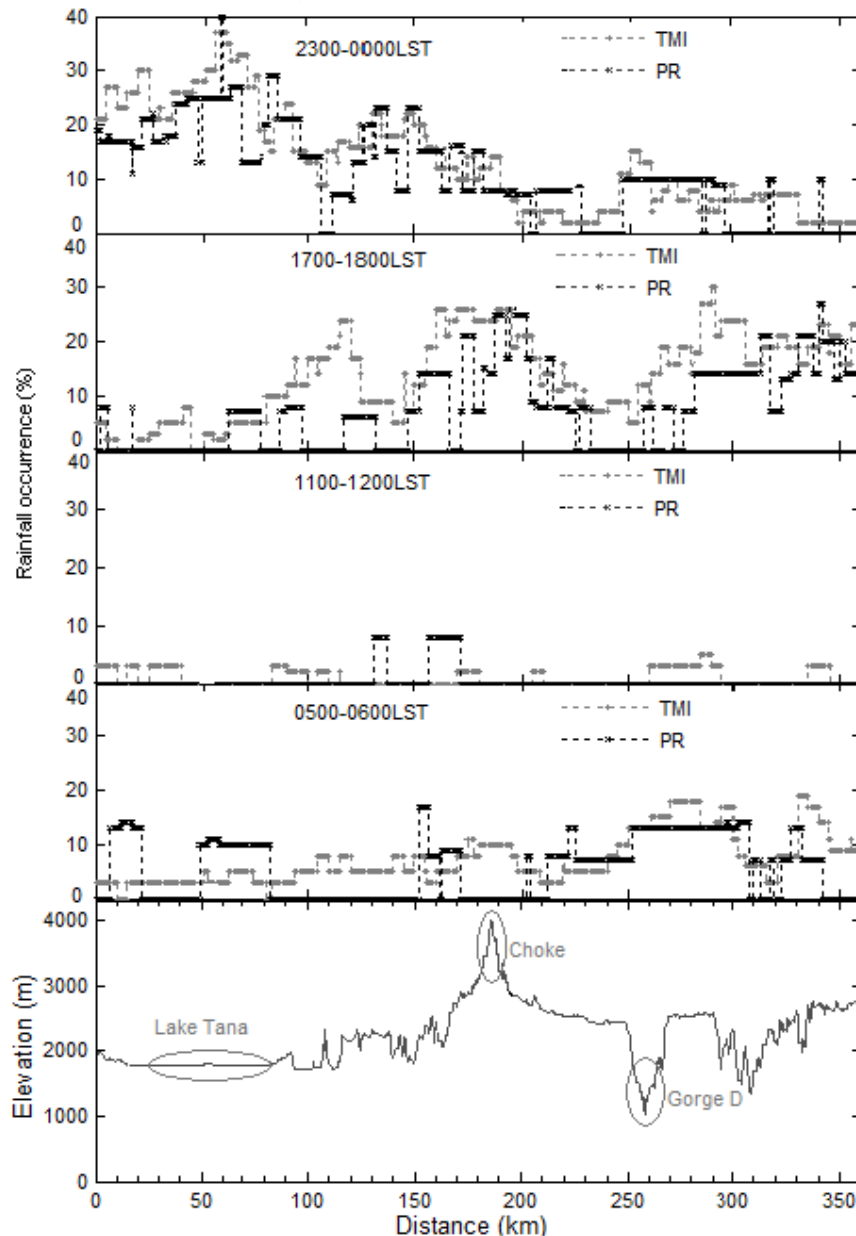
Figure 5.26 Variation of rainfall occurrence along transect YY' for selected LSTs

5.2.8. Rainfall depth estimation from PR and TMI observations

The results of the mean rainfall depth estimated from the PR and TMI observations are shown in figure 5.27. The minimum rainfall depth is observed along the areas of the Blue Nile River (shown by thin dark gray line) and in the northeast areas of the basin (Beshilo sub-basin). From both the PR and TMI estimates, it is shown that the seasonal mean rainfall depth is highest in the central highlands and the southwest parts of the basin. Conway (2000) reported that the areas in the southwest of the basin receive higher amounts of annual rainfall (>2000 mm) compared to the north and northeast parts (around 1000 mm) and 70 % of the annual rainfall occurs during the rainy season (JJAS). According to UNESCO (2004), Kim and Kaluarachchi (2008) and Abtew et al. (2008) the estimated annual rainfall over the basin ranges from 1200 mm to 1600 mm. Since the mean annual rainfall depths reported are point measurements and not interpolated for the entire basin, it is not straightforward to make an implicit comparison between the gauge measurements and the satellite estimates. However, the spatial distribution and magnitude of the mean rainfall depth estimated from PR and TMI seem reasonable. The mean annual rainfall depth is also calculated for the three stations in the basin and the results reveal that the estimated mean rainfall depths from PR are closer to the ground observations than the TMI (see table 5.6). With 70 % of the mean annual rainfall received during the rainy season (ranging from 800-1100 mm for JJAS based on the reports mentioned above), from the comparison with the ground truth in the gauging stations, and showing a more distinct pattern with low estimated rainfall depth along the river line the PR estimated rainfall depth is more reliable. However, unlike PR, TMI does not show a clear pattern along the river line. This could be possibly because of the averaging effect when the TMI observations are down-scaled to 5×5 km pixel size from the original 5×12 km pixel.
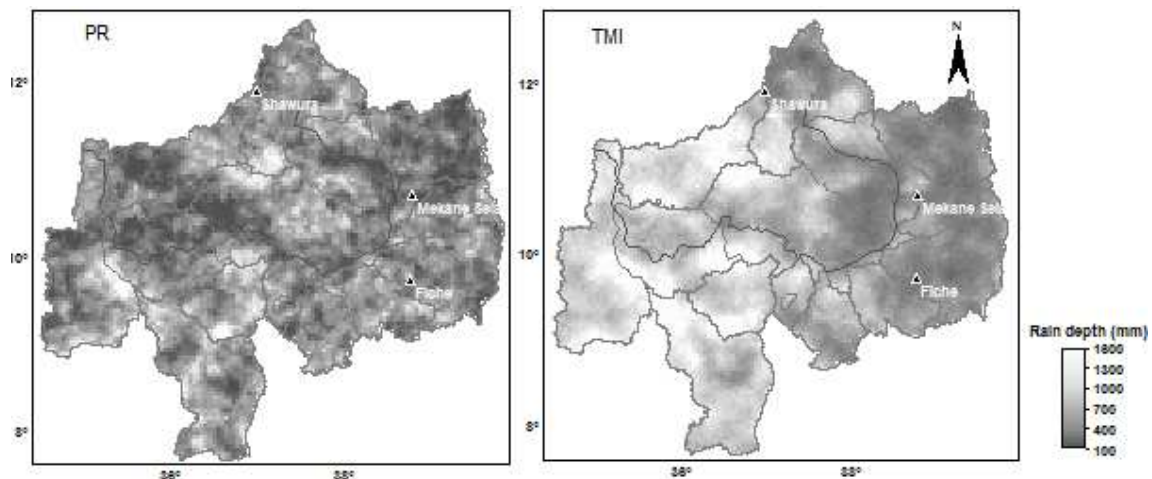
Figure 5.27 Estimated mean rainfall depth for the rainy season (JJAS)

Table 5-6 Mean rainfall depths at the three station sites for JJAS

Station	Rainfall depth (mm)		
	Ground truth	PR	TMI
Fiche	569	540	546
Mekane-selam	428	586	728
Shawura	458	449	928

6.   Conclusions and recommendations

6.1.   Conclusions

Rain rate estimates retrieved from PR and TMI sensors on board of the TRMM satellite are used to assess the diurnal variability of rainfall in French Guiana and the Upper Blue Nile basin. One year (2005) of TMI data for AMJJ and seven years (2002-2008) of PR and TMI data for JJAS are used for French Guiana and the Upper Blue Nile basin respectively. These time periods correspond to the rainy season of the respective study areas. The rainfall diurnal cycle is assessed both in terms of rainfall occurrence and mean rain rate. Moreover, the total number of overpasses of PR and TMI, the difference between PR and TMI mean rain rate estimates and the relation between rainfall and elevation are assessed. Ground based observations are used to validate the TRMM rainfall diurnal cycle estimates.

For French Guiana three hourly aggregated TMI data are used. The number of observations varies spatially between 15 and 21 with a coefficient of variation that ranges from 7 to 15 %. Over most parts of French Guiana the maximum rainfall occurrence and conditional mean rain rate are observed from mid to late afternoon (1500-1800LST). Moreover, the diurnal cycle of the rainfall occurrence from TMI observations show significant correlation with the ground observations at 95 % confidence level. However, the magnitude of the rainfall occurrence from ground observations is higher than TMI estimations in most of the LSTs. This could be because of the difference in data types where the ground observations are accumulated rainfall depths while TMI observations are instantaneous rain rates. In addition, the ground observations represent point rainfall data while TMI represents spatial rainfall observations.

The number of TRMM-PR observations on 1-hourly and 2-hourly periods for the Upper Blue Nile basin varies between 8 to 20 and 19 to 31 respectively. A more uniform sampling is obtained spatially when the PR data is aggregated on 2-hourly periods. The coefficient of variation ranges from 12 to 23 % and 5 to 13% for the 1-hourly and 2-hourly periods respectively. On 1-hourly period, the number of observations from TMI is larger than from PR and ranges from 37 to 50 with a more uniform sampling than PR since the coefficient of variation is between 5 to 9%. The larger number of observations and the more uniform sampling from TMI is due to the wider swath width of the TMI as compared to the PR.

French Guiana and the Upper Blue Nile basin are found at different latitudinal locations. French Guiana is located between 2^0 and 6^0 north latitude whereas the Upper Blue Nile basin is located between 7^0 and 13^0 north latitude. The number of TMI observations ranges from 15-21 for French Guiana from 1-year data (AMJJ) and from 37-50 for the Upper Blue Nile basin from 7-years data (JJAS). This indicates that for the same period of time the number of TMI observations is higher for French Guiana than the Upper Blue Nile basin. As such, the areas near the equator at lower latitude have higher sampling frequency than the areas at higher latitudes. This indicates that the TRMM satellite sampling frequency varies with latitudinal locations of the areas. This can be attributed to the orbital characteristics of the satellite which orbits the earth at 35^0 inclination to the equator.

From PR observations, over most areas of the Upper Blue Nile basin, the rainfall occurrence and conditional mean rain rate are highest between mid to late afternoon (1500-1800LST). However, over Lake Tana and in the southwest and southeast parts of the basin, rainfall occurrence and mean rain rate are maximum during midnight and early morning. Moreover, the southern part of the lake is characterized by higher rainfall occurrence and mean rain rate than the other sides of the lake. Along the Blue Nile River gorge the rainfall occurrence shows a certain pattern with minimum occurrence in most of the LSTs during the day time (0800-1700LST) and maximum during the night (2000-2300LST). This suggests that there is high spatial variability in the pattern of diurnal cycle of rainfall over the Upper Blue Nile basin.

Except differences in magnitude, the diurnal cycles of rainfall distribution observed from TMI observations are close to that of the PR. The comparison of conditional mean rain rate estimations from PR and TMI for the Upper Blue Nile basin indicates that over most areas of the basin (62% of the total area) the PR and TMI rain rate estimates are similar during midday (1100-1200LST). This could be because during the midday in most of the areas there is no rainfall observed. However, for the rest of the LSTs considered, the TMI rain rate estimates are higher than the PR over most of the areas of the basin. As such, in addition to the various factors that affect the rain rate estimates from the sensors, the PR and TMI rain rate estimations are dependent on local time of the day.

For the Upper Blue Nile basin, the comparison of the PR and TMI diurnal cycle estimates with ground observations indicates that the diurnal cycles of rainfall occurrence from PR and TMI observations show similar patterns with the ground observations. The correlation analysis between the satellite estimates and ground observations suggests that the diurnal cycle from PR estimations are closer to the ground observations. The correlation matrix for the diurnal cycle of the mean rain rate also shows that the PR estimates are closer to the ground observations than TMI. However, the correlations of the TRMM estimated and ground truth mean rain rates are weaker and suggest that the satellite estimations are better suited to assess the rainfall occurrence than the rain rate.

In the three station sites of the Upper Blue Nile basin, the patterns of the diurnal cycle from the satellite and ground observations are close. However, the harmonic analysis depicts differences in the mean of the diurnal cycle, amplitude and time of the amplitude among the observations. The first two harmonics explains 65-89 % of the daily variation of rainfall occurrence in the station sites. Except for Mekane-selam, the first harmonics explains most of the variance of the daily variation. Compared to the rainfall occurrence, the variance explained by the sum of the first two harmonics for the conditional mean rain rate is weak (31-66 %). However, in Shawura which is close to Lake Tana a strong diurnal cycle of the mean rain rate is observed with the first harmonic explaining 51-63% of the daily variation.

From the areal average rainfall occurrence diurnal variation it is observed that the first harmonics predominates in Lake Tana, Gilgel Abbay, and Jemma sub-basins. However, the second harmonic explains most of the variance in Belles, Dabus and Muger sub-basins. For the daily variation of the mean rain rate the first harmonic explains 53 % of the daily variation in Lake Tana while the variance explained by the two harmonics is weak (23-50%) for the rest of the sub-basins. For the points selected along the gorge except for the mean rain rate diurnal variation at gorge A, the variance explained by the sum of the first two harmonics is week. In general, differences in the mean of the

diurnal cycle, amplitude and the time of the amplitude are observed among the station sites, the sub-basins and the points selected along the Blue Nile river. As such, spatially varying diurnal cycle is observed over the Upper Blue Nile basin.

The Upper Blue Nile basin is characterized by highly variable topography. Moreover, the orientation of the mountain ranges in relation to the general pattern of air circulation influences the rainfall distribution. Results of this study suggest that high variability of rainfall is related to the variability in topography. By use of two transects from north to south and east to west, it is revealed that more rainfall is observed on the windward side of the high mountain ranges than the leeward side. The areas in the southwest of the mountain ranges (windward side) are characterized by high rainfall occurrence and mean rain rate compared to the other sides of the mountains. This suggests the existence of orographic influences in the basin where the areas in the north and northeast of the mountains are affected by rain shadow effect. Moreover, a direct relation between rainfall and elevation is observed from the two transects especially for 1700-1800LST.

The spatial distribution of the estimated mean rainfall depth for the rainy season of the Upper Blue Nile basin depicts that there is spatial variability of rainfall over the basin. The areas in the southwest and central highlands of the basin receive higher amounts of rainfall than the areas in the north and northeast parts of the basin. Moreover, areas along the Blue Nile River show a distinct pattern particularly from the PR with low amount of rainfall. The PR estimates are closer to the ground observations than TMI and as such the rainfall depth estimates from PR are more reliable than TMI. The TMI estimated mean rainfall depth at Shawura which is located at 9 km from Lake Tana is nearly 2 times greater than the ground truth and PR. This could be possibly because of the presence of mixed pixel with the lake as the resolution of TMI along track direction is around 12 km.

6.2. Recommendations

- This study provides relevant information on the diurnal cycle and spatial variability of rainfall. Information on rainfall variability at intraday time-scales and on areas with high topographic variation such as the Upper Blue Nile basin is required to study for instance erosion processes and for runoff simulation and forecasting. As such, similar and detailed studies can be undertaken for each sub-basin to have more detailed information on the temporal and spatial distribution of rainfall over the basin.

- Only few ground based observations were available to validate the satellite estimates in the basin and hence it is recommended to use/install more ground based meteorological stations with continuous recording devices. This will help to have ground observations not only to validate the satellite based estimates but also to study the rainfall characteristics of the basin at high temporal resolution and improved spatial coverage.

- This study focussed on rainfall variability assessment only for the rainy season AMJJ and JJAS months for French Guiana and the Upper Blue Nile basin respectively. However, further studies can be undertaken to assess the seasonal variability of the diurnal cycle of rainfall and investigate if there exist a diurnal cycle seasonal change over French Guiana and the Upper Blue Nile basin.

- The TRMM PR and TMI observations were used to assess the diurnal cycle and spatial distribution of rainfall. Because of the intermittent nature of sampling of the satellite, however, there might be discrepancies between the satellite sampling and rainfall activity. Therefore, for future studies a suitable approach can be applied to use the TRMM satellite data in combination with data from other satellites. In this regard, the TRMM satellite can be used in combination with MSG-2 which has higher temporal and spatial resolutions or SSM/I which has similar sensors on board with that of the TRMM satellite. In addition, the VIRS sensor can also be used to combine the TRMM observations with those of the geostationary satellites having VIS and IR channels.

- For this study a rain rate threshold of 1 mm h^{-1} is defined. However, further studies can be conducted by defining different thresholds to assess the diurnal cycle and spatial distribution of convective and stratiform rainfall. As such this will help for convective-stratiform partitioning and assess the dominant type of rainfall in the study areas.

- The harmonic analysis is performed for areal averaged rainfall on sub-basin basis; however, the spatial heterogeneity with in the sub-basins may influence the results of the analysis. Therefore, future studies can make use of the application of the analysis for the entire Upper Blue Nile basin. This will help to assess the mean of the diurnal cycle, the amplitude and the time of amplitude of the rainfall diurnal cycle on pixel basis.

- Results from this study indicate that there is spatial variability in the diurnal cycle of rainfall over the Upper Blue Nile basin. Hence, further studies can be undertaken to investigate the mechanisms causing this spatial variability.

- The PR estimated seasonal mean rainfall depth is closer to the ground observations than the TMI. However, to verify the satellite estimated mean rainfall depth, further validations can be carried out taking large number of daily rainfall data from the different parts of the basin.

References

Abtew, W., Melesse, A.M. and Dessalegne, T., 2008. Characteristics of monthly and annual rainfall of the Upper Blue Nile Basin. In: W. Abtew and A.M. Melesse (Editors), Proceedings of the workshop on Hydrology and Ecology of the Nile River Basin under extreme conditions. Addis Ababa, Ethiopia June 16-19, 2008.

Adler, R.F. and Negri, A.J., 1988. A Satellite Infrared Technique to Estimate Tropical Convective and Stratiform Rainfall. Journal of Applied Meteorology, 27(1): 30-51.

Arora, M., Singh, P., Goel, N.K. and Singh, R.D., 2006. Spatial distribution and seasonal variability of rainfall in a mountainous basin in the Himalayan region. Water Resources Management, 20: 489-508.

Artigas, L.F., Vendeville, P., Leopold, M., Guiral, D. and ternon, J.F., 2003. Marine biodiversity in French Guiana: estuarine, costal, and sgelf ecosystems under the influence of Amazonian waters., Gayana (Concepc.) [online], pp. 302-326.

Barros, A.P., Kim, G., Williams, E. and Nesbitt, S.W., 2004. Probing orographic controls in the Himalayas during the monsoon using satellite imagery. Nat. Hazards Earth Syst. Sci., 4(1): 29-51.

Bell, T.L. and Reid, N., 1993. Detecting the Diurnal Cycle of Rainfall Using Satellite Observations. Journal of Applied Meteorology, 32(2): 311-322.

Bielec-Bakowska, Z. and Lupikasza, E., 2009. Long-term precipitation variability on thunderstorm days in Poland (1951-2000). Atmospheric Research, 93(1-3): 506-515.

Bilanow, S. and Slojkowski, S., 2006. TRMM on-orbit performance reassessed after control change. 25th International Symposium on Space Technology and Science, and 19th International Symposium on Space Flight Dynamics.

Buytaert, W., Celleri, R., Willems, P., Bièvre, B.D. and Wyseure, G., 2006. Spatial and temporal rainfall variability in mountainous areas: A case study from the south Ecuadorian Andes. Journal of Hydrology, 329(3-4): 413-421.

Camberlin, P., 1997. Rainfall Anomalies in the Source Region of the Nile and Their Connection with the Indian Summer Monsoon. Journal of Climate, 10(6): 1380-1392.

Camberlin, P., 2009. Nile Basin Climates. In: H.J. Dumont (Editor), The Nile: Origin, Environments, Limnology and Human Use. Monographiiae Biologicae, Springer, pp. 307-333.

Committee on the Future of the Tropical Rainfall Measuring Mission, N.R.C., 2006. Assessment of the Benefits of Extending the Tropical Rainfall Measuring Mission: A Perspective from the Research and Operations Communities, Interim Report, Washington DC, 116, http://www.nap.edu/catalog/11195.html.

Conway, D., 2000. The Climate and Hydrology of the Upper Blue Nile, Ethiopia. The Geographical Journal, 166(1): 49-62.

Conway, D., 2005. From headwater tributaries to international river: Observing and adapting to climate variability and change in the Nile basin. Global Environmental Change Part A, 15(2): 99-114.

Dai, A., 2001. Global Precipitation and Thunderstorm Frequencies. Part II: Diurnal Variations. Journal of Climate, 14(6): 1112-1128.

Dejene, T., 2003. The Regional and Diurnal Variability of the Vertical Structure of Precipitation Systems in Africa, based on TRMM Precipitation Radar Data. University of Wyoming, Laramie pp. 9. http://gest.umbc.edu/student_opp/2003_gssp_reports/TeferiDejene.pdf.

ESA, 2004. EGPM-European Contribution to Global Precipitation Measurement. In: B. Battrick (Editor), Report for Mission Selection: The six candidate Earth Explorer Missions., ESA SP-1279(5). ESA Publications Division, Noordwijk, The Netherlands. http://www.esa.int/esaLP/ESA6KZJE43D_egpm_0.html.

Furuzawa, F.A. and Nakamura, K., 2005. Differences of Rainfall Estimates over Land by Tropical Rainfall Measuring Mission (TRMM) Precipitation Radar (PR) and TRMM Microwave Imager (TMI)-Dependence on Storm Height. Journal of Applied Meteorology, 44(3): 367-383.

Haile, A.T. and Rientjes, T., 2007. Spatio-temporal rainfall mapping from space: setbacks and strengths, In: proceedings of the 5th International symposium on Spatial Data Quality SDQ 2007, Modelling qualities in space and time, ITC, Enschede, The Netherlands, 13-15 June 2007, Enschede, ITC, pp. 9.

Haile, A.T., Rientjes, T., Gieske, A. and Gebremichael, M., 2009a. Multispectral remote sensing for rainfall detection and estimation at the source of the Blue Nile River. International Journal of Applied Earth Observation and Geoinformation, doi: DOI: 10.1016/j.jag.2009.09.001.

Haile, A.T., Rientjes, T., Gieske, A. and Gebremichael, M., 2009b. Rainfall variability over mountainous and adjacent lake areas: the case of Lake Tana basin at the source of the Blue Nile River. Journal of Applied Meteorology and Climatology, 48(8): 1696-1717.

Heinemann, T. and Kerényi, J., 2003. The EUMETSAT Multisensor Precipitation Estimate (MPE): Concept and Validation Proceedings of the EUMETSAT users conference, Weimar, Germany, 2003. .

Heinemann, T., Lattanzio, A. and Roveda, F., 2002. The EUMETSAT Multisensor Precipitation Estimate (MPE), Proceedings of the second International Precipitation Working Group (IPWG) meeting, Madrid, Spain, September 2002

Iguchi, T., Kozu, T., Meneghini, R., Awaka, J. and Okamoto, K., 2000. Rain-Profiling Algorithm for the TRMM Precipitation Radar. Journal of Applied Meteorology, 39(12): 2038-2052.

Ikai, J. and Nakamura, K., 2003. Comparison of Rain Rates over the Ocean Derived from TRMM Microwave Imager and Precipitation Radar. Journal of Atmospheric and Oceanic Technology, 20(12): 1709-1726.

Ji, Y., 2006. Validation of diurnal cycle and intera-seasonal variability of TRMM satellite rainfall. PIERS ONLINE, 2(6): 628-632.

Kidd, C., Kniveton, D.R., Todd, M.C. and Bellerby, T.J., 2003. Satellite Rainfall Estimation Using Combined Passive Microwave and Infrared Algorithms. Journal of Hydrometeorology, 4(6): 1088-1104.

Kim, U. and Kaluarachchi, J.J., 2008. Application of parameter estimation and regionalization methodologies to ungauged basins of the Upper Blue Nile River Basin, Ethiopia. Journal of Hydrology, 362(1-2): 39-56.

Kim, U., Kaluarachchi, J.J. and Smakhtin, V.U., 2008. Generation of Monthly Precipitation Under Climate Change for the Upper Blue Nile River Basin, Ethiopia. JAWRA Journal of the American Water Resources Association, 44(5): 1231-1247.

Kishtawal, C.M. and Krishnamurti, T.N., 2001. Diurnal Variation of Summer Rainfall over Taiwan and Its Detection Using TRMM Observations. Journal of Applied Meteorology, 40(3): 331-344.

Kousky, V.E., 1980. Diurnal Rainfall Variation in Northeast Brazil. Monthly Weather Review, 108(4): 488-498.

Kummerow, C., Barnes, W., Kozu, T., Shiue, J. and Simpson, J., 1998. The Tropical Rainfall Measuring Mission (TRMM) Sensor Package. Journal of Atmospheric and Oceanic Technology, 15(3): 809-817.

Kummerow, C., Hong, Y., Olson, W.S., Yang, S., Adler, R.F., McCollum, J., Ferraro, R., Petty, G., Shin, D.-B. and Wilheit, T.T., 2001. The Evolution of the Goddard Profiling Algorithm (GPROF) for Rainfall Estimation from Passive Microwave Sensors. Journal of Applied Meteorology, 40(11): 1801-1820.

Kummerow, C., Simpson, J., Thiele, O., Barnes, W., Chang, A.T.C., Stocker, E., Adler, R.F., Hou, A., Kakar, R., Wentz, F., Ashcroft, P., Kozu, T., Hong, Y., Okamoto, K., Iguchi, T., Kuroiwa, H., Im, E., Haddad, Z., Huffman, G., Ferrier, B., Olson, W.S., Zipser, E., Smith, E.A., Wilheit, T.T., North, G., Krishnamurti, T. and Nakamura, K., 2000. The Status of the Tropical Rainfall Measuring Mission (TRMM) after Two Years in Orbit. Journal of Applied Meteorology, 39(12): 1965-1982.

Kuraji, K., Punyatrong, K. and Suzuki, M., 2001. Altitudinal increase in rainfall in the Mae Chaem watershed, Thailand. Journal of the Meteorological Society of Japan, 79(1B): 353-363.

Levizzani, V., Amorati, R. and Menguzzo, F., 2002. A review of satellite-based rainfall estimation methods European Commission Project MUSIC Report (EVK1-CT-2000-00058), pp. 66. http://www.isac.cnr.it/~meteosat/pub.shtml

Levizzani, V. and Mungnai, A., 2004. Rainfall measurement from space: where are we?, Proc. 14th Int. Conf. on Clouds and Precipitation Bologna, 18-23 July, 1123-1126. http://www.isao.bo.cnr.it/~meteosat/pub.html.

Lim, G.-H. and Suh, A.-S., 2000. Diurnal and Semidiurnal Variations in the Time Series of 3-Hourly Assimilated Precipitation by NASA GEOS-1. Journal of Climate, 13(16): 2923-2940.

Maathuis, B., Gieske, A., Retsios, V., Leeuwen, B.V., Mannaerts, C. and Hendrikse, J., 2006. Meteosat-8: from temperature to rainfall. ISPRS Tech. Commission VII, Mid Term Symposium, 8-11 May 2006.

Meisner, B.N. and Arkin, P.A., 1987. Spatial and Annual Variations in the Diurnal Cycle of Large-Scale Tropical Convective Cloudiness and Precipitation. Monthly Weather Review, 115(9): 2009-2032.

Negri, A.J., Bell, T.L. and Xu, L., 2002. Sampling of the Diurnal Cycle of Precipitation Using TRMM. Journal of Atmospheric and Oceanic Technology, 19(9): 1333-1344.

Nesbitt, S.W. and Zipser, E.J., 2003. The Diurnal Cycle of Rainfall and Convective Intensity according to Three Years of TRMM Measurements. Journal of Climate, 16(10): 1456-1475.

Nesbitt, S.W., Zipser, E.J. and Kummerow, C.D., 2004. An Examination of Version-5 Rainfall Estimates from the TRMM Microwave Imager, Precipitation Radar, and Rain Gauges on Global, Regional, and Storm Scales. Journal of Applied Meteorology, 43(7): 1016-1036.

Oki, T. and Musiake, K., 1994. Seasonal Change of the Diurnal Cycle of Precipitation over Japan and Malaysia. Journal of Applied Meteorology, 33(12): 1445-1463.

Schouppe, M. and Ghazi, A., 2007. European commission research for global climate change studies: Towards improved water observations and forecasting capability. In: V. Levizzani, P. Bauer and F. Joseph Turk (Editors), Measuring precipitation from space : EURAINSAT and the future Advances in global change research. Springer Verlag pp. 737.

Sen, Z. and Habib, Z., 2000. Spatial precipitation assessment with elevation by using point cumulative semivariogram technique. Water Resources management, 14(4): 311-325.

Simpson, J., Adler, R.F. and North, G.R., 1988. A Proposed Tropical Rainfall Measuring Mission (TRMM) Satellite. Bulletin of the American Meteorological Society, 69(3): 278-295.

Sorooshian, S., Gao, X., Hsu, K., Maddox, R.A., Hong, Y., Gupta, H.V. and Imam, B., 2002. Diurnal Variability of Tropical Rainfall Retrieved from Combined GOES and TRMM Satellite Information. Journal of Climate, 15(9): 983-1001.

Todd, M.C., Kidd, C., Kniveton, D. and Bellerby, T.J., 2001. A Combined Satellite Infrared and Passive Microwave Technique for Estimation of Small-Scale Rainfall. Journal of Atmospheric and Oceanic Technology, 18(5): 742-755.

UNESCO, 2004. National Water Development Report for Ethiopia. UN-WATER/WWAP/2006/7, World Water Assessment Program, report, MOWR: 284.

Vondou, D.A., Nzeukou, A. and Kamga, F.M., 2009. Diurnal cycle of convective activity over the West of Central Africa based on Meteosat images. International Journal of Applied Earth Observation and Geoinformation, doi:10.1016/j.jag.2009.09011.

Walther, A., Jeong, J.H. and Chen, D., 2009. Spatio-temporal characteristics of the diurnal precipitation cycle over Sweden and the linkage to large-scale circulation. Geophysical Research, 11.

Werkineh, 2002. Some aspects of meteorological drought in Ethiopia. In: M.H. Glantz (Editor), Drought and hunger in Africa: Denying famine a future. Cambridge University Press, UK, pp. 23-36.

Wu, Q., 2004. Diurnal variation of tropical rainfall using five years TRMM data. MSc Thesis, A and M University, Texas, 45 pp.

Yates, D.N. and Strzepek, K.M., 1998. Modeling the Nile Basin under Climatic Change. Journal of Hydrologic Engineering, 3(2): 98-108.
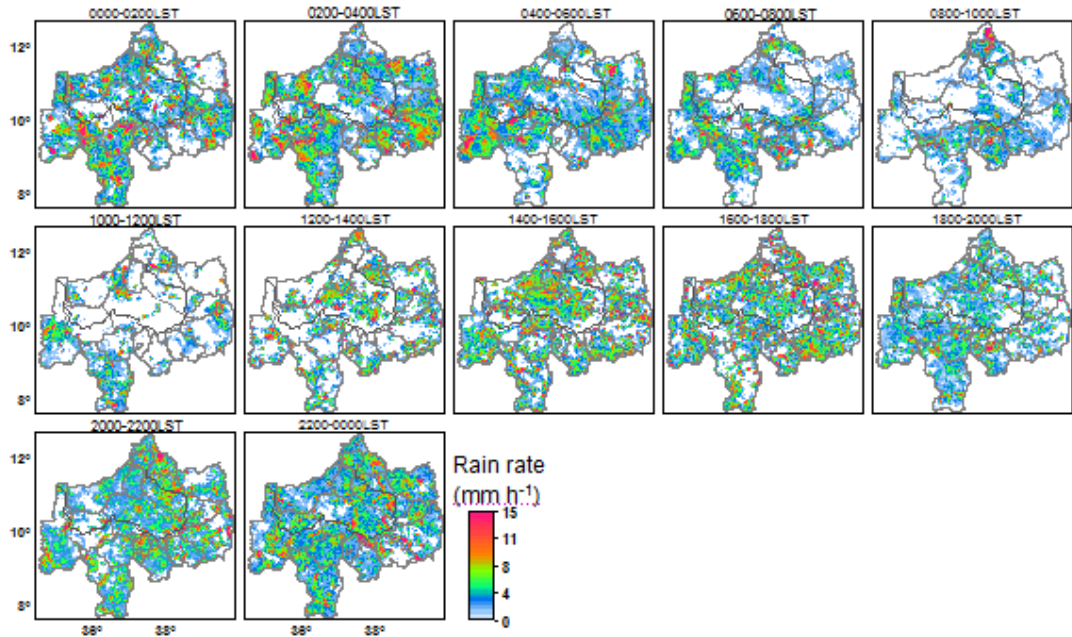
Appendices
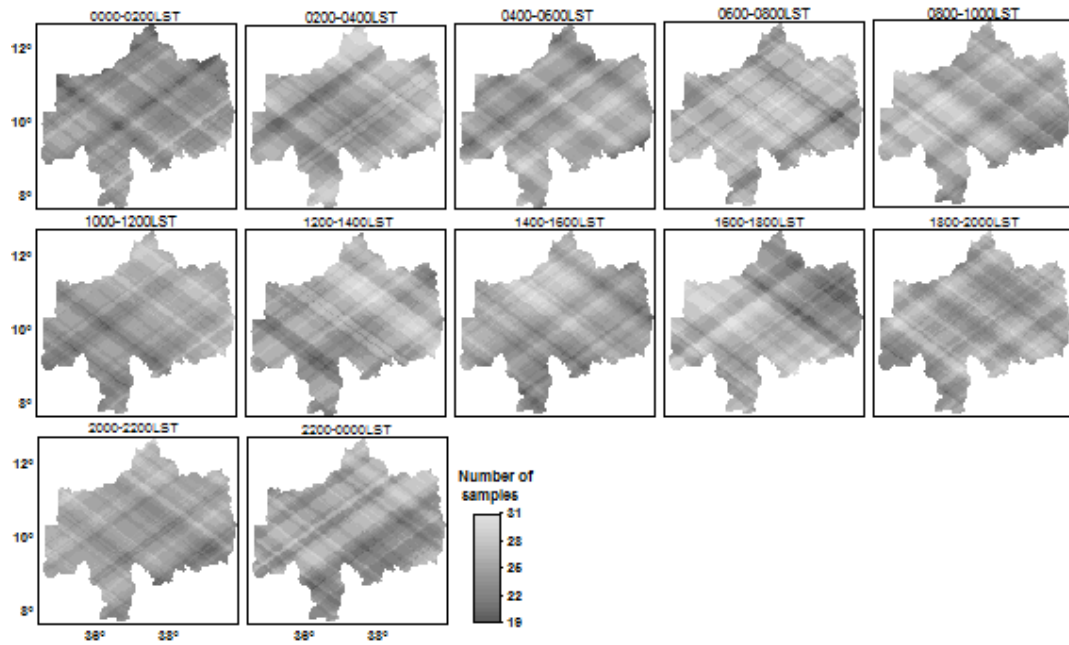
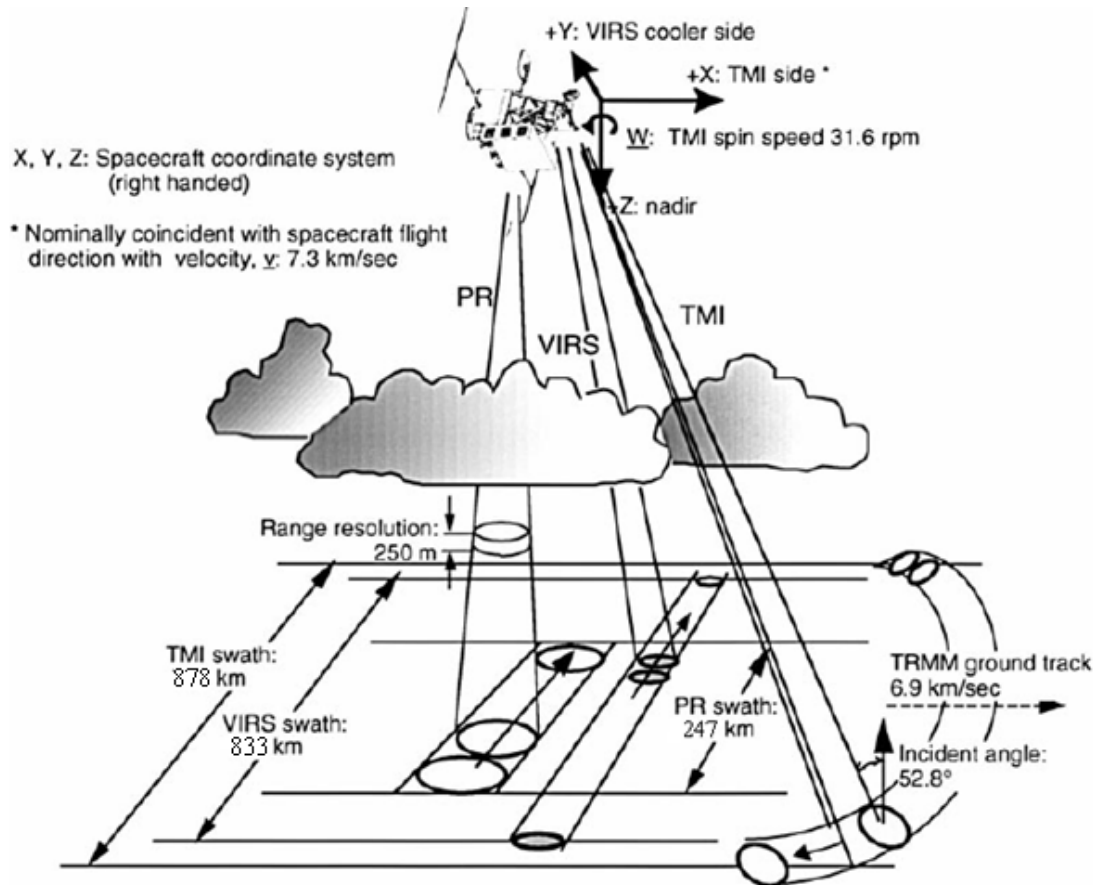I. The number of PR observations for the Upper Blue Nile Basin on 2-hourly periods.
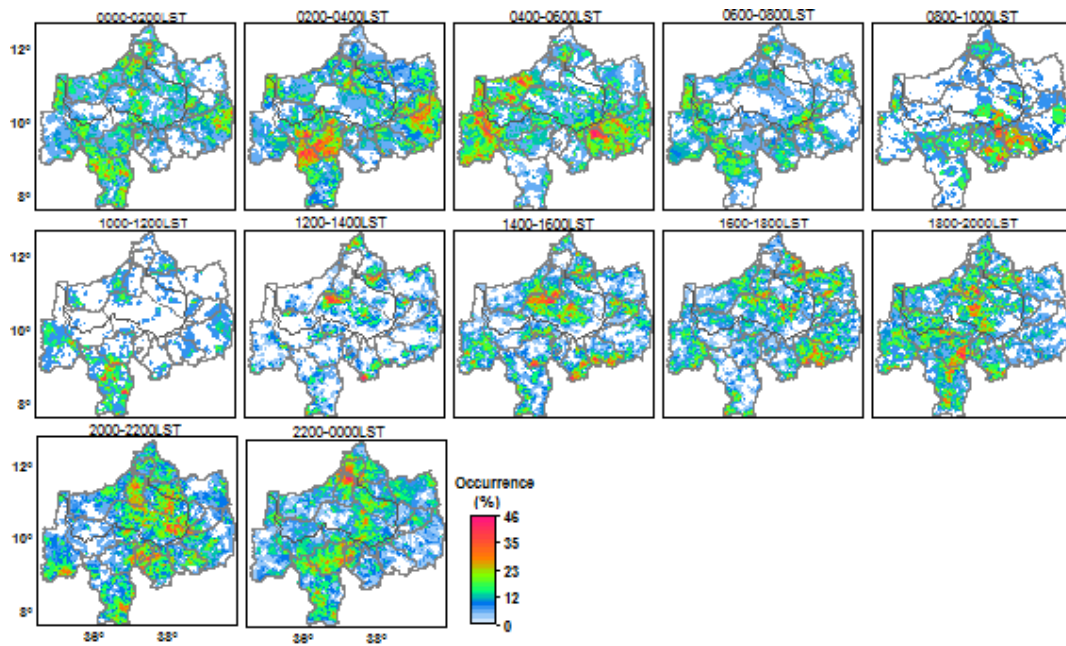
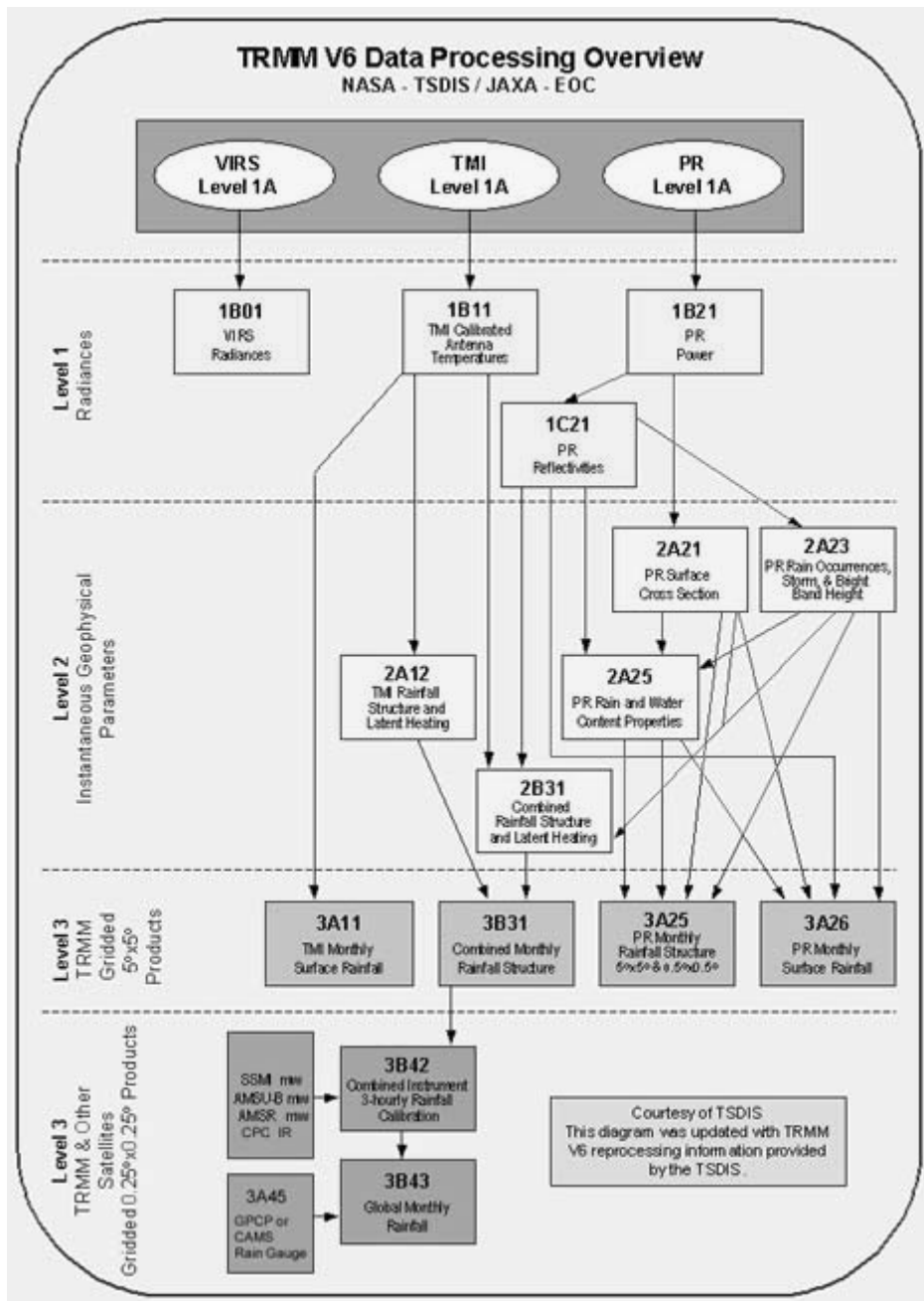II. Diurnal variation of rainfall occurrence using PR data on 2-hourly periods.

III. Diurnal variation of conditional mean rain rate using PR data on 1-hourly period.

IV. Schematic view of the scan geometries of the three TRMM primary rainfall sensors (PR, TMI and VIRS). Source: Kummerow et al., 1998, TRMM sensor package.

V. TRMM version 6 algorithm flow diagram. (source: http://trmm.gsfc.nasa.gov/)